Predicting the effects of ankle-foot orthoses on the gait of patients with calf muscle weakness

A predictive forward dynamics simulation study

MSc Thesis

Delft University of Technology

February 2021

Bernadett Kiss

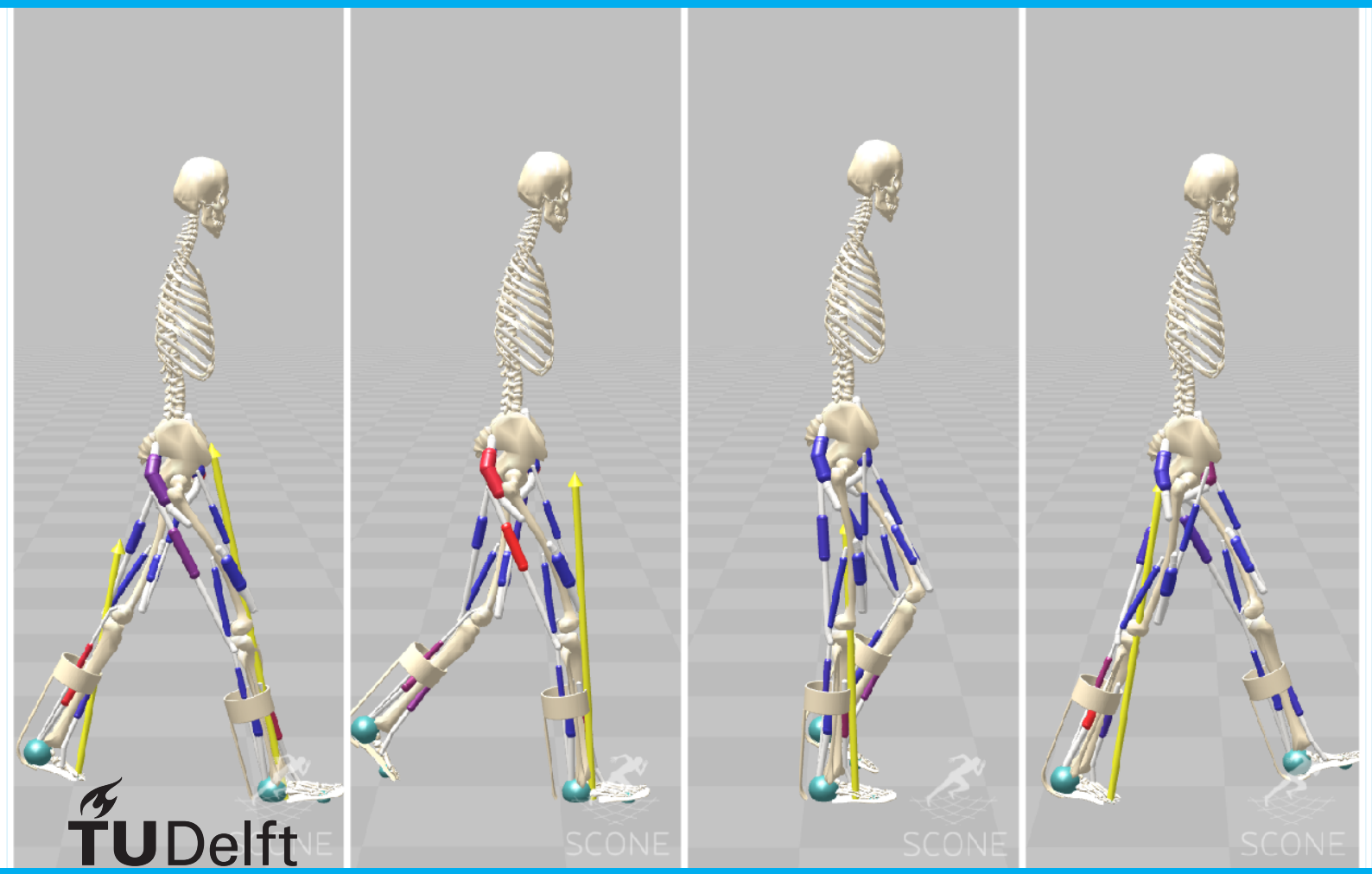

TU Delft

Predicting the effects of ankle-foot orthoses on the gait of patients with calf muscle weakness

A predictive forward dynamics simulation study

by

Bernadett Kiss

to obtain the degree of Master of Science
at the Delft University of Technology,
to be defended publicly on Wednesday February 24, 2021 at 12:30.

Student number:	4788427	
Project duration:	January 6, 2020 – February 24, 2021	
Thesis committee:	Prof. Dr. Ir. Jaap Harlaar	TU Delft, supervisor
	Dr. Ir. Ajay Seth	TU Delft, supervisor
	Dr. Ir. Gerwin Smit	TU Delft
	Dr. Ir. Riender Happee	TU Delft
Thesis advisor:	Dr. Niels F. J. Waterval	VU Medical Center Amsterdam, daily supervisor

An electronic version of this thesis is available at http://repository.tudelft.nl/.

TU Delft

Abstract

Various neuromuscular disorders such as spinal cord injury, Charcot-Marie-Tooth disease and poliomyelitis lead to calf muscle weakness, which limits the patient's ability to propel their body forward during gait. Their abnormal gait pattern is characterized by increased ankle dorsiflexion, excessive knee flexion during stance and reduced ankle push-off power which leads to decreased walking speed and increased energy cost of gait.

To improve walking ability, dorsal leaf spring (DLS) ankle-foot orthoses (AFOs) are often worn that provide stiffness around the ankle joint which is its most important characteristic. Selecting optimal AFO stiffness is important because it can substantially reduce the net metabolic cost of gait, while improper AFO stiffness can lead to discomfort, fatigue and overall reduced activity. Experimental data shows that the effect of AFOs is dependent on the individual characteristics of the patients, such as level of muscle weakness, spasticity and body mass. Despite the importance of AFO stiffness, empirically determining the stiffness of the applied AFO remains time-consuming and ad hoc.

This master thesis aims to uncover the mechanism relating AFO stiffness to the metabolic cost of transport (CoT) as observed in experimental trends from individuals with calf muscle weakness. We used predictive forward musculoskeletal simulations to reproduce the experimental trends and analyzed our simulations to explain the relationship between AFO stiffness and metabolic CoT.

The predicted optimal AFO stiffness was within $1\,\mathrm{Nm/deg}$ of the patient's experimentally measured one. From the experimentally observed effects, all kinematic and kinetic trends were predicted within $0.5-2.5$ SD from the mean of the experimental slopes of all patients' results. Moreover, the differences between the slopes of the simulation results were mostly lower compared to the modelled patient's individual experimental slopes than compared to the experimental slope of the group average results.

We identified a reduction in the vasti muscle metabolic cost due to larger external knee extension moments with increasing AFO stiffness as the main mechanism resulting in the net metabolic CoT trend. Limitations on translating our findings to patient behavior include: modelled calf muscle strength, where the model may be significantly stronger or weaker than the patient, and the relative importance of metabolic cost minimization to other goals during walking, such as minimizing the loading rate at heel strike.

Acknowledgments

I would like to thank Prof. Dr. Ir. Jaap Harlaar for giving me the opportunity to work on this exciting research project, Dr. Ir. Ajay Seth for guiding my work with his indispensable and constructive observations, and Dr. Niels Waterval for his continuous feedback and helpful suggestions. Besides my supervisors, I would like to express my gratitude towards my family and friends for their endless support during the past years.

Bernadett Kiss
Delft, February 2021

Contents

List of Figures

List of Tables

Acronyms

Table 1: Nomenclature

AFO	Ankle-Foot Orthosis
DLS	Dorsal Leaf Spring
DF	Dorsiflexion
PF	Plantarflexion
RoM	Range of Motion
CoT	Cost of Transport
GRF	Ground Reaction Force
CoP	Center of Pressure
DoF	Degree of Freedom

1 Introduction

1.1. Calf muscle weakness

Various neuromuscular disorders such as spinal cord injury, Charcot-Marie-Tooth disease and poliomyelitis affect the strength and control of the lower leg muscles, causing spasticity and/or paresis (weakness) of these muscles [2][46][56]. It can affect the plantarflexor (calf muscles) and/or the dorsiflexor muscles as well.

In case of calf muscle weakness, ankle push-off power is reduced which limits the patients' ability to propel their body forward. This results in reduced walking speed and abnormal gait patterns, such as excessive dorsiflexion of the ankle, and excessive knee flexion during stance [58]. These gait deviations lead to increased metabolic energy cost during walking [12] which can deteriorate the patients' quality of life by limiting them in their daily physical activities [47].

1.2. Ankle-foot orthoses (AFOs)

To improve walking ability and quality of life in patients with calf muscle weakness, AFOs are often provided [29]. AFOs are assistive devices which encompass the ankle joint and provide support to it and the foot, intended to mechanically compensate for (part of) the lost function of the calf muscles.

AFOs can be active or passive devices depending on whether the device provides external energy sources for walking or not. Passive devices are more common, as powered AFOs are currently too heavy, too expensive and less reliable to use in daily life [64].

The most important characteristic defining a passive AFO's effect is its stiffness around the ankle joint, the resistance against sagittal plane rotation of the AFO. The stiffness determines the energy storage and return capacity of the AFO which can have a significant effect on gait performance [38] and on the energy cost of walking [88][11][15].

These devices can be articulated, named spring-hinged (SH) AFOs or non-articulated, named dorsal leaf spring (DLS) AFOs. SH-AFOs (Fig. 1.1.) have a mechanical joint at the ankle around which a cylindrical spiral spring is providing moment when the ankle is in PF or DF depending on the position of the spring(s). In SH-AFOs the DF and PF stiffness can be varied independently. In DLS-AFOs (Fig. 1.1.) a leaf spring is attached to the posterior side of the orthosis which provides additional moment around the ankle when it is not in neutral position. Stiffness is affected by the leaf spring's material, its thickness, shape and trimline [79]. Contrary to SH-AFOs, in DLS-AFOs the DF and PF stiffness can not be varied independently. In the current thesis, the focus will be on passive DLS-AFOs.

1.3. Kinetic and kinematic effects of AFOs

Increased ankle dorsiflexion, excessive knee flexion during stance and reduced ankle push-off power [58] are characteristic of the gait of patients with calf muscle weakness which leads to elevated energy cost of gait [12]. The use of AFOs aims to prevent excessive ankle DF and persistent knee flexion by providing PF moment when the ankle is dorsiflexed during stance [31] but the degree of compensation for impaired calf muscle function depends largely on the stiffness setting of the applied AFO.

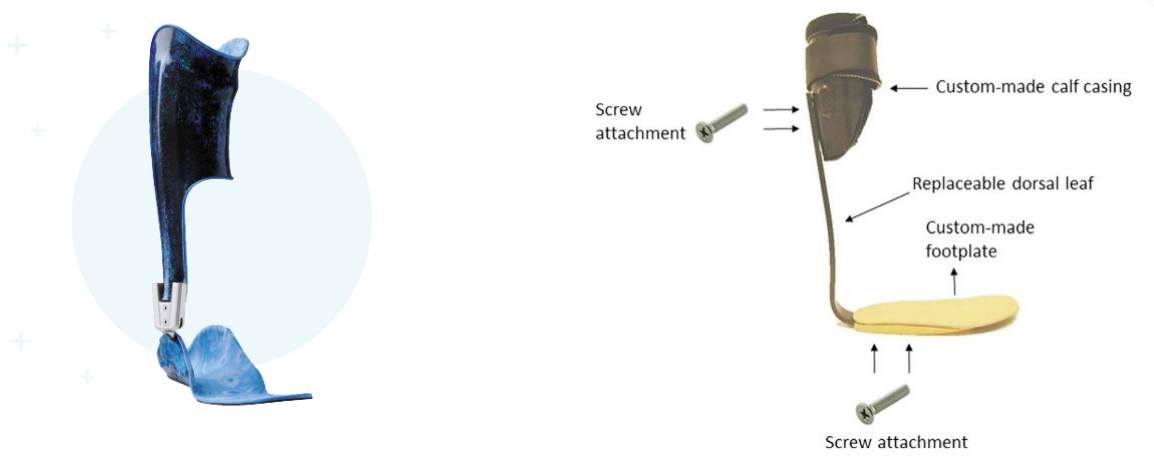

Figure 1.1: Example of a spring-hinged (SH) AFO [1] (left) and of a dorsal leaf spring (DLS) AFO [88] (right)

The positive effects of increasing AFO stiffness identified from studies on patients with impaired calf muscles were the following. With increasing AFO stiffness less biological ankle moment contribution is needed to the net ankle joint moment [10][6][78], and ankle- and knee angles and moments will be closer to normal [88][59]. Moreover, by low stiffnesses, the total ankle push-off power is increasing.

However, by further increasing the AFO stiffness, negative effects develop on the ankle range of motion (RoM) [10][28][35][6][33][88][59] inducing limits on the maximal ankle PF angular velocity [10][11] which results in lower net ankle power generation at push-off [88][59]. By higher stiffnesses, this can lead to compensations at the hip joint. Some studies reported increased hip flexion angles [33] and increased hip work [10] by excessive AFO stiffness levels.

Accordingly, AFOs support but also constrain calf muscle function which means that there should be an optimum setting to balance out these two opposing effects.

1.4. Effect of AFOs on the metabolic cost of transport

Due to changes in the gait pattern of patients, AFOs can lower the metabolic energy cost of their gait. Experimental studies [10][15][33][20][88][59] on healthy and pathological subjects corroborate that AFOs reduce the mean metabolic cost of gait of the measured group compared to walking barefoot or with shoes only, in a range of 5.8% to 19.5% (Fig. 1.2.). This percentage was shown to be even larger when the average of the individual metabolic cost reductions were considered, 7.7%[59] to 22.7% [88]. The results of simulations on healthy models showed similar levels of metabolic cost of transport (CoT) reduction of 7.2% [83] and 8% [65].

The level of metabolic energy cost reduction depends partly on the AFO design (Fig. 1.2.) but these studies also found that tuning AFO stiffness of each investigated design could reduce the metabolic cost by $3.2 - 12.2\%$ with the most efficient setting of the group compared to the least efficient setting of the group.

Studies on patients with non-spastic calf muscle weakness also showed that the energy cost decrease was even larger on an individual basis [88][59]. By the individual best setting of the patients their metabolic energy cost was on average 9.5%[59] and 10.7%[88] less than by their individual worst setting. This is a statistically significant difference because it is larger than the smallest detectable difference for metabolic energy cost reported in poliomyelitis patients (9.4%[12]). Also, it is considered clinically relevant because it is meaningful to the patient.

The stiffness which optimally supports the patient is hypothesized to depend on their individual characteristics such as level of muscle weakness, spasticity, RoM and body mass. This shows in the wide spread of individual metabolic CoT trends of the patients from the measurements of Waterval et al.[88] in Fig. 1.3. If the stiffness of the AFO is not set correctly, it can worsen the patient's gait pattern and cause excessive stress on the legs, which can lead to discomfort, fatigue and future pathologies [76][63][21]. Since the individual metabolic CoT results are widespread (Fig. 1.3), the trend resulting from their mean (Fig. 1.2) does not display a quadratic trend as the number of measured patients

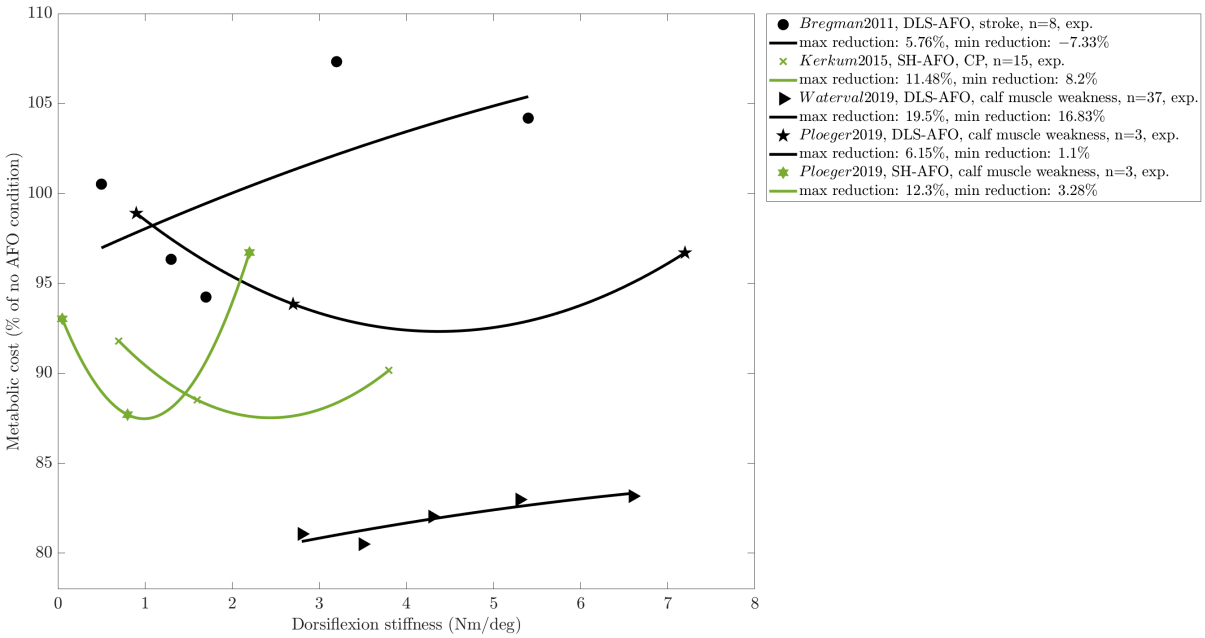

Figure 1.2: Mean metabolic energy cost decrease of all patients in the studies walking with AFO in the percentage of the metabolic energy cost of subjects walking without AFO against AFO stiffness
DLS-AFO: dorsal leaf spring AFO (black); SH-AFO: spring hinged AFO (green); CP: cerebral palsy;
min. and max. reduction: compared to the no-AFO condition; fitted curves are quadratic polynomials
*Bregman*2011 - [10], *Kerkum*2015 - [33], *Waterval*2019 - [88], *Ploeger*2019 - [59]

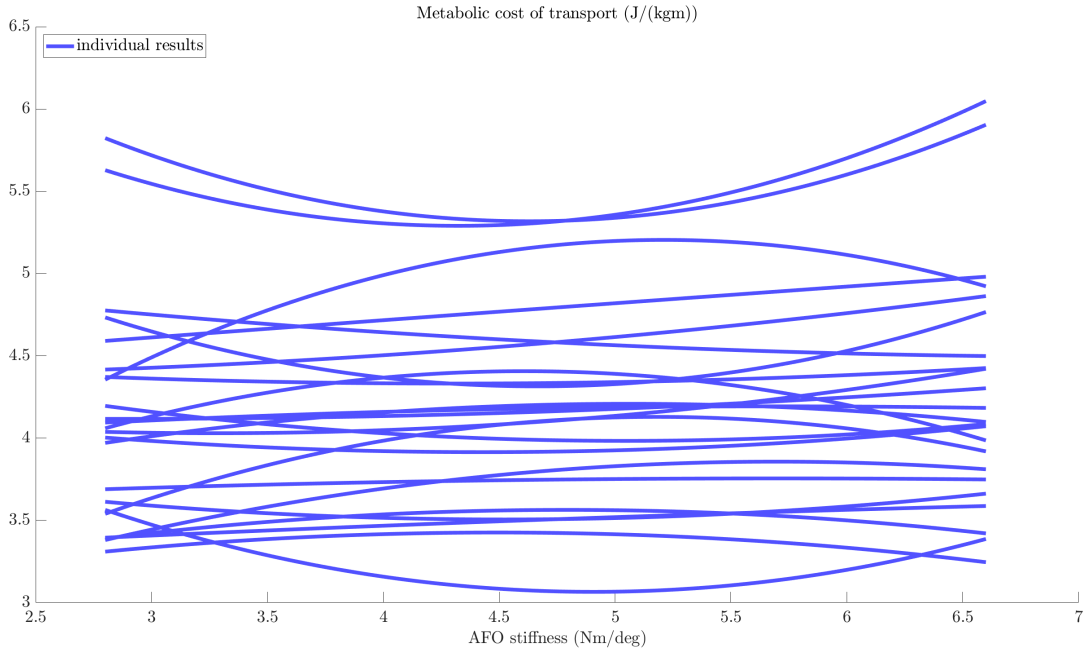

Figure 1.3: Experimental metabolic energy cost trend against AFO stiffness for each bilateral affected patient walking with AFO in the study of Waterval et al.[88]

increases.

The trade-off between the opposing effects of AFO stiffness determines the individual optimum for each patient. The positive and negative effects on gait kinematics and kinetics, identified from the literature on pathological population in the previous subsection, cause reduction and rise in the net metabolic cost of gait, respectively. The main metabolic CoT reducing factor was hypothesized to be connected to the decrease of the energy consumption of the quadriceps muscles as AFO stiffness

increases by subjects with calf muscle impairments, and the rise of the metabolic CoT was assumed to be due to the decrease in ankle push-off power generation and compensation strategies at the hip joint by excessive AFO stiffness levels [88][13][33][36][59][7]. However, these muscle activation level changes were not yet measured experimentally, so further investigation is needed.

1.5. Problem statement

As the low number of significant effects in literature also shows, the effects of AFO stiffness are highly individual in both rate and extent depending on the severity of the patient's impairment (Fig. 1.3). In a few cases, the effects can be very limited [57], but generally, enough stiffness is needed for the above described positive effects on the joint kinematics and kinetics, but the stiffness setting cannot be too high to avoid the negative effects on the ankle push-off power. Thus, the optimal stiffness is individual and difficult to find for each patient.

Currently, guidelines about the optimal stiffness for different patients are not yet available. Consequently, orthotists usually rely on their experience, time-consuming trial and error iterations and the feedback of the patient, when they are determining the stiffness setting of the applied AFO. Thus, frequently improper AFO stiffness is chosen which leads to suboptimal gait biomechanics and energy costs [87]. Great efforts have been made to make this process faster by analysing the patient's gait and determining the optimal stiffness by instrumented AFOs [9][34] and by simulations [11][17].

Instrumented AFOs have many drawbacks because each prototype is designed with a single desired functionality in mind which limits the potential assistance strategy. Moreover, their design and development take years and the developed equipment is expensive. Finding the optimal settings still includes many trials and it is time-consuming to individualize the method for different patient needs.

Recently, human-in-the-loop optimizations [95][91] were developed during which continuously optimized device control laws are generated and applied on the worn exoskeleton during walking by an emulator system. The aim is to maximize human performance by minimizing the energy cost of walking. Using this method a wide range of assistance strategies can be applied on the exoskeleton worn by the user, mitigating the need to build new prototypes.

Simulations are less limited than human-in-the-loop optimizations because a wider range of assistance strategies can be applied to a model without causing any physical harm or exhausting the user which is especially important in the case of patients. However, some aspects of simulations, such as the selection of the modelled attributes and objective functions are not flawless yet which complicates the validation process.

Most of the published simulations are non-predictive [65][83][7][93] which means that they can reach similar results to experiments and could partly explain the underlying causes, but predictive, forward simulations [78][11] would be needed to forecast the adaptation of the patients to different assistance strategies without the need to build new hardware [49].

Furthermore, the general effects of the AFO device's attributes (e.g. stiffness, neutral angle, mass) and the patients' characteristics (e.g. body mass, muscle strength, muscle stiffness) could be isolated with the help of predictive forward simulations.

The ultimate goal of this research is to find the AFO settings (stiffness and neutral angle) for each individual patient that maximizes her/his performance. To reach this goal, the mechanical relationship between AFO stiffness and metabolic cost of transport (CoT) in patients with calf muscle weakness has to be explored. The first step to find these underlying mechanisms is to validate the predictive forward simulation results by evaluating the effects of varying stiffness on metabolic CoT, gait kinematics and kinetics.

1.6. Research questions

The main research question of the study is: By what mechanism does the metabolic cost of transport change with AFO stiffness as observed in experimental trends in individuals with calf muscle weakness? To answer this question, the aims of this study are: to reproduce experimental trends in musculoskeletal simulations and to analyze the simulations to explain the experimental trends. The experimental outcomes were measured on 37 patients with non-spastic calf muscle weakness, wearing AFOs with varying stiffnesses [88].

To answer our main question, the following sub questions have to be evaluated:

1. Using a scaled model of a patient with calf muscle weakness and matching the simulation's minimum walking speed to his experimental minimum, how accurately can predictive forward simulations forecast the same patient's trend of metabolic cost of transport change as AFO stiffness is varied?
2. How accurately can forward simulations predict the trend in gait kinetics and kinematics with varying AFO stiffness as observed in experimental data?
    2.1. How accurately can these predictive forward simulations forecast the trend of gait kinetic and kinematic changes seen in experimental group data as AFO stiffness is varied?
    2.2. How accurate are the trend predictions compared to the same patient's experimental kinetic- and kinematic results?
3. What are the possible reasons for the differences between simulation and experimental results?

1.7. Thesis overview

First, the modelling method of the DLS-AFO; secondly, the scaling and inverse simulation of the neuromuscular patient model wearing the DLS-AFO device will be presented. Then, the predictive forward simulation framework, SCONE, will be introduced and the properties of the optimizations will be described and explained in detail. The methods of data analysis are closing this section.

Next, the results of the optimizations will be presented and compared with experimental data from the study of Waterval et al.[88]. Afterwards, the discussion of the results, the answers to the research questions will be detailed. Last, the limitations of the study, future work and the conclusion will follow.

2

Methods

2.1. Modelling methods

2.1.1. Human model

The neuromuscular patient model was designed in *OpenSim 3.3* [19][72]. The human model is based on [18][92][4][5], it is a modified version of the *gait10dof18musc* model [75].

The final model (Fig. 2.1) is planar, it has 9 degrees of freedom: pelvis translation in the sagittal plane horizontally and vertically, pelvis forward/backward tilt, right and left hip flexion/extension, right and left knee flexion/extension, right and left ankle PF/DF. These are actuated by 18 muscles, two contact forces between each foot and the ground, and a coordinate limit force at each knee joint. The 9 major muscle groups per leg are: tibialis anterior (TA), soleus (SOL), gastrocnemius (GAS), vasti (VAS), rectus femoris (RF), biceps femoris short head (BFSH), biarticular hamstrings (HAMS), iliopsoas (ILIO), gluteus maximus (GMAX). The muscles' behaviour is based on the *Millard 2012* muscle model [74] [44]. The coordinate limit forces at the knees apply stiffness ($2\,\mathrm{Nm/deg}$) and damping ($0.2\,\mathrm{Nm/(deg/s)}$) on the knee joint if the knee angles are outside the $5 - 120\,^\circ$ flexion range. This aims to put physiological limits on knee movement [70]. The basal and individual muscle metabolic energy cost calculation is based on the work of Uchida et al.[80] and Umberger et al.[81]. The slow-twitch fiber ratios for the muscles can be found in the Appendix A. They were set according to Johnson et al.[32] and Garrett et al.[23], similarly to the settings in the study of Ong et al.[49].

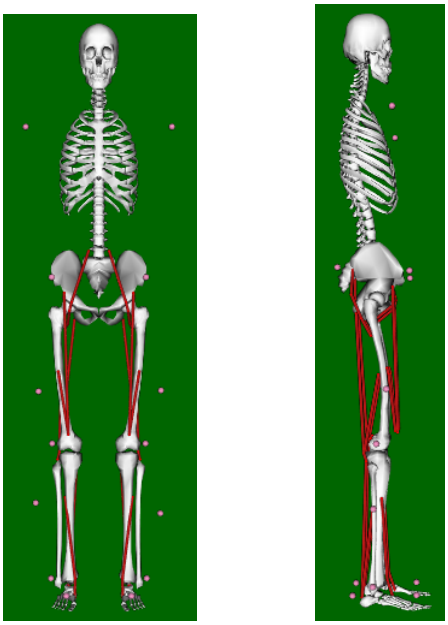

Figure 2.1: The scaled OpenSim model, based on the *gait10dof18musc* model [75] with the scaling markerset

2.1.2. Non-spastic calf muscle weakness modelling

Biodex tests were done on the patients in the work of Waterval et al.[88] but it is questionable how this data relates to percentage weakness as we do not have extensive reference values. Thus, the maximum isometric muscle strength of the patients is uncertain, an informed guess was made based on the minimization of residual ankle moments during the inverse simulations using experimental data. The maximum isometric muscle strength of the soleus and gastrocnemius muscles was set to 40% of its original, healthy value (60% muscle weakness).

In contrast to other papers [49], passive fiber- and tendon force-length curves were modified so that the healthy passive force-length curves are maintained. This was needed because the relation between maximal isometric force and passive force generation is different by patients than by healthy subjects [55]. The final passive fiber- and tendon force-length curve parameters can be found in Appendix B.

2.1.3. Contact parameter settings

To generate forces between the ground and the foot, a compliant contact model was used. One contact sphere was placed at the heel and one at the toe of each foot. Predictive forward simulations are highly influenced by the used foot contact model settings [43], so the results of Veerkamp et al.[82] were used in this study (Appendix C). They tuned the position (x, y, z) and size of the contact spheres in *SCONE* tracking optimizations to best fit experimental kinematic- and ground reaction force data. They set the Hunt-Crossley force parameters (stiffness, dissipation and friction) according to previous studies.

2.1.4. Ankle-foot orthosis modelling

The AFO was modelled in two parts using *Solidworks® 2019* (Dassault Systèmes Corp.). One part is the calf casing of the AFO and the other part encompasses the footplate of the AFO and the shoe (Fig. 2.2). Uniform mass distribution and their experimental mass (calf casing - $0.2\,\mathrm{kg}$, footplate and shoe - $0.5\,\mathrm{kg}$) [88] was set for both parts. The modelled parts were imported into OpenSim and connected with weld joints to the body (calf casing to tibia, footplate and shoe to calcaneus).

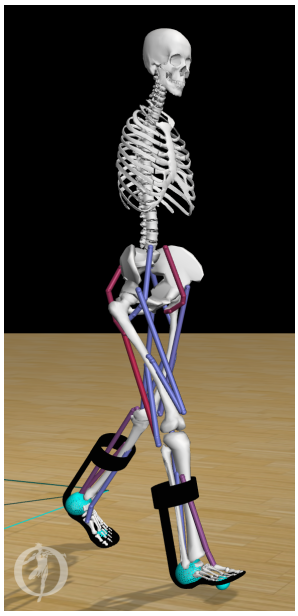

Figure 2.2: The scaled OpenSim model with AFO and contact spheres

The stiffness property of the AFO was added as a coordinate limit force in OpenSim, acting on the ankle joint. The stiffness and neutral angle range were set according to experimental data. The AFO exerts moments on the ankle joint only when the ankle angle is outside of the neutral angle range (Fig. 2.3). By DLS-AFOs, this small range depends on the material and manufactured geometry of the AFO, and its fitting on the subject's leg. The neutral angle range was defined as the ankle angle range during swing phase of the subject for each leg because in swing phase the AFO should not exert moments on the ankle joint [62] (Fig. 2.4).

According to experimental kinematic data, the neutral angle range was asymmetric for the subject. This was probably caused by asymmetries in calf or foot geometry of the subject, or slight misalignment of the AFO. To simplify the model to a symmetric controller, we used the neutral angle of the right leg for both legs (Fig. 2.4).

The damping factor of the coordinate limit force was set to $0.001\,\mathrm{Nm/(deg/s)}$ and the width of the transition region from zero to the set stiffness as the ankle angle exceeds the limit of the neutral angle range was set to $0.01\,\mathrm{deg}$ which does not modify the linear behavior of the AFO model substantially.

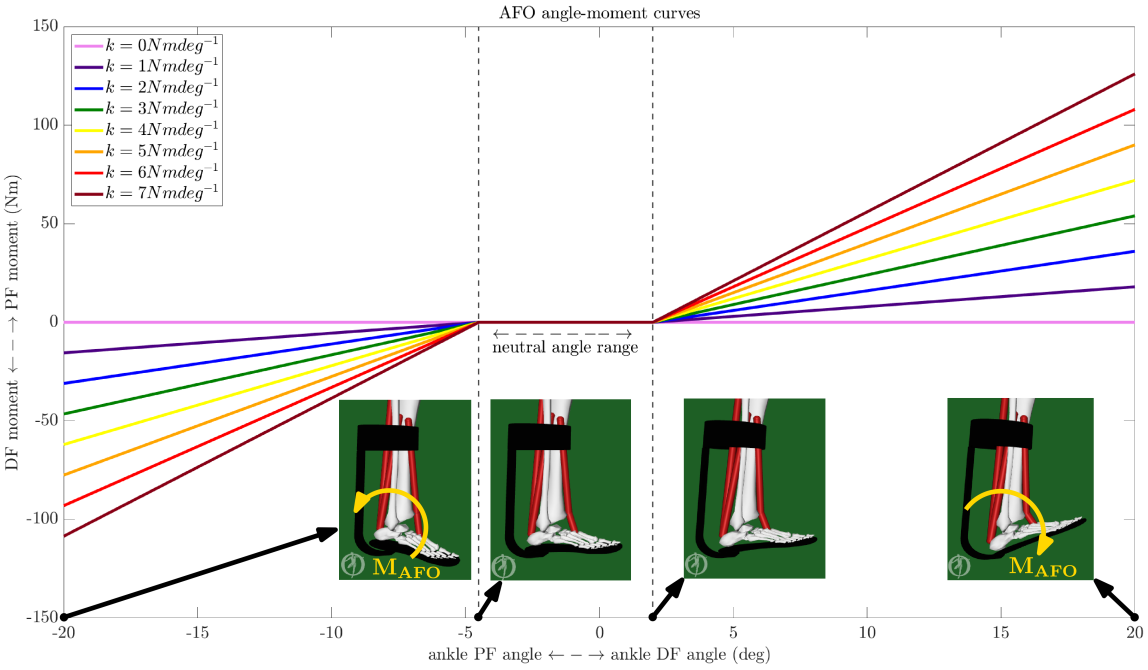

Figure 2.3: AFO moment - angle curves by the stiffnesses that were used in the forward simulations (PF - plantarflexion, DF - dorsiflexion

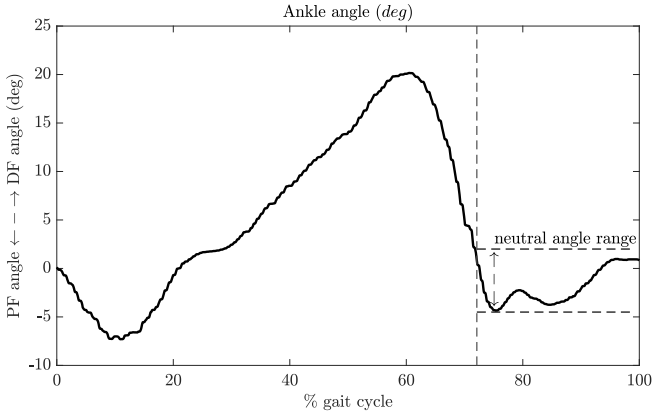

Figure 2.4: Experimental right ankle angle curve, showing the neutral angle range in swing

2.2. Simulation methods

A patient model wearing an AFO was designed and scaled according to experimental marker data of one of subjects from the study of Waterval et al. [88]. This model was used during inverse simulations to process the provided experimental data [88], and during the predictive forward simulations as well. This subject was chosen from the bilaterally affected patients based on the quality of the marker and metabolic CoT data recordings. The baseline characteristics of this subject can be seen in Table 2.1.

Table 2.1: Baseline characteristics of the patient whose data was used for the scaling of the used musculoskeletal model

Age	$38\,\mathrm{years}$
Sex	Male
Height	$177\,\mathrm{cm}$
Weight	$81\,\mathrm{kg}$
Unilateral/bilateral affected	Bilateral
MRC plantar flexion of legs	4 (both sides)
Diagnosis	Myotonic dystrophy

2.2.1. Inverse simulation

The experimental protocol for data recording can be found in [88]. A trial without AFO and a trial with one AFO stiffness was used during the inverse simulation. Three additional degrees of freedom were added to the above described model before scaling so that the model markers can follow the experimental markers better and the marker error evaluation is more accurate. These degrees of freedom were: horizontal pelvis translation in the frontal plane, hip adduction/abduction and hip internal/external rotation.

Scaling and Inverse Kinematics

Each body segments' size and mass was matched to the experimental data using the *Scaling Tool* in *OpenSim*. The marker errors were checked using the *Inverse Kinematics Tool*. During inverse kinematics analysis the joint angles and body translations, allowed by the degrees of freedom of the model, are calculated. This is done by solving a least-squares problem to minimize the difference between the model- and experimental marker positions.

First, the model was scaled without AFO and checked against video recordings of the subject. Secondly, the same scaling ratios were used for the model with AFO since it was the same subject. Then, the marker placements were slightly adjusted to reduce marker errors.

The steps of the scaling process used on the model without AFO:

1. The markers on the unscaled model were placed by hand according to the video recordings and anatomical marker placement definitions.

2. The unscaled model was scaled to match the height of the subject.

3. According to marker errors during static trial, the marker placements were modified by hand on the unscaled model. This model was scaled using this new markerset without the markers on the shoulders (*model-scaled-1*).

4. According to marker errors during static trial, the marker placements were modified by hand on the *model-scaled-1*. This model was scaled using this new markerset without the markers on the shoulder (*model-scaled-2*).

5. The upper body of *model-scaled-2* was scaled using the markers on the shoulders. If the height of the model did not match the height of the subject, the upper body was rescaled to match that but the location of the shoulder markers with respect to the ground was not changed.

   The upper body was scaled separately because the location of the shoulder markers was the most uncertain since the model did not have arms.

6. The markers on non-bony landmarks were adjusted to match the experimental ones.

During static trials, the marker errors were maximally $2\,\mathrm{cm}$ and their RMSE (root-mean squared error) value was below $1\,\mathrm{cm}$. During walking trials the maximum error was $3.5\,\mathrm{cm}$ with an RMSE below $2\,\mathrm{cm}$. According to the *OpenSim* documentation [54], these are within the recommended limits.

Ground reaction force extrapolation
Only two force plates were used in the data collection [88] which is not sufficient for analysing a whole gait cycle. The ground reaction force data was extrapolated to the length of the marker data, assuming the same force profiles by each step of the same leg. The time intervals of ground contacts were calculated from the foot markers' recordings.

Residual Reduction Algorithm
The purpose of residual reduction algorithm (RRA) is to make the kinematics of the model dynamically more consistent with the ground reaction force data [53]. In order to reach this goal, reserve actuators provide torques at the joints for each degree of freedom, and residual actuators provide forces and torques at the center of mass of the pelvis. The residuals are minimized during RRA by small adjustments to the center of mass of the torso and to the kinematic data. The algorithm also makes suggestions to change the body mass.

RRA actuator optimal forces and kinematics tracking weights were defined for each degree of freedom of the model. The tracking weights and residual optimal forces were tuned until the maximum and RMS errors were below the recommended $2\,\mathrm{cm}$ or $2\,\mathrm{deg}$ values [53], and the residual forces and moments were as low as possible.

Computed Muscle Control
Using the adjusted model after RRA and the extended ground reaction force data, computed muscle control (CMC) algorithm was run to compute the muscle activations which drive the model to track the kinematics from the RRA results. CMC applies reserve actuators to provide moments at the joints for each degree of freedom if the muscles fail to reproduce the desired torques. Additionally, residual forces and moments are applied on the pelvis of the model to make the kinematics and ground reaction forces dynamically consistent, like in RRA [50]. The same kinematics tracking weights were set as during RRA.

The peak isometric strength of the soleus and gastrocnemius muscles was tuned so that the reserve moments at the ankle joint, of the model without and with AFO as well, would be negligible, maximum less than $25\,\mathrm{Nm}$, RMS value less than $10\,\mathrm{Nm}$ [50].

From the results of CMC, the work contributions of the muscles, reserves and residuals can be calculated.

2.2.2. Predictive forward simulation

SCONE (v1.6.0) control and optimization framework [24] was used to compute the effects of using an AFO with non-spastic calf muscle weakness without any experimental data. The muscle activation patterns were computed by a reflex-based gait controller and used to generate the forward simulations. The above described model's equations of motion were defined and integrated using OpenSim, as the plant of the optimization process. The calculated joint- and muscle states of the model were used as a sensory feedback to the gait controller to close the feedback loop. In each loop, an objective function was evaluated based on the forward simulation results, and its outcomes were used in the Covariance Matrix Adaptation Evolutionary Strategy (CMA-ES) optimization method to compute the new controller parameters which are the variables of the optimization problem [49] (Fig. 2.5).

Gait controller
The used reflex-based controller is an implementation of the work of Geyer & Herr [25] in the form of high level states conditioning low-level controls.

The controller encompasses 5 high-level states: early stance (ES), late stance (LS), lift-off (LO), swing (S), and landing (L). 4 of the transitions are defined by 4 thresholds which are variables in the optimization problem. These are: 1) L to ES: normalized leg load on stance foot (ipsilateral) is above a threshold, 2) ES to LS: relative sagittal foot position of the stance foot (ipsilateral) is below a threshold, 3) LO to S: normalized leg load on stance foot (ipsilateral) is below a threshold, 4) S to L: relative sagittal foot position of the stance foot (ipsilateral) is above a threshold. Additionally, LS to LO transition happens when the contralateral leg goes from L to ES.

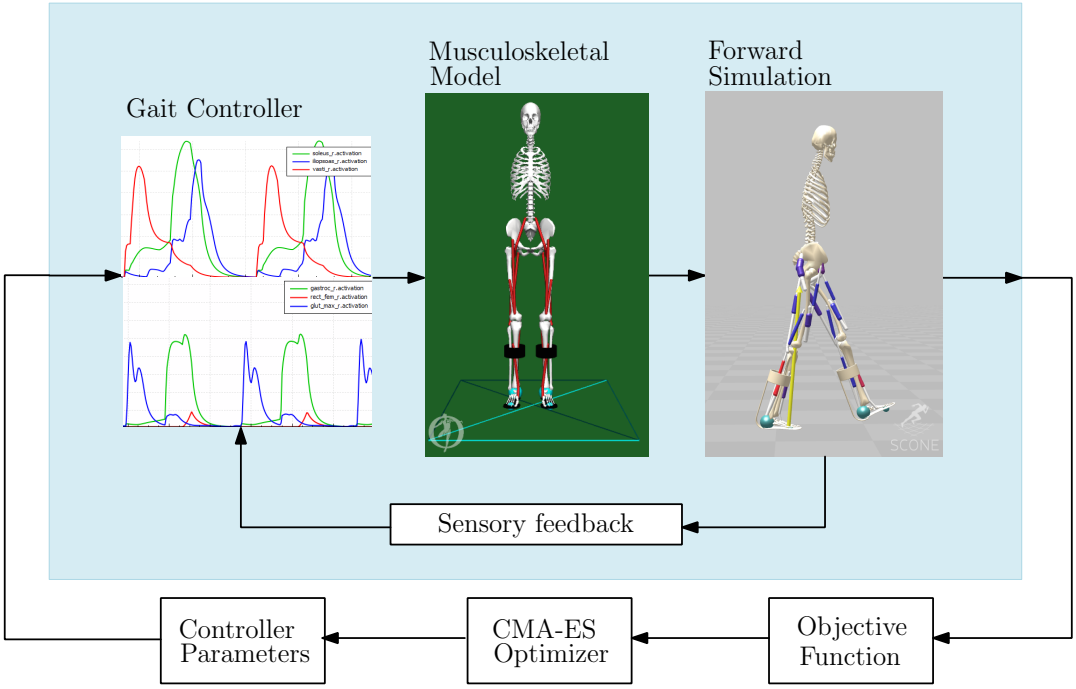

Figure 2.5: Block diagram of the optimization method (adapted from [49])

State / Target	Stance			Swing	
	ES	**LS**	**LO**	**S**	**L**
TA	L+ F-$_{(SOL)}$	L+ F-$_{(SOL)}$	L+ F-$_{(SOL)}$	L+ F-$_{(SOL)}$	L+ F-$_{(SOL)}$
SOL	F+	F+	F+		
GAS	F+	F+	F+		
VAS	F+ cond. *knee*	F+ cond. *knee*			
RF	L+	L+	L+	L+	L+
BFSH				L+	
HAMS	PD+ $_{(pelv.tilt)}$	PD+ $_{(pelv.tilt)}$	PD- $_{(pelv.tilt)}$	F+	F+
ILIO	PD- $_{(pelv.tilt)}$	PD- $_{(pelv.tilt)}$	PD+ $_{(pelv.tilt)}$	L+ PD+ $_{(pelv.tilt)}$ L-$_{(HAM)}$	L+ PD+ $_{(pelv.tilt)}$ L-$_{(HAM)}$
GMAX	PD+ $_{(pelv.tilt)}$	PD+ $_{(pelv.tilt)}$	PD- $_{(pelv.tilt)}$	F+	F+

Figure 2.6: Gait controller with high level states and low level controls (muscle reflex - white, conditional muscle reflex - blue, DoF/PD reflex - green background)

The high-level states define when and which low-level control is active. These low-level controls represent the muscle reflexes. Three type of reflex control laws were used: muscle reflex, conditional muscle reflex and degree of freedom (DoF) reflex (Fig. 2.6).

The inputs for muscle reflexes are force feedback (F), length feedback (L) and/or velocity feedback (V) of the same muscle except for the case when a *source* muscle is defined. The output of the muscle reflex is the muscle excitation (U) of the *target* actuator which is calculated the following way: [69]

$$U = C0 + KF[(F(t - t_{\mathrm{D}}) - F0)]_{+} + KL[(L(t - t_{\mathrm{D}}) - L0)]_{+} + KV[(V(t - t_{\mathrm{D}}) - V0)]_{+} \tag{2.1}$$

where $C0$ is a constant actuation; KF,KL and KV are the force-, length- and velocity feedback gains, based on normalized muscle force ($F/F_{\max}$), normalized contractile element (CE) length (L/L_{opt}) and normalized CE velocity (V/V_{opt}); $F0$,$L0$ and $V0$ are the force-, length- and velocity feedback offsets. These are variables in the optimization problem. $[]_{+}$ indicates that the result is always equal or larger than zero. Additionally, the neuromuscular delay (t_{D}) of each muscle reflex is defined.

Conditional muscle reflexes are muscle reflexes which are only activated when a predefined degree of freedom (DoF) is within a certain range. The name of the DoF and a minimum and/or a maximum position for that DoF are used as additional variables. The minimum and maximum positions are a variables in the optimization problem. [66]

The inputs for DoF reflexes are the position (P) and velocity (V) of a predefined DoF, so it can also be called proportional-derivative (PD) control. The predefined DoF is the *source*, and the *target*'s muscle excitation is the output which is calculated the following way: [67]

$$U = C0 + KP[(P(t - t_{\mathrm{D}}) - P0)]_{+} + KV[(V(t - t_{\mathrm{D}}) - V0)]_{+} \tag{2.2}$$

where $C0$ is a constant actuation; KP and KV are the position- and velocity feedback gains; $P0$ and $V0$ are the target position and -velocity for the *source*. $[]_{+}$ indicates that the result is always equal or larger than zero. Additionally, the neuromuscular delay(t_{D}) of each DoF reflex is defined.

Objective function

An objective function (J) was defined to evaluate the goodness of the current control parameter set in each iteration of the simulation. J comprises of the desired high-level tasks during gait of patients wearing an AFO, represented by the following measures, which were minimized during the optimization process.

$$J = w_{\mathrm{Gait}} \cdot J_{\mathrm{Gait}} + w_{\mathrm{Effort}} \cdot J_{\mathrm{Effort}} + w_{\mathrm{MuscleActLim}} \cdot J_{\mathrm{MuscleActLim}} + w_{\mathrm{DOFLim}} \cdot J_{\mathrm{DOFLim}} + w_{\mathrm{GRFJerk}} \cdot J_{\mathrm{GRFJerk}} + w_{\mathrm{HeadAcc}} \cdot J_{\mathrm{HeadAcc}} \tag{2.3}$$

w_{a} represents the weight associated to a high-level task J_{a}.

In the gait measure, J_{Gait}, the minimum velocity was defined as $1.22\,\mathrm{m/s}$ with 0.01 threshold, without maximum speed setting, to keep the model walking during the forward simulation with a similar speed as the subject walked during the experiments with AFO. In the experimental data, taking all AFO stiffness settings into account, the subject's overall minimum velocity was $1.216\,\mathrm{m/s}$ [88]. Since walking speed and leg length are related [3][37], using one of the scaled subject models meant that the corresponding minimal walking velocity should be set.

Additionally, a relative termination height of 0.85 was set in the gait measure which was used to detect the fall of the model. The simulation was terminated when the current center of mass height was below the initial center of mass height times the defined relative termination height [68].

In the effort measure, J_{Effort}, the total CoT was defined to be minimized. The calculation method was based on the work of Uchida et al.[80] and Umberger et al.[81]. There is no consensus in literature what cost function humans are using to minimize their energy expenditure during walking. Application of total CoT, sum of squared muscle activations or a combination of both cost functions can be found in previous papers [71][22].

In this work, no measure for minimizing the sum of squared muscle activations was used in the final optimizations because initial trials showed that the minimization of both measures combined leads to divergent results. Our goal was to find the gait pattern by each AFO stiffness setting which has the lowest total CoT, so the objective has to represent that to drive the optimization in this direction.

Table 2.2: Weights of the used measures in the objective function

Measure	Weight
J_{Gait}	10^9
J_{Effort}	1.5
$J_{\text{MuscleActLim}}$	1000
J_{DOFLim}	0.10 for ankle 0.01 for knee
J_{GRFJerk}	0.05
J_{HeadAcc}	0.1

However, as a substitute, an additional 50% maximum activation limit ($J_{\text{MuscleActLim}}$) was introduced for the soleus and gastrocnemius muscles because they were activated maximally for $10-20\%$ of the gait cycle in the initial trials without this limit. This is unrealistic because by maximum activation the muscles would fatigue immediately [8][60] but by 50% maximum activation the muscles may be able to work without substantial fatigue and damage. No other muscles were maximally activated during the gait cycle in the simulations, so no maximum limit was introduced for their activation level.

To penalize out-of-range ankle- and knee motion, J_{DOFLim} measure was used. Penalty was added when the ankle angle was outside of the $[-60, 60]$ deg range or when the absolute coordinate limit force acting on the knee joint was larger than $5\,\text{Nm}$.

The objective function contains the term J_{GRFJerk} to minimize the impact stress on the legs. This measure minimizes the sum of ground reaction force derivatives for both legs in both sagittal plane directions, normalized by the travelled distance.

To stabilize the head during gait, excessive head accelerations were penalized [14][61]. J_{HeadAcc} measure minimizes the sum of head accelerations in both sagittal plane directions, normalized by the travelled distance.

The weights were chosen based on previous studies [86] and trial and error (Tab. 2.2). The largest weights were associated to the minimization of the gait measure and the maximum activation limit measure on the calf muscles, so their contribution to the final optimization scores was negligible. From the remaining measures, the effort measure had the largest weight and it contributed about 90% of the final optimization scores.

Optimizer algorithm

Covariance Matrix Adaptation Evolution Strategy (CMA-ES) [27] was used to optimize the control parameters which already proved to be successful for similar optimization problems [49]. This is a stochastic method for real-parameter optimization of non-linear and non-convex problems.

The algorithm calculates a new set of variable values according to the result of the objective function evaluation in each iteration, called generation, by taking only a sample of the variable space, called population size (λ). The mean (m), covariance matrix (C) and the step size (σ) is updated in each generation. Updating the step size in each iteration prevents premature convergence but it does not ensure that the optimization will find the global optimum [27].

The dimension (n) of the problem is the number of optimization parameters which was 100 in our optimization. This contains 7 parameters for the initial state, defining the joint position offsets, 4 parameters for the gait phase transition thresholds and 89 for the variables of the gait controller.

The population size was set to its recommended value, calculated according to [27]:

$$\lambda = 4 + \text{floor}(3 \cdot \ln(n)) = 17 \tag{2.4}$$

Initialization

To initialize an optimization in *SCONE* the simulation objective, the random seed, the minimum progress value, the init file and the initial step size (standard deviation for the parameter values) has to be defined.

The simulation objective contains the model-, controller- and measure file, and the length of the simulation. The length of the simulation was set to $10\,\text{s}$. The random seed, which determined the randomness of the optimization, was set to default. Since 5 optimizations were run in parallel in each round, the random seed values were $1-5$.

The minimum progress value defines the minimum improvement in optimization score, below which the optimization will be terminated. This was set to 0.0001 in all optimizations.

The init file defines the initial optimization parameter values. The final init file and optimization strategy was chosen after multiple trials.

As a base, the same init file, named *ORG*, was used as in previous studies [86] who selected this init file based on trial and error, and used it successfully in gait optimizations for healthy- and patient (non-spastic calf muscle weakness) models.

Firstly, this *ORG* init file was used in optimizations with a patient model wearing an AFO with $2.8\,\mathrm{Nm/deg}$ stiffness. The comparison of these results to experimental kinematics with the same stiffness setting contributed to the fine-tuning of the used objective function terms and their weight factors, to setting the initial step size and to finding the right number of optimizations to run in parallel. After similar kinematic outcomes were reached in the optimizations as in the experimental data, these new optimized parameter values were used as the *NEW* init file. The practice of using the best results of previous optimizations as the new init file for further optimizations with different objectives was also seen in [49] who used the same type of optimizer algorithm. The *NEW* init file was used in simulations with patient models wearing an AFO with different stiffness settings, and further optimizations were done with the best results as new init files. Additionally, the AFO stiffness was added to the control variables to be optimized but the optimization seemed to be more prone to get stuck in local minimums. The trends of the outcomes were highly dependent on the init file, the results were inconclusive because of this bias.

Instead, the same *ORG* init file was used in optimizations with a patient model wearing AFOs with 8 different stiffness values (0, 1, 2, 3, 4, 5, 6 and $7\,\mathrm{Nm/deg}$) and with a patient and healthy subject model not wearing an AFO. The initial step size (σ), also called standard deviation of the parameters, was set to 0.05, according to trial and error iterations where the goal was to provide a large enough initial standard deviation so that the optimization can explore the variable space, but not too large to avoid unnecessarily slow convergence.

To check the robustness of our results, multiple optimizations were run in a chain with two distinctive init files for their first round. 5 parallel optimization instances with different random seeds were run in each round, with each model that were mentioned above. Running chains of optimizations was already successfully implemented in the study of Song et al.[77] and Ong et al.[48] who used the same type of optimizer algorithm. This means that the best results of an optimization were used to initialize the next optimization with the same model (same AFO stiffness setting) and the same initial step size. Since the trend of the results was not changing qualitatively between the first and second round of optimizations (see Appendix D), only two rounds of optimizations were done in a chain. Firstly, the above mentioned *ORG* init file parameters were used to initialize the first round of simulation in one of the chains. Secondly, the first round of the other chain was initialized by the *Patient* init file. This *Patient* parameter value file was the result after two rounds of optimizations using the patient model without AFO, where the first round was initialized by the *ORG* init file.

In the first round of optimizations using the *ORG* init file, one additional optimization parameter was calculated, the initial offset value of the dissipated energy as one of the state variables. The effect of this additional parameter is negligible on the outcomes of the simulation but it is important to take note of it so that the optimization results can be reproduced.

The results of the second round of the *ORG* init file chain will be presented and analyzed in the next sections of this study.

Data reduction to one gait cycle

As mentioned above, the length of a simulation was set to $10\,\mathrm{s}$, so the resulting data had to be averaged to one gait cycle for evaluation.

First, the whole simulation was divided into right gait cycles, starting with the initial contact of the right leg. Next, the simulation was also divided into left gait cycles, starting with the initial contact of the left leg. The gait cycles were normalized by time. Since there was larger variability in the first two gait cycles during the simulation, those were not taken into account. From the rest of the gait cycles the mean of the ipsilateral leg's data was calculated, the right leg's data from the right gait cycles and the left leg's data from the left gait cycles. Finally, these two mean data sets were averaged. This data set was used for all analyses.

2.2.3. Gait phases

For data analysis purposes, the gait cycle was divided into gait phases according to the definitions of Whittle [89] (Fig. 2.7.). The limits of the gait phases were defined according to the changes in the ground reaction force curve (Fig. 2.7.). Loading response (LR) starts with the initial contact of the ipsilateral leg and ends with the toe-off of the contralateral leg where the midstance (MS) begins. MS ends and terminal stance (TS) begins at heel-off of the ipsilateral leg which inflicts the second peak of the ground reaction force. TS ends and pre-swing (PS) begins with the initial contact of the contralateral leg. PS ends and swing (SW) begins at toe-off of the ipsilateral leg. TS and PS together defines the push-off (PO) phase of the ipsilateral leg.

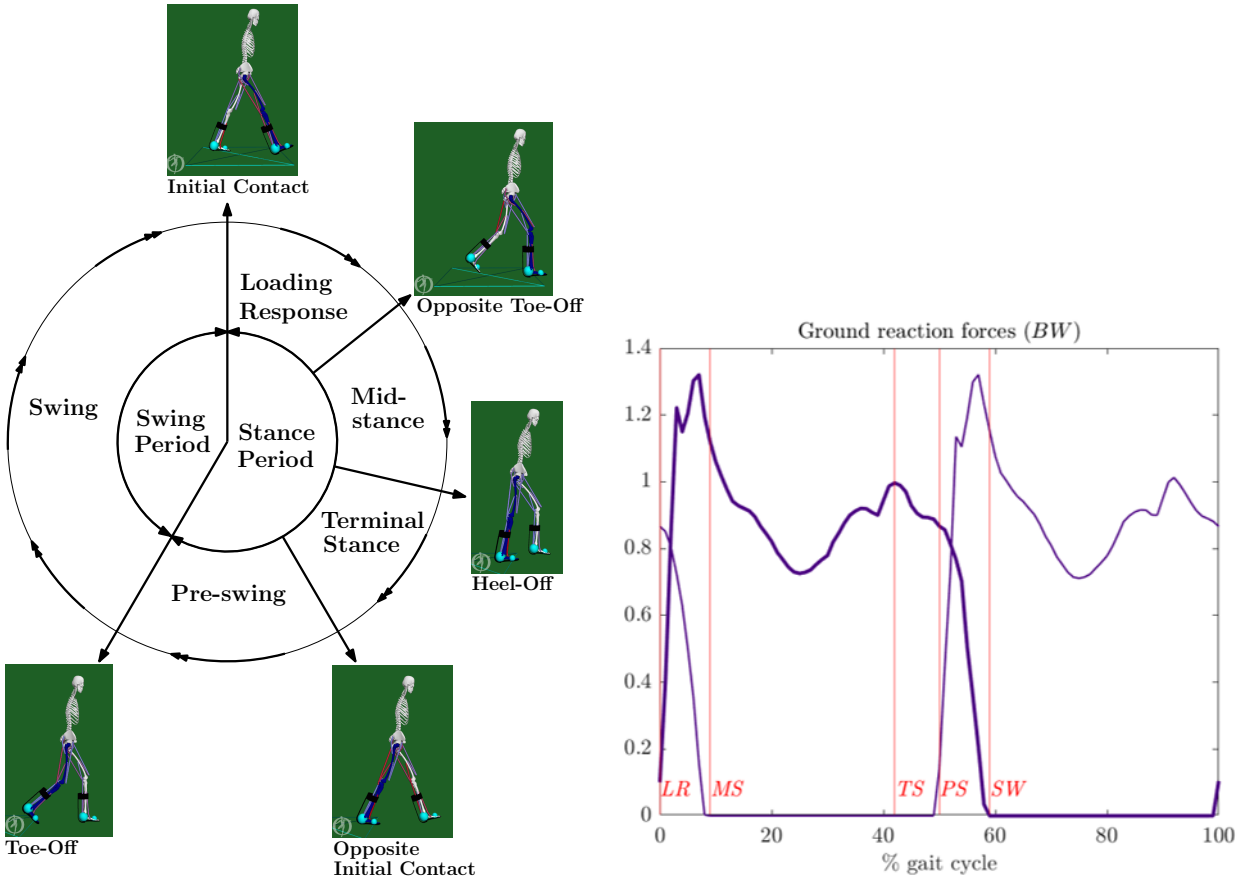

Figure 2.7: Whittle's gait cycle adapted from [89] (left), example of the gait phase limits according to the ground reaction force data (right)

2.2.4. Power and work calculation

The inverse and forward simulation results were further processed by the Analysis Tool in *OpenSim*. It calculated the joint moments, muscle-, reserve- and residual actuator powers from the CMC results of the inverse simulation, and it calculated the joint moments from the forward simulation results exported from *SCONE*. The joint powers were calculated using the following formula:

$$P_{\mathrm{j}} = M_{\mathrm{j}} \cdot \omega_{\mathrm{j}} \tag{2.5}$$

where M_{j} is the internal joint moment exported by the Analysis Tool, ω_{j} is the same joint's angular velocity calculated during the simulations, and P_{j} is the same joint's power. Positive P_{j} means that power is generated at the joint, negative P_{j} means that power is absorbed from the system at the joint.

Joint work was calculated using the trapezoidal numerical integration of joint power. To calculate the cumulative work curves during the whole gait cycle, the $cumtrapz$ function was used in *MATLAB® R2020b* (MathWorks Inc.) [39].

2.3. Data analysis methods

2.3.1. Data normalization

Joint moment, power and work outcomes were normalized by body mass. The ground reaction force data was normalized by body weight (BW). The metabolic energy cost was normalized by body mass, mean walking speed and simulation duration to get the total metabolic CoT over a gait cycle in $\mathrm{J/(kgm)}$.

2.3.2. Trend comparison methods

The comparison between simulation- and experimental result trends was based on the quadratic or linear models fitted to the data. The fitting was done in *MATLAB® R2020b* (MathWorks Inc.), using the polyfit function [40]. Quadratic curves were fitted to the metabolic CoT data points across stiffnesses as in the study of Collins et al. [15]. The similarity of quadratic trends was evaluated by comparing their minimum value and the corresponding optimal stiffness values. Lines were fitted to the kinetic and kinematic data points across stiffnesses as in the work of Waterval et al.[88]. The similarity of the trends was evaluated by the difference between the simulation slope and experimental slope.

The slope of the experimental group results was calculated as the mean of the slopes of the lines fitted individually to all 37 patients' results from the study of Waterval et al.[88]. In simulation results, line was fitted only to nonzero stiffness values (from 1 to $7\,\mathrm{Nm/deg}$) in ankle moment and power data series because at zero stiffness, AFO moment and power is zero which creates an outlier in these trends.

The goodness of fit of the models was assessed by their coefficient of determination value (R^2), calculated in *MATLAB® R2020b* (MathWorks Inc.) [90]. This value shows whether the fitted model is a good representation by explaining the variability in the data. The goodness of fit value for the experimental group results was calculated as the mean of the coefficient of determination values of the fitted models to the 37 patients' results.

Additionally, the mean and standard deviation of the slopes of the individual linear fits of all 37 subjects from the work of Waterval et al. [88] was calculated and the slope difference between this mean and the simulation was expressed as multiple of the standard deviation.

2.3.3. The compared outcomes

Kinetic, kinematic and metabolic CoT outcomes of the simulation were compared with the experimental group results from the study of Waterval et al. [88], and they were also compared with the same patient's results that was used for scaling and minimum walking speed setting in the simulation.

In the case of data comparison between simulation and experimental group results, the mean AFO stiffness values and mean outcome values of the affected leg(s) of all 37 subjects was used in the comparison of kinetic and kinematic outcomes. In the case of metabolic CoT comparison, the mean outcome values of only the bilaterally affected patients were used since the energy consumption of the unilateral patients are affected differently and asymmetrically.

In the work of Waterval et al. [88], all patients had an individual optimal stiffness, so their metabolic energy consumption was affected by AFO stiffness on an individual level. However, four clinically important gait features were identified for the whole patient group based on the expected effects of AFO use on the ankle- and knee joints:

1. peak ankle dorsiflexion angle
2. peak total ankle power
3. peak knee extension angle
4. peak internal knee flexion moment

These were tested and showed significantly changing trends with AFO stiffness in the study of Waterval et al. [88]. Therefore, these are the main outcomes that should be predicted by the simulation.

Furthermore, linear models were fitted to some additional simulation outcomes to better understand the changes in the main gait features:

1. peak biological and AFO provided ankle joint moments
2. peak biological and AFO provided ankle joint powers
3. peak knee flexion angle in stance

To investigate if the underlying mechanism affecting the metabolic CoT is the same in the simulation as in experimental results, the simulation was compared to the experimental individual- and group results as well, on all the above listed outcomes.

The final goal of creating these type of simulations is to find the individual optimal AFO stiffness for each patient, so the effect of individualization by only scaling and minimum speed matching delivers useful information for future research. Evidence was found by healthy subjects that a relationship exists between body mass and knee angle [30], and between gait speed and joint moments [26], so the question is how much the individualization of the patient model helps the simulation reach even more similar kinematic and kinetic trends to the individual experimental ones than to experimental group results.

2.3.4. Evaluating the reliability of the optimizations

The reliability of the optimization results was assessed based on the standard deviation of the metabolic CoT data from the optimization instances with different random seeds at the same stiffness. This standard deviation of the first and second round of optimizations from the above defined *ORG* init file chain were compared. Furthermore, the trend change in metabolic CoT data between first and second round optimizations were compared as well.

3

Results

3.1. Inverse simulation results

During the residual reduction step (RRA), the residual forces could not be reduced to an insignificant level. Therefore, after computed muscle control (CMC) analysis the residual forces were large and their contribution to the total work was comparable to the AFOs' contribution (Fig. 3.1.). This means that the experimental GRF data is inconsistent with the model kinematics, its use would lead to unreliable results and conclusions. Therefore, only the experimental kinematic data and the trends of the experimental kinetic data by varying AFO stiffness can be used for the validation of the forward simulations.

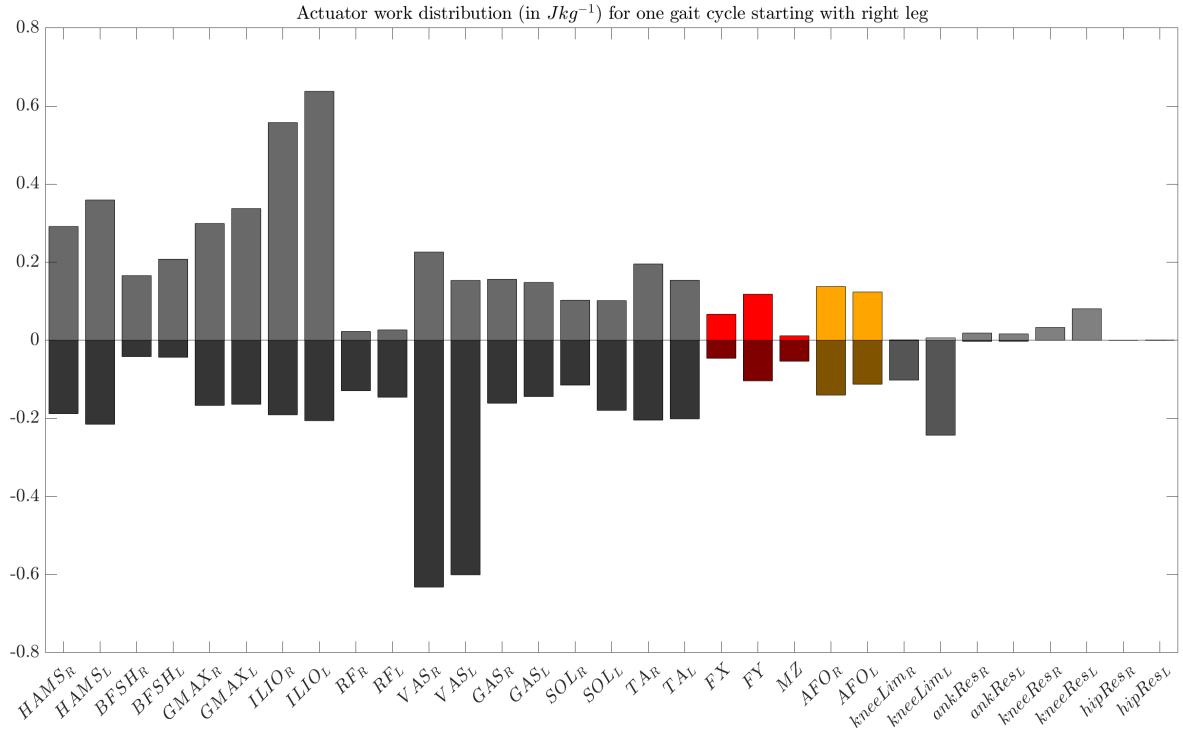

Figure 3.1: The contributions of the model actuators to the total work during one gait cycle; from left to right: muscle work (dark grey), work of the residual forces and moment: *FX, FY, MZ* (red), AFO work (orange), work of the knee limit force: *kneeLim* (grey), work of reserve moments acting on the ankle-, knee- and hip joints (grey); *R* and *L* in underscores indicate right and left legs

3.2. Predictive forward simulation results

The simulated joint angle, -moment and -power curves are comparable to normal reference data [85]. The largest differences to normal curves can be seen in the knee- and hip joint moment curves (Fig. 3.2).

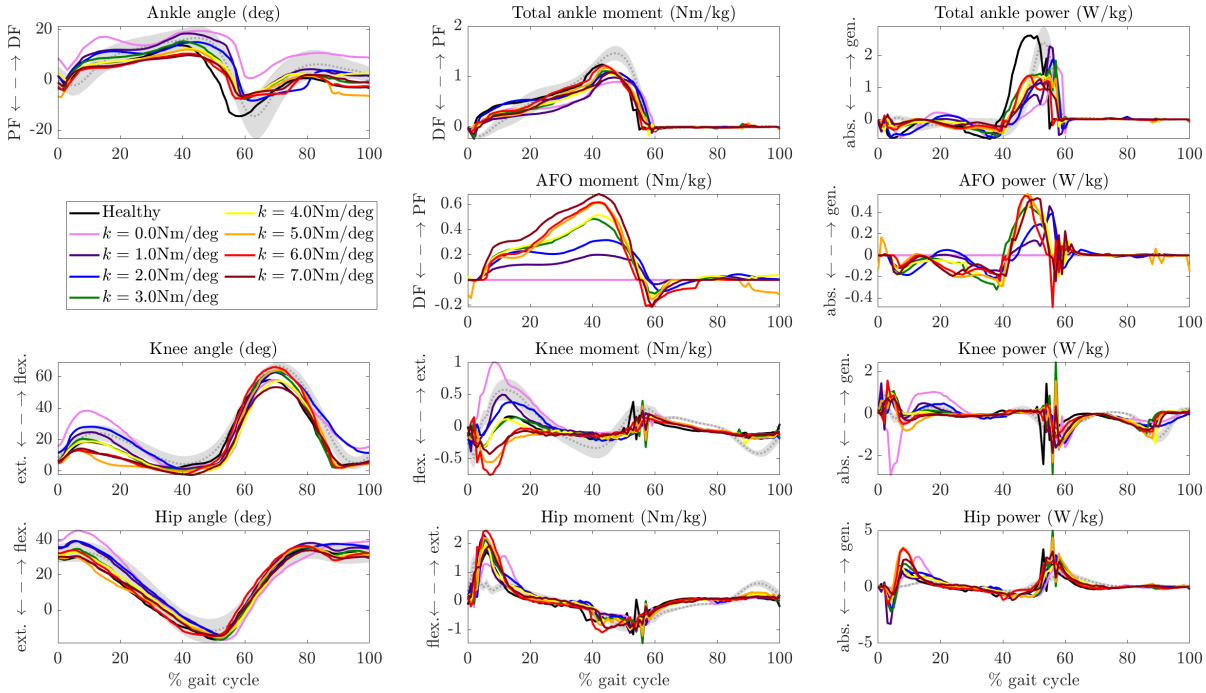

Figure 3.2: Ankle, AFO, knee and hip angles, (internal) moments and powers in the forward simulations with the same model with healthy calf muscle settings and with non-spastic calf muscle weakness settings wearing an AFO with stiffnesses $0-7\,\mathrm{Nm/deg}$. Gray curves and shading is normal data ± 1 SD [85].

3.2.1. Metabolic cost of transport trend comparison

Total metabolic CoT shows quadratic trend in simulation with $R^2 > 0.8$, similarly to the individual experimental data. The predicted optimal stiffness is less than $1\,\mathrm{Nm/deg}$ apart from the same patient's experimental one. The corresponding minimum metabolic CoT is lower in simulation results by 11.27% than in individual experimental results. Furthermore, the individual experimental trend is more sensitive to stiffness change than the simulation trend (Fig. 3.3., Tab. 3.1.).

Experimental group results, as the average of the patients, did not show a quadratic trend due to the varying individual optimal stiffnesses as the large standard deviation of these results also shows (Fig. 3.3., Tab. 3.1.). Since only the minimum walking velocity was defined in the simulations, it is important to point out that gait speed does not change with AFO stiffness, so it is not an influencing factor on the metabolic CoT trend (Tab. 3.1.).

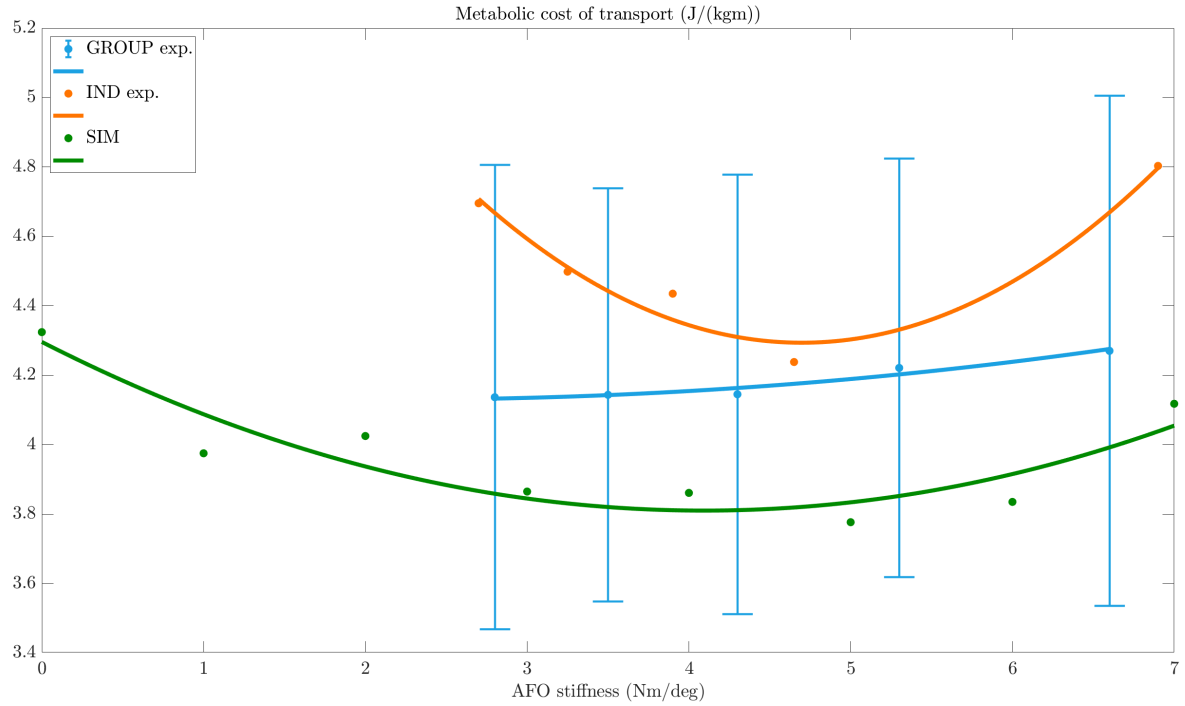

Figure 3.3: Metabolic CoT as AFO stiffness is varied from $0 - 7\,\mathrm{Nm/deg}$. The results of simulation (green), experimental on group level (blue) with ± 1 SD (only bilaterally affected patients results), and experimental of one of the patients (the same as the one who was used for scaling and minimum walking speed matching) (orange) is shown. The best fitting quadratic trends are plotted with the same color as the data.

Table 3.1: Equation, goodness of fit of quadratic curve, minimum of metabolic CoT and optimal stiffness value calculated from the fitted curve; slope and goodness of fit of line to walking speed data across stiffnesses (CoT: metabolic CoT)

	Forward sim.	**Exp. on group level**	**Exp. on individual level**
equation of fitted curve	$0.029x^2 - 0.237x + 4.296$	$-0.007x^2 + 0.033x + 4.166$	$0.104x^2 - 0.976x + 6.586$
R^2	0.835	0.949	0.954
min. CoT (J/(kgm))	**3.812**	**3.500**	**4.296**
optimal stiffness (Nm/deg)	**4.086**	**4.210**	**4.692**
slope – walking speed (m/s per 1 Nm/deg)	0.000	-0.012	-0.002
R^2 **– walking speed**	0.041	0.948	0.057

3.2.2. Comparison of the clinically important gait feature trends

The predicted slopes of the clinically important gait features match well the experimental group slopes (within 1 SD) except the peak internal knee flexion moment slope (Fig. 3.4, Tab. 3.2).

Peak ankle DF angle is decreasing with AFO stiffness in simulation and in experimental results (Fig. 3.4). The slope difference of the fitted lines between simulation and individual experimental results is lower than compared to the group average experimental results (Tab. 3.3). The slope of the line fitted to the simulation results is within 0.5 SD of the mean of all patients' fitted slopes (Tab. 3.2). The linear trends explain more than 95% of the variability in the data series of the simulation and individual experimental results (Tab. 3.3).

Peak total ankle power is decreasing with increasing AFO stiffness in both forward simulation and experimental data on group and individual level (Fig. 3.4 and 3.2). The slope of the line fitted to the simulation results is within 1 SD of the mean of all patients' fitted slopes (Tab. 3.2). However, the simulation result is not a good match to the individual experimental results which is almost insensitive to AFO stiffness change (Fig. 3.4).

Peak knee extension angle shows an increasing trend in simulation and in experimental results as well (Fig. 3.4). The slope of the linear trends fitted to the simulation and experimental group results are not a close match but the simulation's slope is within 1 SD of the mean of all patients' fitted slopes (Tab. 3.2). The simulation's slope fits better the individual experimental result's trend, the slope difference is only $0.107\,^\circ\ \mathrm{per}\ 1\,\mathrm{Nm/deg}$ AFO stiffness change. The fitted linear trends explain more than 70% of the variation in these two data sets (Tab. 3.3).

Peak internal knee flexion moment is increasing in simulation and in experimental group and individual results as well but the simulation does not match the experiments closely, the change is more extreme in the simulation (Tab. 3.3, Fig. 3.4 and 3.2). The line's slope fitted to the simulation is within 2.5 SD of the mean of all patients' fitted slopes (Tab. 3.2).

Additionally, since the standard deviation of the experimental trials of the patient is small, its results are reliable (Fig. 3.4).

Table 3.2: Slope of peak DF angle, peak total ankle power, peak knee extension angle in stance and peak internal knee flexion moment in stance trends as AFO stiffness is varied from $0 - 7\,\mathrm{Nm/deg}$. From left to right: slope of the line fitted to the forward simulation result, mean of the slope of the lines fitted to all 37 patients' results [88], standard deviation (SD) of the slope of the lines fitted to all 37 patients' result [88], difference between the simulation slopes and the mean of the experimental slopes divided by the standard deviation of the experimental slopes

	Sim.	Group exp.	Group exp. SD	Diff. (in SDs)
slope - peak DF angle (deg per 1 Nm/deg)	−1.417	−1.163	0.794	**0.320**
slope - peak total ankle power (W/kg per 1 Nm/deg)	−0.166	−0.107	0.071	**0.832**
slope - peak knee extension angle (deg per 1 Nm/deg)	−0.574	−0.248	0.631	**0.516**
slope - peak internal knee flexion moment (Nm/kg per 1 Nm/deg)	−0.069	−0.012	0.024	**2.378**

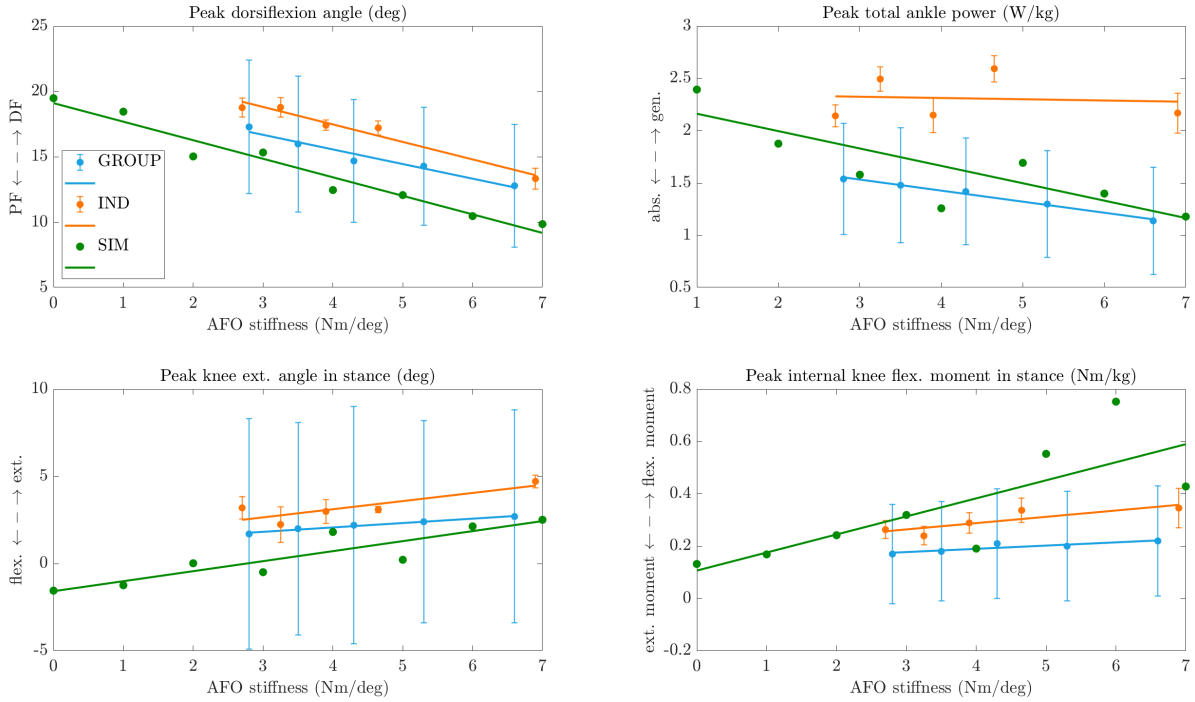

Figure 3.4: Peak dorsiflexion angle, peak total ankle power, peak knee extension angle in stance and peak internal knee flexion moment in stance as AFO stiffness is varied from $0-7\,\mathrm{Nm/deg}$. The results of simulation (SIM - green), experimental on group level (GROUP - blue) with ± 1 SD (all subjects' results), and experimental of one of the patients (the same as the one who was used for scaling and minimum walking speed matching) (IND - orange) ± 1 SD (standard deviation of all trials) is shown. The best fitting linear trends are plotted with the same color as the data. The slope, their relative differences and the linear trends goodness of fit (R^2) value is in Tab. 3.3. The time of the peak internal knee flexion moments in stance varies in the simulation results, it depends on stiffness (see Fig. 3.2.)

Table 3.3: Slope and goodness of fit of line (R^2) to peak DF angle, peak total ankle power, peak knee extension angle in stance and peak internal knee flexion moment in stance trends as AFO stiffness is varied from $0-7\,\mathrm{Nm/deg}$. From left to right: forward simulation result, experimental group result, difference between forward simulation and experimental group result, individual experimental result of the patient that was used for the scaling of the model, difference between forward simulation and individual experimental result

	Sim.	Group exp.	Diff. (sim. vs. group)	Ind. exp.	Diff. (sim. vs. ind.)
slope - peak DF angle (deg per 1 Nm/deg)	−1.417	−1.163	−0.254	−1.336	−0.081
R^2 **- peak DF angle**	0.956	0.689		0.961	
slope – peak total ankle power (W/kg per 1 Nm/deg)	−0.166	−0.107	−0.059	−0.012	−0.154
R^2 **- peak total ankle power**	0.836	0.649		0.008	
slope - peak knee ext. angle (deg per 1 Nm/deg)	0.574	0.248	0.326	0.467	0.107
R^2 **- peak knee ext. angle**	0.817	0.356		0.717	
slope – peak int. knee flex. moment (Nm/kg per 1 Nm/deg)	0.069	0.012	0.057	0.024	0.045
R^2 **– peak int. knee flex. moment**	0.610	0.433		0.735	

3.2.3. Comparison of additional gait feature trends

The trends of peak AFO- and ankle moment and -power of the simulation are matching well the experimental slopes, but the trend of peak knee flexion angle in stance is a worse match (Fig. 3.5 and 3.2). The fitted lines to simulation results are mostly within 1 SD of the slopes of the mean experimental results (Tab. 3.4).

Peak AFO moments show good similarity between the slopes of the fitted lines of simulation and both individual and group experimental results (Tab. 3.5.), and the experimental group result's slope is within 1.1 SD of the experimental group slope. These linear trends explain more than 90% of the variability in the simulation and individual experimental data (Tab. 3.5).

Peak biological ankle moment was decreasing in simulation and experimental result on group level but slightly increasing in individual experimental result with a low goodness of fit for the linear trend (Fig. 3.5). Nonetheless, the slope of the simulation results was within 0.5 SD of the slope of the experimental group results (Tab. 3.4).

The peak AFO power trend of the simulation is not a close match to either experimental results' slope (Tab. 3.5) but the slope of the simulation is within 1 SD of the slope the experimental group results (Tab. 3.4).

The slopes of the lines fitted to the simulation and experimental individual and group results on peak biological ankle power are similarly decreasing by all three data sets with a goodness of fit higher than 0.55 (Tab. 3.5). Furthermore, the slope of the simulation results is within 0.5 SD of the experimental group result's slope (Tab. 3.4).

As a consequence of the similarities and differences between peak AFO moment trends and peak biological ankle moment trends, peak total ankle moment is slightly increasing in all three data sets but their slopes are not matching well, the individual experimental results are increasing more extremely than the other two slopes. Moreover, the slope of the simulation results is within 1 SD of slope of the experimental group results (Tab. 3.4).

Additionally, peak knee flexion angles in stance showed a decreasing trend with AFO stiffness increase in the simulations while they were insensitive to stiffness change in the experiments (Fig. 3.5 and 3.2, Tab. 3.5 and 3.4).

Table 3.4: Slope of peak total ankle moment, peak AFO moment, peak biological ankle moment, peak AFO power, peak biological ankle power, peak knee flexion angle in stance trends as AFO stiffness is varied from $0 - 7\,\mathrm{Nm/deg}$. From left to right: slope of the line fitted to the forward simulation result, mean of the slope of the lines fitted to all 37 patients' results [88], standard deviation (SD) of the slope of the lines fitted to all 37 patients' result [88], difference between the simulation slopes and the mean of the experimental slopes divided by the standard deviation of the experimental slopes

	Sim.	Group exp.	Group exp. SD	Diff. (in SDs)
slope - peak AFO moment (Nm/kg per 1 Nm/deg)	0.078	0.040	0.035	**1.086**
slope - peak biol. ankle moment (Nm/kg per 1 Nm/deg)	−0.047	−0.030	0.040	**0.431**
slope - peak AFO power (W/kg per 1 Nm/deg)	0.025	−0.009	0.054	**0.617**
slope - peak biol. ankle power (W/kg per 1 Nm/deg)	−0.126	−0.095	0.074	**0.427**
slope - peak total ankle moment (Nm/kg per 1 Nm/deg)	0.022	0.001	0.028	**0.746**
slope - peak knee flexion angle in stance (deg per 1 Nm/deg)	−3.252	−0.018	0.469	**6.900**

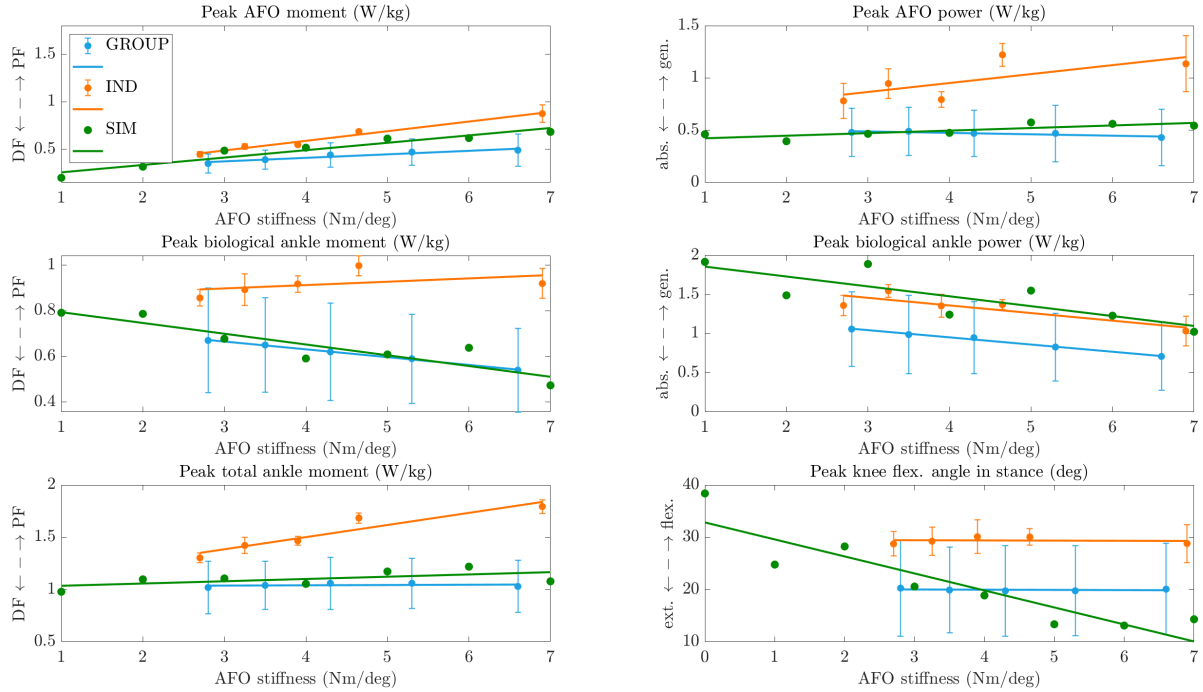

Figure 3.5: Peak AFO moment and power, peak biological ankle moment and power, peak total ankle moment and peak knee flexion angle in stance as AFO stiffness is varied from $0 - 7\,\mathrm{Nm/deg}$. The results of simulation (SIM - green), experimental on group level (GROUP - blue) with ± 1 SD (all subjects' results), and experimental of one of the patients (the same as the one who was used for scaling and minimum walking speed matching) (IND - orange) ± 1 SD (standard deviation of all trials) is shown. The best fitting linear trends are plotted with the same color as the data. The slope, their relative differences and the linear trends goodness of fit (R^2) value is in Tab. 3.5

Table 3.5: Slope and goodness of fit of line (R^2) to peak AFO moment and power, peak biological ankle moment and power, peak total ankle moment and peak knee flexion angle in stance trends as AFO stiffness is varied from $0-7\,\mathrm{Nm/deg}$. From left to right: forward simulation result, experimental group result, difference between forward simulation and experimental group result, individual experimental result of the patient that was used for the scaling of the model, difference between forward simulation and individual experimental result

	Sim.	Group exp.	Diff. (sim. vs. group)	Ind. exp.	Diff. (sim. vs. ind.)
slope - peak AFO moment (Nm/kg per 1 Nm/deg)	0.078	0.040	0.038	0.101	−0.023
R^2 **- peak AFO moment**	0.923	0.620		0.979	
slope - peak biol. ankle moment (Nm/kg per 1 Nm/deg)	−0.047	−0.030	−0.017	0.015	−0.062
R^2 **- peak biol. ankle moment**	0.820	0.415		0.214	
slope – peak AFO power (W/kg per 1 Nm/deg)	0.025	−0.009	0.034	0.086	−0.061
R^2 **- peak AFO power**	0.663	0.433		0.496	
slope – peak biol. ankle power (W/kg per 1 Nm/deg)	−0.126	−0.095	−0.031	−0.097	−0.029
R^2 **- peak biol. ankle power**	0.648	0.563		0.736	
slope – peak total ankle moment (Nm/kg per 1 Nm/deg)	0.022	0.001	0.021	0.116	−0.094
R^2 **– peak total ankle moment**	0.359	0.364		0.898	
slope – peak knee flex. angle in stance (deg per 1 Nm/deg)	−3.252	−0.018	−3.234	−0.036	−3.216
R^2 **– peak knee flex. angle in stance**	0.827	0.272		0.008	

3.2.4. Muscle metabolic consumption trends

The trends of vasti, hamstrings and iliopsoas muscles metabolic energy cost is changing more than $0.01\,\mathrm{J/(kgm)}$ by $1\,\mathrm{Nm/deg}$ AFO stiffness change, so these changes have the largest effects on the total metabolic CoT trend (Fig. 3.6).

The decrease in the metabolic consumption of vasti muscles happens in loading response and midstance, it is the main contributor to the total metabolic CoT trend (Fig. 3.8). Additionally, the metabolic consumption of the hamstrings muscles slightly increases in early stance (Fig. 3.8) and the metabolic consumption of the iliopsoas muscle slightly increases at the end of midstance and in push-off (Fig. 3.10). The metabolic energy cost of the calf muscles, gastrocnemius and soleus, is not changing substantially by AFO stiffness increase (Fig. 3.6).

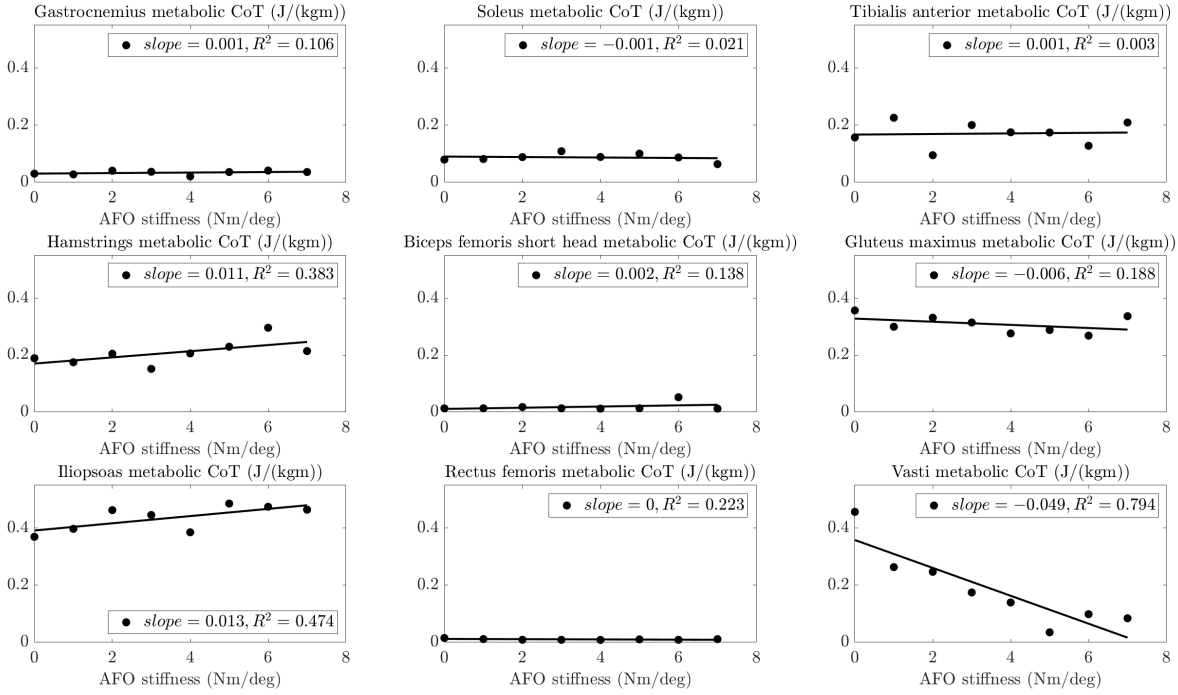

Figure 3.6: Total metabolic energy consumption of all 9 muscles during one whole gait cycle with fitted lines

3.2.5. Joint work trends

Effects on the ankle joint

Negative biological ankle work shows a slightly decreasing trend in loading response as AFO stiffness increases and AFO work has a negligible contribution in loading response by all AFO stiffnesses.

Negative biological ankle joint work decreases and negative AFO work increases with stiffness in midstance, so AFO loading happens instead of biological ankle joint loading. Biological ankle work slightly increases in push-off until the stiffness reaches $3\,\mathrm{Nm/deg}$, by larger stiffnesses biological ankle work generation decreases (Fig. 3.7). That is, larger stiffnesses influence negatively the power generation at the ankle.

As AFO stiffness increases, AFO power generation occurs earlier in the gait cycle. AFO work is larger in terminal stance than in pre-swing by stiffnesses larger than $3\,\mathrm{Nm/deg}$ and biological ankle work is larger in pre-swing than in terminal stance by all stiffness settings (Fig. 3.7).

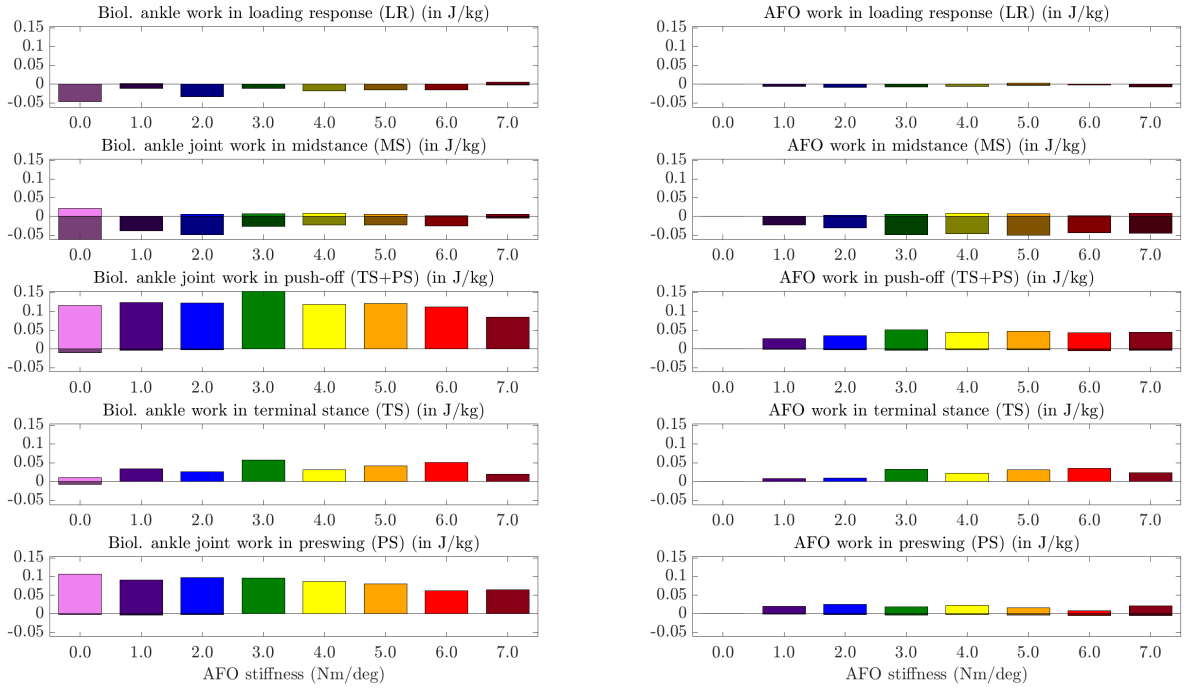

Figure 3.7: AFO and biological ankle joint work contribution in loading response (LR), midstance (MS) and push-off (PO) phase which consists of the terminal stance (TS) phase ending with heel-off of the ipsilateral leg, and pre-swing (PS) phase ending with toe-off of the ipsilateral leg

Effects on the knee joint

The knee flexion moment curve had an extension peak which turned into a flexion peak in stance as stiffness increased which means that external knee extension moment increased (Fig. 3.8). Additionally, peak knee flexion angle in early stance decreased and peak knee extension angle in midstance increased with increasing stiffness.

While positive knee joint work, generated by the vasti muscles, decreases, negative knee joint work, generated by the hamstrings muscles, increases. As AFO stiffness increases, the knee starts to absorb energy instead of generating it (Fig. 3.9).

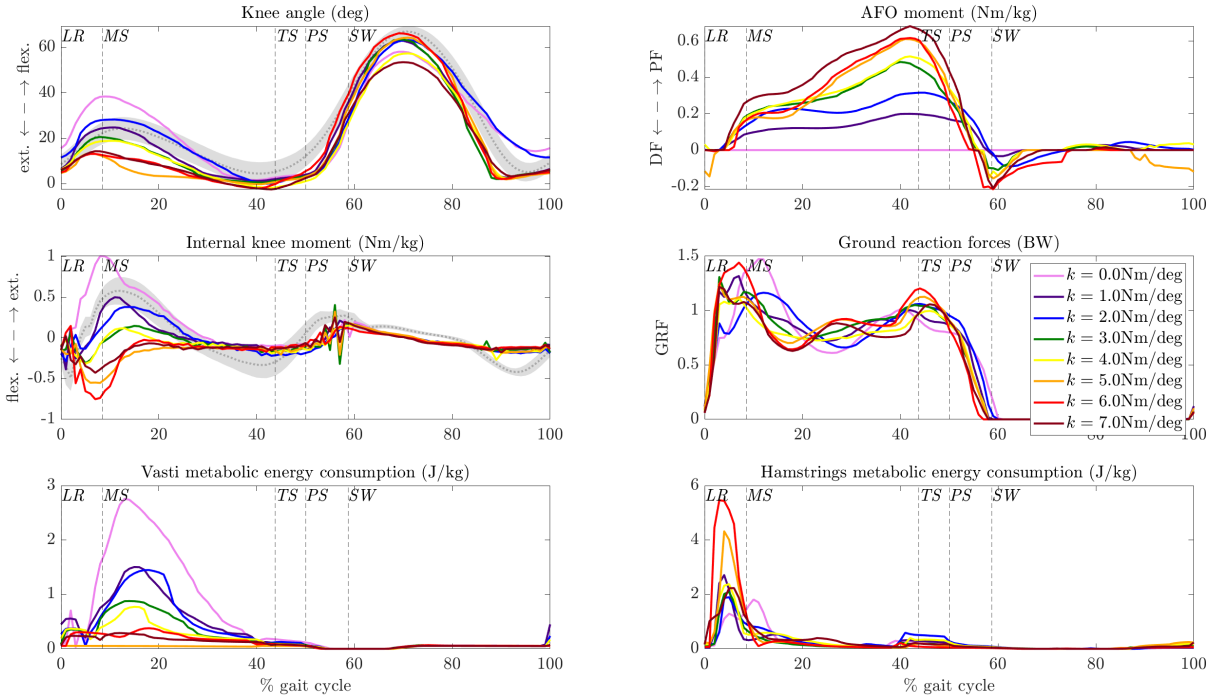

Figure 3.8: Knee joint angle, -moment, GRF, AFO moment, vasti- and hamstrings metabolic energy consumption curves across stiffnesses. Gray curve and shading is normal data ± 1 SD [85].

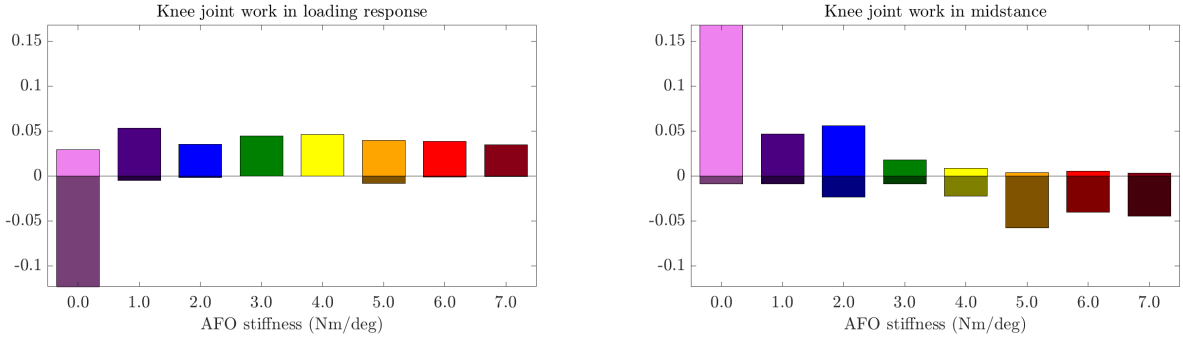

Figure 3.9: Knee joint work in loading response and midstance across stiffnesses

Effects on the hip joint

Negative hip work increases in midstance while sum negative work from midstance and push-off does not increase with increasing AFO stiffness (Fig. 3.10). Positive hip work during pre-swing changes in a similar but not increasing manner to iliopsoas metabolic consumption trend with AFO stiffness change (Fig. 3.6 and 3.10.). Additionally, negative hip joint work is decreasing in loading response and positive hip joint work is increasing in midstance as AFO stiffness increases (Fig. 3.11.). Also, hip extension moment is increased in early stance by higher stiffnesses (Fig. 3.2).

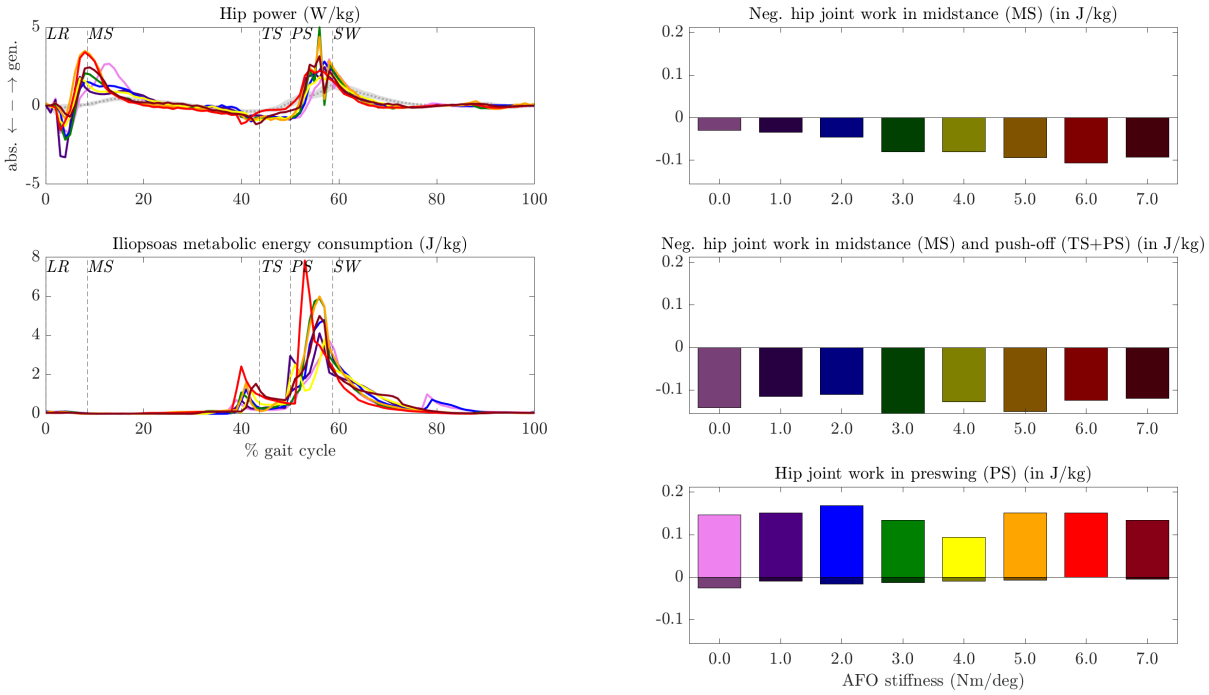

Figure 3.10: Hip joint power curves, iliopsoas metabolic energy consumption curves and hip joint work contribution across stiffnesses in push-off (PO) phase which consists of the terminal stance (TS) phase ending with heel-off of the ipsilateral leg, and pre-swing (PS) phase ending with toe-off of the ipsilateral leg. Gray curve and shading is normal data ± 1 SD [85].

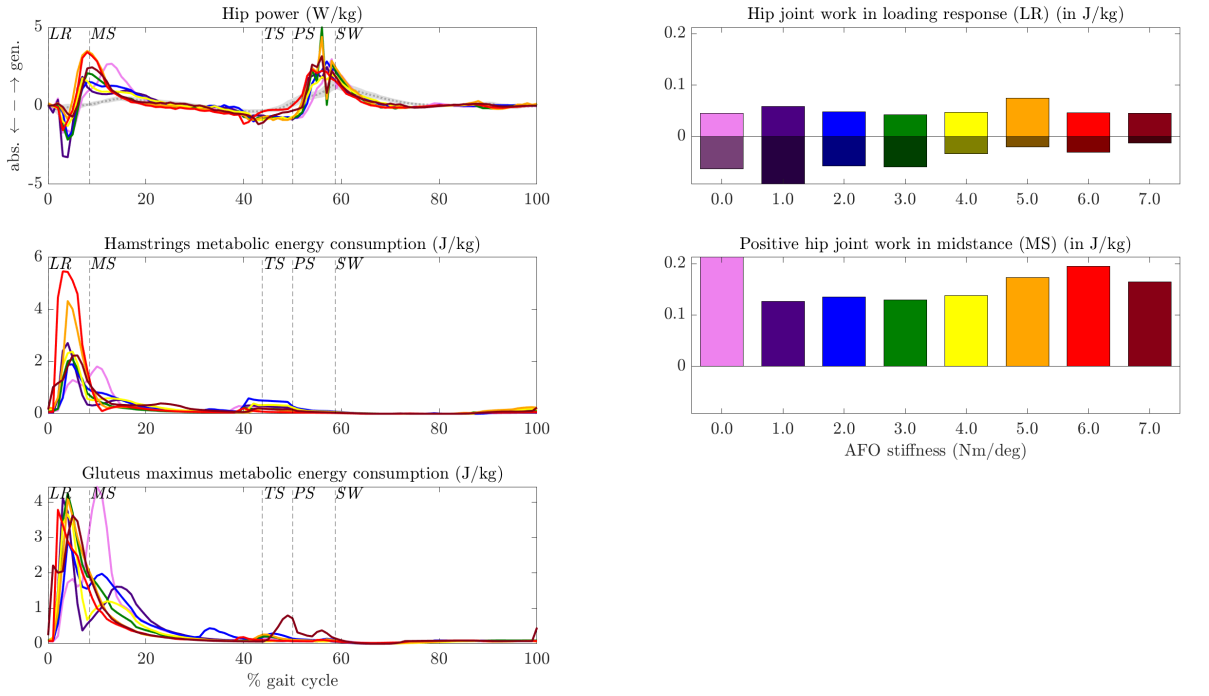

Figure 3.11: Hip joint power curve, hamstrings and gluteus maximus metabolic energy consumption curves, work contribution in loading response and positive hip joint work contribution in midstance across stiffnesses. Gray curve and shading is normal data ± 1 SD [85]

3.2.6. Variability of the optimization results

The mean standard deviation of total CoT, resulting from the same optimization trials but with different random seed values (R1-R5), is halved between the first and the second round of optimizations (Fig. 3.12). The mean standard deviation of the first round is $0.209\,\mathrm{J/(kgm)}$, while in the second round this is only $0.094\,\mathrm{J/(kgm)}$.

Furthermore, the trend of minimum CoT values (Fig. 3.12), the found kinematic, kinetic and individual muscle metabolic cost trends do not change substantially between the two rounds (Appendix D).

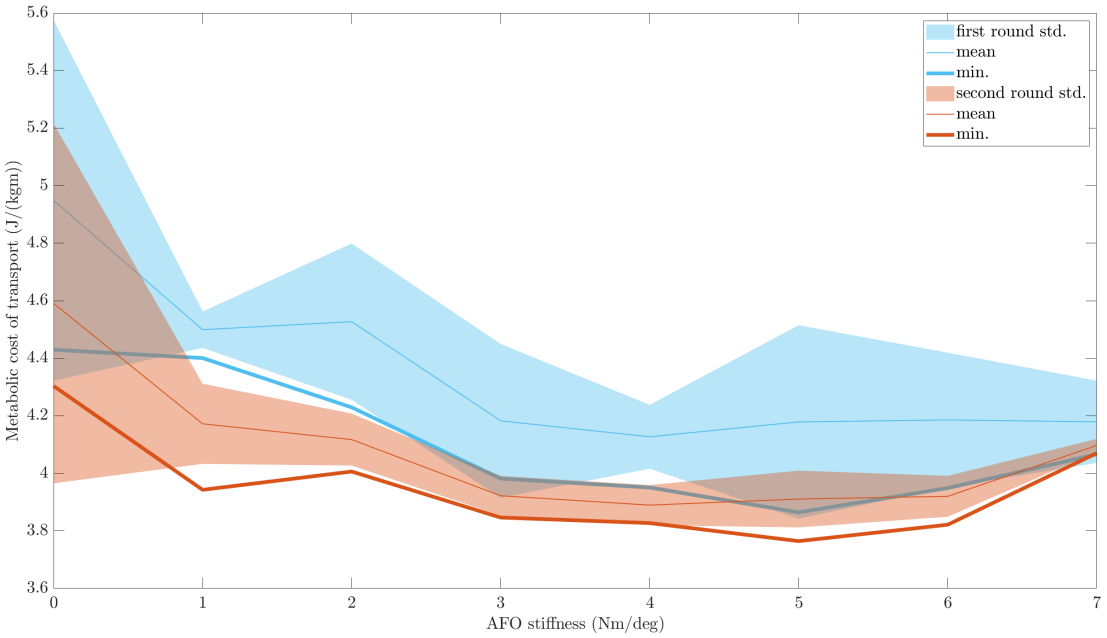

Figure 3.12: Mean (thinner lines), standard deviation (shading) and minimum (thicker lines) of the metabolic CoT values resulting from the same optimization trials but with different random seed values (R1-R5). *ORG* init file chain first (blue) and second (orange) optimization rounds.

4

Discussion

The main aim of this study was to uncover the mechanism relating AFO stiffness to the metabolic CoT as observed in experimental trends from individuals with calf muscle weakness.

To reach this goal, first the results of predictive forward musculoskeletal simulations were compared to experimental trends to evaluate if the AFO affects the simulation in a similar way as in experiments. The simulations predicted the same direction of change in most of the outcomes as the experiments and the metabolic CoT trend was quadratic similarly to the modelled patient's experimental result. According to this evidence, the same mechanism could explain the changes in the experiments as in the simulation.

The reduction in the vasti muscle metabolic cost due to larger external knee extension moments with increasing AFO stiffness was identified as the main contributor to the net metabolic CoT trend. Additionally, a slight increase in the metabolic cost of hamstrings and iliopsoas muscles leads to the increase of net metabolic CoT by higher AFO stiffness values. According to the accuracy of the simulation's predictions, limitations on translating our findings to patient behavior were found, such as the uncertainty of the modelled calf muscle strength, and the relative importance of metabolic cost minimization to other goals during walking.

4.1. Accuracy of the predictions

Total CoT shows quadratic trend in simulation similarly to the individual experimental data and many other measurements on pathological populations [33][20][59]. The predicted optimal stiffness is within $1\,\mathrm{Nm/deg}$ of the patient's experimental optimal stiffness. The simulated metabolic energy cost values were lower by 11.27% which can be explained by the planar model which requires no medio-lateral stabilization that can decrease the total metabolic energy consumption by 10% according to Matsubara et al. [41].

The individual experimental metabolic CoT trend is more sensitive to stiffness change than the simulation trend, possibly due to the inaccuracy of the used objective function for the optimization. The improper weighting of the terms could lead to an incorrect representation of the patient's objectives during gait [49]. It is important to note that even though only a minimum was set in the simulation for the gait speed, it was insensitive to AFO stiffness change, therefore the metabolic CoT trend is not influenced by the effects of varying walking speed.

Bregman et al. [11] also found a minimum in metabolic CoT trend in their predictive forward simulations but our results show greater similarity to experimental observations in the range of metabolic CoT and optimal stiffness value as well. This is probably due to the absence of active muscular system in their model since they used a frictionless planar model with only hip actuation.

Even though the metabolic CoT trends showed a large variation between patients, four outcomes (peak ankle dorsiflexion angle, peak total ankle power, peak knee extension angle and peak knee flexion moment) showed significantly changing trends in the work of Waterval et al. [88] which implies that these changes are occurring by all individuals and should be predicted by the simulation. All four of these outcomes showed changes in the same direction in the simulation as in the measurements by increasing AFO stiffness levels.

Simulation results and both group and individual experimental results showed linearly decreasing peak ankle dorsiflexion angles which is one of the most presented effects of AFO stiffness in literature [10][28][35][6][33][88][59]. The simulations predictions are accurate as the slope differences between simulation and both experimental results can be considered negligible. Peak total ankle power showed decreasing trends in both simulation and experimental group results, with negligible slope difference, but it was almost constant in the individual experimental data as AFO stiffness increased. These decreasing trends were also showed in other studies on patients [59][36]. Similarly, peak AFO and biological ankle moment and -power slopes of the forward simulation are within 1.1 SD of the mean experimental slopes of all patients, thus the simulation results deviation from the experimental group results concerning ankle kinetics can be considered small. Additionally, peak AFO moments and peak biological ankle power showed great similarity between simulation results and individual experimental results. Despite the fact that the simulation did not predict all the individual trends related to the ankle joint kinetics, it predicted the average group trend with high accuracy which implies that the impaired calf muscle property settings of the model could be more similar to the group average than to the chosen individual. This could happen due to inaccuracies in calf muscle property settings of the patient which was set according to an informed guess, as detailed above in Chapter 2.

The knee joint is less flexed at initial contact (Fig. 3.8) as AFO stiffness increases, which results in increased external knee extension moments as the CoP progresses and the GRF action line moves anterior to the knee. Consequently, less internal knee extension moment is required in early stance in the simulation (Fig. 3.8) and peak internal knee flexion moment is increasing in stance which is shown in the simulation and in experimental individual and group results as well but the slopes showed large differences. Evidence from literature also shows similar trends [33][59][36]. The rate of increase was more extreme by the simulation results, its slope was outside of 2 SD of the mean of all patients' slope.

The increasing external knee extension moments result in earlier knee extension (Fig. 3.8) in the simulation as AFO stiffness increases which results in decreased peak knee flexion angles in early stance. This extreme reaction to AFO stiffness did not happen in either experimental result and can be explained by the excessive increase in external extension moment in early stance.

As another consequence of the increased external knee extension moment, peak knee extension angle increased as AFO stiffness increased in the simulation and experimental results as well. This is also a commonly observed outcome in literature [59][33][36]. The slopes of the fitted lines were more similar between simulation and individual experimental results than compared to group experimental outcomes. However, the slope of the simulation results was still within 1 SD of the mean of all patients' slope which means that the deviations between the experimental and simulation trends of peak knee extension angles are small, so the prediction accuracy is high.

The inaccuracies in peak internal knee flexion moment, peak knee flexion angle in early stance and peak knee extension angle predictions could be due to the used objective function for the optimization [49]. The weighting of the terms, such as too high weight on CoT minimization, or lacking terms could drive the optimization into abnormal patterns.

The change in the variability of the metabolic CoT results in the two subsequent rounds of optimizations showed that the results of the second round are more reliable since the mean standard deviation of the metabolic CoT results in the optimizations with different random seeds decreased by 55.024% and the minimal metabolic CoT trend proved to be robust, since the optimal stiffness did not change substantially between the two rounds. Furthermore, the found kinematic, kinetic and individual muscle metabolic cost trends were also similar in the two rounds. Therefore, if more rounds would be optimized, they would not change the found optimal stiffness value and the found underlying mechanism considerably which proves its reliability.

The clinically important gait feature trends that were identified from the experiments changed in the same direction in the simulation results as AFO stiffness increased. The simulation predicted most of the kinetic and kinematic trends with high accuracy. The knee flexion moment trend showed the largest, not negligible difference between simulation and experimental trends which can be explained by the uncertainty of the weighting on the terms in the objective function. According to this evidence, the same mechanism could be responsible for the changes in the metabolic CoT in the experiments as in the simulation.

4.2. Mechanisms explaining the metabolic CoT trend

The main metabolic CoT reducing factors were hypothesized to be connected to the decrease in the energy consumption of the quadriceps muscles as AFO stiffness increased by patients with calf muscle impairments, and the rise of the metabolic CoT was assumed to be due to the decrease in ankle push-off power generation and compensation strategies at the hip joint by excessive AFO stiffness levels [88][13][33][36][59][7]. These hypotheses proved to be true in the simulations.

The lack of effects of the calf muscles' metabolic energy consumption changes in push-off phase on the total metabolic CoT could be explained by the calf muscle weakness of the subjects since the weaker muscles weigh less therefore they consume less metabolic energy. This is in contrast to findings on healthy subjects where the calf muscle function can be partly substituted by the AFO, according to calf muscle activation decrements measured by Collins et al. [15]. Only one study was found that measured lower leg muscle activations of patients with unilateral lower limb salvage and found significant decrease only in gastrocnemius muscle activation and more flexed knee in early stance as stiffness increased [28]. However, their tested stiffness range was small and these results are not directly applicable to our patients with mainly bilateral calf muscle weakness.

The decrease in the metabolic consumption of vasti muscles was found to be the main contributor to the total metabolic CoT trend. The knee flexion moment curve had an extension peak which turned into a flexion moment in stance as stiffness increased which means that external knee extension moment increased (Fig. 3.8). This happens because the increasing AFO moment on the ankle restricts the ankle movement into dorsiflexion so the tibia forward rotation will be limited and the knee can not move forward, thus the knee will be less flexed at initial contact (Fig. 3.8). Then, as the CoP progresses, the GRF action line will be anterior to the knee, inducing knee extension moment which extends the knee even more and earlier. Consequently, less internal knee extension moment is needed to extend the knee in midstance, so less vasti work is needed. Since more extended knee in stance is linked to decreased CoT [84][13], the probable reason why the optimizations were driven to this loading pattern is the relatively high weight on the minimization of CoT in the objective function. Additionally, the decreased hip power absorption and increased hip power generation in early stance supports that the excessive knee extension is exploited at the hip joint too (Fig. 3.11). The biarticular hamstrings muscle acts like a strap which aids in hip extension when the knee extends. Slight increase in hamstrings metabolic energy consumption were shown in early stance (Fig. 3.6), as it counteracts the increasing external extension moment to decelerate knee extension and to facilitate hip extension.

Due to this strategy, the knee will not go into flexion in early stance (Fig. 3.8), so shock absorption will be limited [16]. Landing with a straighter knee leads to increased GRF loading rates (derivative of GRF curve) as AFO stiffness increases (Fig. 4.1). The high loading rates raise the risk of lower limb stress fractures [16][73][94]. The found peak loading rate values are more than twice as high as the loading rate on healthy subjects during walking at $1.3\,\mathrm{m/s}$ in the work of Cook et al. [16], but lower than the loading rate on healthy subjects during running ($\sim 80\,\mathrm{BW/s}$) found by Milner et al. [45].

Additionally, iliopsoas metabolic consumption slightly increases with AFO stiffness at the end of midstance and in push-off but the changes in hip work does not fully explain this increase (Fig. 3.10). The increasing negative work at the end of midstance may be aiding in AFO loading as a compensation strategy, so that hip extension is counteracted earlier before push-off as stiffness increases. Positive hip work during pre-swing (Fig. 3.10) changes in a similar but not increasing manner to iliopsoas metabolic consumption trend which could also be a compensation strategy for the missing ankle work at push-off.

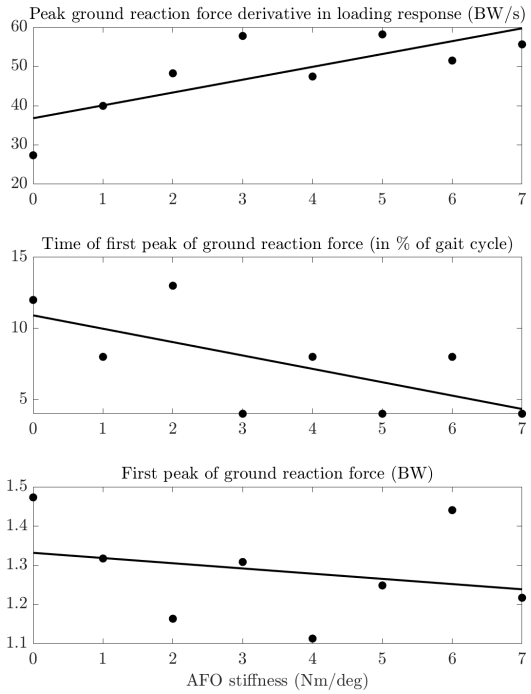

Figure 4.1: Peak loading rate (GRF derivative) in loading response, time of the first peak of GRF, height of the first peak of the GRF across $0 - 7\,\mathrm{Nm/deg}$ stiffnesses

5

Limitations of the study

The aim of our simulations was to represent reality from a point of view that is relevant to answer our research questions. Therefore, certain limitations of the model, the objectives and optimization have to be taken into account when interpreting the results of this study.

A limitation of the used musculoskeletal model is that it is planar, no medio-lateral stabilization is needed in the simulation which could explain why the total metabolic CoT is lower by $\sim 10\%$ [41] in the simulation than in the experiments. By non-optimal AFO settings the out-of-plane compensation, such as trunk motions, could have become more extreme as Meyns et al.[42] found significant increase in trunk rotation range of motion by increasing AFO stiffness. This could justify why the sensitivity of the metabolic CoT trend to AFO stiffness is lower in the simulation than in reality.

Furthermore, the calf muscles could be stronger in the experiments than simulated and their metabolic consumption could change more substantially as AFO stiffness increases which could have a larger impact on the total metabolic CoT trend than seen in the simulations. The calf muscle weakness property of the model was uncertain because it is questionable how the experimentally measured Biodex data relates to percentage weakness as no extensive reference values are available. Another limitation originates from the fact that the AFO neutral angle while wearing a shoe was not measured experimentally on each patient, only an informed guess was made based on inverse simulation results. It was set symmetrically in the forward simulation because a symmetric controller was used, while in inverse simulation the neutral angle range was shown to be asymmetric. These factors could cause inaccuracy in the modelled AFO's neutral angle setting which could cause shifts in all outcome trends according to Kobayashi et al. [36]. This limitation could alter the found optimal stiffness and ankle kinetics.

The objective function represents those goals of human walking which are useful to answer our research questions. To find the most suitable setting, multiple initial trials were done to test the effect of different objective functions. However, other not used factors could be contributing as well or the weights on the terms could be inaccurate since the goals of human gait are individual, especially in pathological population, which makes its fine tuning even more difficult. The largest deviation between the simulation results and the experiments shows by the internal knee flexion moment trends which is the main indicator of the found mechanism. Also, some other factors could have a larger role in modifying the experimental metabolic CoT trend than simulated. One of these factors is, that in reality the loading rate could be more restricted to avoid lower limb stress fractures. To verify the hypothesized effect of the objective function on the simulation outcomes, two rounds of simulation were run with the same optimization settings and same scaled subject but with healthy calf muscle property settings. The knee is flexed in early stance, the kinematics are close to the normal reference data (Fig.3.2) but less knee extension moment is generated than normal (Fig.3.2). Also, the high weight on metabolic cost minimization drives the healthy model into a similar knee extension strategy as it does with a patient wearing an AFO with $3 - 4\,\mathrm{Nm/deg}$ stiffness setting.

Moreover, the minimum walking speed of the simulation was set as measured experimentally and could cause restrictions in the optimization and have an effect on the kinetic and kinematic outcomes [49].

Additionally, the optimization solutions are probably local minima and not global minima since the optimization problem at hand is a non-convex optimization problem and the CMA-ES algorithm is a

stochastic optimizer. To gain confidence in the solutions, multiple optimizations were run in parallel and previous best result was used to initialize next optimizations as in the work of Ong et al.[48] and Song & Geyer [77]. Furthermore, two different initial files were used, and their results were compared after two rounds of optimizations. The resulting kinetic and kinematic trends are similar, they are insensitive to the initial conditions, but the resulting optimal stiffnesses are slightly different (Appendix E).

6

Future work

To address the limitations of the model, more degrees of freedom to allow out-of-plane compensation could be added. The predictions of the forward simulation were especially good fits to individual results except for outcomes directly related to the ankle joint. Also, scaling and minimum speed matching could have already a large effect on reaching similar conclusions to a patient's experimental results but this still needs further investigation with multiple individualized models, more accurate muscle property and neutral angle settings. By introducing asymmetries into the model, and additional limb length and circumference measurements, the models could be even more individualized. Sensitivity analysis could be carried out to evaluate the effect of model properties, such as body weight, muscle weakness and muscle spasticity. A further goal of this research area may be to isolate the effects of neutral angle range of the AFO and optimize it to the individuals as well.

In future objective functions, higher weight on minimizing the loading rate (derivative of GRF) could help in reaching more realistic simulation results. Moreover, the effect of free speed in forward simulation, without lower limit setting should be explored to gain knowledge on how it affects the mechanism found in this study.

7

Conclusion

The main aim of this study was to identify the mechanism relating AFO stiffness to the metabolic CoT as observed in experimental trends from individuals with calf muscle weakness. To reach this goal, first the results of predictive forward musculoskeletal simulations were compared to experimental trends from the study of Waterval et al. [88] to evaluate if the AFO affects the simulation in a similar way as in experiments.

Forward simulations predicted the optimal stiffness within $1\,\mathrm{Nm/deg}$ of the patient's experimental optimal stiffness and the minimal metabolic CoT was $\sim 10\%$ less in simulation than measured which can be explained by the simplifications of the used model. From the trends in peak ankle DF angle, AFO-, biological- and total ankle moment and -power, knee extension and flexion angle in stance, and internal knee flexion moment, only the fitted slope of the peak knee flexion moments was outside 1.1 SD of the mean of the experimental slope of all patients' results. The linear trends fitted to simulation results had even more similar slopes to the individual experimental trend slopes than to the group except for the gait features concerning ankle kinetics, which may indicate a limitation of this study that the calf muscle properties were not set accurately in the model due to the lack of reference data.

Since the metabolic CoT, the kinematic and kinetic trends changed in the same direction in the simulations as in the experiments and most of these trends were well comparable, the mechanism behind the trends of the simulation is relatable to the mechanism behind the trends of the experiments. As AFO stiffness increases, external extension moments on the knee increase which results in earlier knee extension and aids in hip extension. The increasing external knee extension moment allows the internal knee extension moment from the vasti muscles to decrease, thus decreasing the net metabolic CoT. Moreover, a slight increase in hamstrings and iliopsoas metabolic cost contributed to the total metabolic CoT trend. While this is metabolically more efficient according to our simulations, it leads to the absence of shock-absorbing knee flexion in early stance.

Based on the limitations of the simulation, the uncovered mechanism plays a role in reality as well but additional factors may affect it. One of these factors is that the metabolic CoT change of the calf muscles could be larger in reality than simulated, and the other one is that the loading rate in early stance could be more restricted in reality than in the simulation to lower the risk of lower limb stress fractures.

The used model and optimization method helped in identifying parts of the mechanism behind the effects of AFO stiffness on metabolic CoT, and proved to be a good starting point for further simulations aiming at predicting the optimal AFO stiffness for each individual in a pathological population.

Bibliography

[1] FIOR & GENTZ Orthopädietechnik mit System. URL https://www.fior-gentz.de/.

[2] Atefeh Aboutorabi, Mokhtar Arazpour, Monireh Ahmadi Bani, Hassan Saeedi, and John S. Head. Efficacy of ankle foot orthoses types on walking in children with cerebral palsy: A systematic review. *Annals of Physical and Rehabilitation Medicine*, 60(6):393–402, 11 2017. ISSN 18770665. doi: 10.1016/j.rehab.2017.05.004.

[3] R. Alexander McN. Optimization and gaits in the locomotion of vertebrates. *Physiological Reviews*, 69(4):1199–1227, 1989. ISSN 00319333. doi: 10.1152/physrev.1989.69.4.1199.

[4] Frank C. Anderson and Marcus G. Pandy. A dynamic optimization solution for vertical jumping in three dimensions. *Computer Methods in Biomechanics and Biomedical Engineering*, 2(3):201–231, 1999. ISSN 10255842. doi: 10.1080/10255849908907988. URL https://www-tandfonline-com.tudelft.idm.oclc.org/doi/abs/10.1080/10255849908907988.

[5] Frank C Anderson and Marcus G Pandy. Dynamic optimization of human walking. *Journal of Biomechanical Engineering*, 123(5):381–390, 2001. ISSN 01480731. doi: 10.1115/1.1392310.

[6] Elisa S. Arch and Steven J. Stanhope. Passive-Dynamic Ankle–Foot Orthoses Substitute for Ankle Strength While Causing Adaptive Gait Strategies: A Feasibility Study. *Annals of Biomedical Engineering*, 43(2):442–450, 2 2015. ISSN 15739686. doi: 10.1007/s10439-014-1067-8. URL http://www.ncbi.nlm.nih.gov/pubmed/25023660.

[7] Elisa S. Arch, Steven J. Stanhope, and Jill S. Higginson. Passive-dynamic ankle–foot orthosis replicates soleus but not gastrocnemius muscle function during stance in gait: Insights for orthosis prescription. *Prosthetics and Orthotics International*, 40(5):606–616, 10 2016. ISSN 0309-3646. doi: 10.1177/0309364615592693. URL http://journals.sagepub.com/doi/10.1177/0309364615592693.

[8] B. Bigland-Ritchie, E. Cafarelli, and N. K. Vollestad. Fatigue of submaximal static contractions. *Acta Physiologica Scandinavica*, 128(SUPPL. 556):137–148, 1986. ISSN 00016772.

[9] Nicholas B. Bolus, Caitlin N. Teague, Omer T. Inan, and Geza F. Kogler. Instrumented Ankle–Foot Orthosis: Toward a Clinical Assessment Tool for Patient-Specific Optimization of Orthotic Ankle Stiffness. *IEEE/ASME Transactions on Mechatronics*, 22(6):2492–2501, 12 2017. ISSN 1083-4435. doi: 10.1109/TMECH.2017.2761746. URL http://ieeexplore.ieee.org/document/8065054/.

[10] D.J.J Bregman. *The Optimal Ankle Foot*. PhD thesis, VU Amsterdam, 2011.

[11] D.J.J. Bregman, M.M. van der Krogt, V. de Groot, J. Harlaar, M. Wisse, and S.H. Collins. The effect of ankle foot orthosis stiffness on the energy cost of walking: A simulation study. *Clinical Biomechanics*, 26(9):955–961, 11 2011. ISSN 02680033. doi: 10.1016/j.clinbiomech.2011.05.007. URL https://linkinghub.elsevier.com/retrieve/pii/S0268003311001380.

[12] Merel Anne Brehm, Frans Nollet, and Jaap Harlaar. Energy demands of walking in persons with postpoliomyelitis syndrome: Relationship with muscle strength and reproducibility. *Archives of Physical Medicine and Rehabilitation*, 87(1):136–140, 2006. ISSN 00039993. doi: 10.1016/j.apmr.2005.08.123.

[13] Merel Anne Brehm, Jaap Harlaar, and Michael Schwartz. Effect of ankle-foot orthoses on walking efficiency and gait in children with cerebral palsy. *Journal of Rehabilitation Medicine*, 40(7):529–534, 7 2008. ISSN 16501977. doi: 10.2340/16501977-0209.

[14] Blandine Bril and Annick Ledebt. Head coordination as a means to assist sensory integration in learning to walk. *Neuroscience and Biobehavioral Reviews*, 22(4):555–563, mar 1998. ISSN 01497634. doi: 10.1016/S0149-7634(97)00044-4.

[15] Steven H. Collins, M. Bruce Wiggin, and Gregory S. Sawicki. Reducing the energy cost of human walking using an unpowered exoskeleton. *Nature*, 522(7555):212–215, 6 2015. ISSN 0028-0836. doi: 10.1038/nature14288. URL http://www.nature.com/articles/nature14288.

[16] Thomas M Cook, Kevin P Farrell, Iva A. Carey, Joan M. Gibbs, and Gregory E. Wiger. Effects of restricted knee flexion and walking speed on the vertical ground reaction force during gait. *Journal of Orthopaedic and Sports Physical Therapy*, 25(4):236–244, 1997. ISSN 01906011. doi: 10.2519/jospt.1997.25.4.236. URL www.jospt.org.

[17] Charles A. Crabtree and Jill S. Higginson. Modeling neuromuscular effects of ankle foot orthoses (AFOs) in computer simulations of gait. *Gait & Posture*, 29(1):65–70, 1 2009. ISSN 09666362. doi: 10.1016/j.gaitpost.2008.06.004. URL https://linkinghub.elsevier.com/retrieve/pii/S0966636208001549.

[18] Scott L. Delp, J. Peter Loan, Melissa G. Hoy, Felix E. Zajac, Eric L. Topp, and Joseph M. Rosen. An Interactive Graphics-Based Model of the Lower Extremity to Study Orthopaedic Surgical Procedures. *IEEE Transactions on Biomedical Engineering*, 37(8):757–767, 1990. ISSN 15582531. doi: 10.1109/10.102791.

[19] Scott L Delp, Frank C Anderson, Allison S Arnold, Peter Loan, Ayman Habib, Chand T John, Eran Guendelman, and Darryl G Thelen. OpenSim: Open-source software to create and analyze dynamic simulations of movement. *IEEE Transactions on Biomedical Engineering*, 54 (11):1940–1950, 2007. ISSN 00189294. doi: 10.1109/TBME.2007.901024. URL http://ieeexplore.ieee.org.

[20] Miha Dežman, Tadej Debevec, Jan Babič, and Andrej Gams. Effects of Passive Ankle Exoskeleton on Human Energy Expenditure: Pilot Evaluation. In *Advances in Intelligent Systems and Computing*, volume 540, pages 491–498. Springer Verlag, 2017. ISBN 9783319490571. doi: 10.1007/978-3-319-49058-8_53. URL http://link.springer.com/10.1007/978-3-319-49058-8{_}53.

[21] Nicola Eddison, Nachiappan Chockalingam, and Stephen Osborne. Ankle foot orthosis–footwear combination tuning: An investigation into common clinical practice in the United Kingdom. *Prosthetics and Orthotics International*, 39(2):126–133, 4 2015. ISSN 17461553. doi: 10.1177/0309364613516486. URL http://www.ncbi.nlm.nih.gov/pubmed/24567349.

[22] Antoine Falisse, Gil Serrancolí, Christopher L. Dembia, Joris Gillis, Ilse Jonkers, and Friedl De Groote. Rapid predictive simulations with complex musculoskeletal models suggest that diverse healthy and pathological human gaits can emerge from similar control strategies. *Journal of the Royal Society Interface*, 16(157):20190402, aug 2019. ISSN 17425662. doi: 10.1098/rsif.2019.0402. URL https://royalsocietypublishing.org/doi/10.1098/rsif.2019.0402.

[23] W. E. Garrett, J. C. Califf, and F. H. Bassett. Histochemical correlates of hamstring injuries. *American Journal of Sports Medicine*, 12(2):98–103, mar 1984. ISSN 03635465. doi: 10.1177/036354658401200202. URL http://journals.sagepub.com/doi/10.1177/036354658401200202.

[24] Thomas Geijtenbeek. SCONE: Open Source Software for Predictive Simulation of Biological Motion. *Journal of Open Source Software*, 4(38):1421, jun 2019. ISSN 2475-9066. doi: 10.21105/joss.01421. URL http://joss.theoj.org/papers/10.21105/joss.01421.

[25] Hartmut Geyer and Hugh Herr. A Muscle-reflex model that encodes principles of legged mechanics produces human walking dynamics and muscle activities. *IEEE Transactions on Neural Systems and Rehabilitation Engineering*, 18(3):263–273, 2010. ISSN 15344320. doi: 10.1109/TNSRE.2010.2047592.

[26] Saryn R Goldberg and Steven J Stanhope. Sensitivity of joint moments to changes in walking speed and body-weight-support are interdependent and vary across joints. *Journal of Biomechanics*, 46(6):1176–1183, 2013. ISSN 00219290. doi: 10.1016/j.jbiomech.2013.01.001.

[27] Nikolaus Hansen. The CMA Evolution Strategy: A Comparing Review. In *Towards a New Evolutionary Computation*, pages 75–102. Springer Berlin Heidelberg, jun 2007. doi: 10.1007/3-540-32494-1_4. URL www.springerlink.com.

[28] Nicole G. Harper, Elizabeth Russell Esposito, Jason M. Wilken, and Richard R. Neptune. The influence of ankle-foot orthosis stiffness on walking performance in individuals with lower-limb impairments. *Clinical Biomechanics*, 29(8):877–884, 9 2014. ISSN 02680033. doi: 10.1016/j.clinbiomech.2014.07.005. URL https://linkinghub.elsevier.com/retrieve/pii/S0268003314001739.

[29] Amy K. Hegarty, Anthony J. Petrella, Max J. Kurz, and Anne K. Silverman. Evaluating the effects of ankle-foot orthosis mechanical property assumptions on gait simulation muscle force results. *Journal of Biomechanical Engineering*, 139(3), 3 2017. ISSN 15288951. doi: 10.1115/1.4035472.

[30] Martin Hora, Vladimír Sládek, Libor Soumar, Kateřina Stráníková, and Tomáš Michálek. Influence of body mass and lower limb length on knee flexion angle during walking in humans. *Folia Zoologica*, 61(3-4):330–339, nov 2012. ISSN 01397893. doi: 10.25225/fozo.v61.i3.a15.2012. URL http://www.bioone.org/doi/10.25225/fozo.v61.i3.a15.2012.

[31] J D Hsu, J Michael, and J Fisk. *AAOS Atlas of Orthoses and Assistive Devices E-Book*. Elsevier Health Sciences, 2008. ISBN 9780323076319. URL https://books.google.hu/books?id=mFmoyOesaIMC.

[32] M. A. Johnson, J. Polgar, D. Weightman, and D. Appleton. Data on the distribution of fibre types in thirty-six human muscles. An autopsy study. *Journal of the Neurological Sciences*, 18 (1):111–129, 1973. ISSN 0022510X. doi: 10.1016/0022-510X(73)90023-3. URL https://pubmed-ncbi-nlm-nih-gov.tudelft.idm.oclc.org/4120482/.

[33] Yvette L. Kerkum, Annemieke I. Buizer, Josien C. Van Den Noort, Jules G. Becher, Jaap Harlaar, and Merel Anne Brehm. The effects of varying ankle foot orthosis stiffness on gait in children with spastic cerebral palsy who walk with excessive knee flexion. *PLoS ONE*, 10(11), 11 2015. ISSN 19326203. doi: 10.1371/journal.pone.0142878.

[34] Yvette L. Kerkum, Jaap Harlaar, Annemieke I. Buizer, Josien C. van den Noort, Jules G. Becher, and Merel-Anne Brehm. An individual approach for optimizing ankle-foot orthoses to improve mobility in children with spastic cerebral palsy walking with excessive knee flexion. *Gait & Posture*, 46:104–111, 5 2016. ISSN 09666362. doi: 10.1016/j.gaitpost.2016.03.001. URL https://linkinghub.elsevier.com/retrieve/pii/S0966636216000734.

[35] Toshiki Kobayashi, Aaron K.L. Leung, Yasushi Akazawa, and Stephen W. Hutchins. Design of a stiffness-adjustable ankle-foot orthosis and its effect on ankle joint kinematics in patients with stroke. *Gait & Posture*, 33(4):721–723, 4 2011. ISSN 09666362. doi: 10.1016/j.gaitpost.2011.02.005. URL https://linkinghub.elsevier.com/retrieve/pii/S0966636211000397.

[36] Toshiki Kobayashi, Michael S. Orendurff, Grace Hunt, Lucas S. Lincoln, Fan Gao, Nicholas LeCursi, and K. Bo Foreman. An articulated ankle–foot orthosis with adjustable plantarflexion resistance, dorsiflexion resistance and alignment: A pilot study on mechanical properties and effects on stroke hemiparetic gait. *Medical Engineering & Physics*, 44:94–101, 6 2017. ISSN 13504533. doi: 10.1016/j.medengphy.2017.02.012. URL http://www.ncbi.nlm.nih.gov/pubmed/28284572http://www.pubmedcentral.nih.gov/articlerender.fcgi?artid=PMC5415412https://linkinghub.elsevier.com/retrieve/pii/S1350453317300644.

[37] Françoise Leurs, Yuri P. Ivanenko, Ana Bengoetxea, Ana Maria Cebolla, Bernard Dan, Francesco Lacquaniti, and Guy A. Cheron. Optimal walking speed following changes in limb geometry. *Journal of Experimental Biology*, 214(13):2276–2282, jul 2011. ISSN 00220949. doi: 10.1242/jeb.054452. URL www.statsoft.com.

[38] R E Major, P J Hewart, and A. M. Macdonald. A new structural concept in moulded fixed ankle foot orthoses and comparison of the bending stiffness of four constructions. *Prosthetics and Orthotics International*, 28(1):44–48, 4 2004. ISSN 03093646. doi: 10.3109/03093640409167924. URL http://www.ncbi.nlm.nih.gov/pubmed/15171577.

[39] MathWorks. Trapezoidal numerical integration - MATLAB trapz - MathWorks Benelux. URL https://nl.mathworks.com/help/matlab/ref/cumtrapz.htmlhttps://nl.mathworks.com/help/matlab/ref/trapz.html.

[40] MathWorks. Polynomial curve fitting - MATLAB polyfit - MathWorks United Kingdom, 2016. URL https://nl.mathworks.com/help/matlab/ref/polyfit.htmlhttps://uk.mathworks.com/help/matlab/ref/polyfit.html{%}0Ahttps://se.mathworks.com/help/matlab/ref/polyfit.html{%}0Ahttps://uk.mathworks.com/help/matlab/ref/polyfit.html.

[41] J H Matsubara, M Wu, and K E Gordon. Metabolic cost of lateral stabilization during walking in people with incomplete spinal cord injury. *Gait and Posture*, 41(2):646–651, 2015. ISSN 18792219. doi: 10.1016/j.gaitpost.2015.01.015.

[42] P Meyns, Y L Kerkum, M A Brehm, J G Becher, A I Buizer, and J Harlaar. Ankle foot orthoses in cerebral palsy: Effects of ankle stiffness on trunk kinematics, gait stability and energy cost of walking. *European Journal of Paediatric Neurology*, 26:68–74, 2020. ISSN 15322130. doi: 10.1016/j.ejpn.2020.02.009. URL https://doi.org/10.1016/j.ejpn.2020.02.009.

[43] Matthew Millard and Katja Mombaur. A quick turn of foot: Rigid foot-ground contact models for human motion prediction. *Frontiers in Neurorobotics*, 13, 2019. ISSN 16625218. doi: 10.3389/fnbot.2019.00062.

[44] Matthew Millard, Thomas Uchida, Ajay Seth, and Scott L. Delp. Flexing computational muscle: Modeling and simulation of musculotendon dynamics. *Journal of Biomechanical Engineering*, 135 (2), 2013. ISSN 01480731. doi: 10.1115/1.4023390.

[45] Clare E. Milner, Reed Ferber, Christine D. Pollard, Joseph Hamill, and Irene S. Davis. Biomechanical factors associated with tibial stress fracture in female runners. *Medicine and Science in Sports and Exercise*, 38(2):323–328, feb 2006. ISSN 01959131. doi: 10.1249/01.mss.0000183477.75808.92. URL http://journals.lww.com/00005768-200602000-00019.

[46] Ryo Momosakr, Masahiro Abo, Shu Watanabe, Wataru Kakuda, Naoki Yamada, and Shoji Kinoshita. Effects of ankle-foot orthoses on functional recovery after stroke: A propensity score analysis based on Japan rehabilitation database. *PLoS ONE*, 10(4), 4 2015. ISSN 19326203. doi: 10.1371/journal.pone.0122688.

[47] Frans Nollet, Anita Beelen, Martin H. Prins, Marianne De Visser, Anthony J Sargeant, Gustaaf J. Lankhorst, and Bareld A De Jong. Disability and functional assessment in former polio patients with and without postpolio syndrome. *Archives of Physical Medicine and Rehabilitation*, 80(2):136–143, 1999. ISSN 00039993. doi: 10.1016/S0003-9993(99)90110-7.

[48] Carmichael F. Ong, Jennifer L. Hicks, and Scott L. Delp. Simulation-Based Design for Wearable Robotic Systems: An Optimization Framework for Enhancing a Standing Long Jump. *IEEE Transactions on Biomedical Engineering*, 63(5):894–903, may 2016. ISSN 0018-9294. doi: 10.1109/TBME.2015.2463077. URL http://ieeexplore.ieee.org/document/7173005/.

[49] Carmichael F Ong, Thomas Geijtenbeek, Jennifer L Hicks, and Scott L Delp. Predicting gait adaptations due to ankle plantarflexor muscle weakness and contracture using physics-based musculoskeletal simulations, 2019. ISSN 1553-7358. URL https://doi.org/10.1101/597294.

[50] Opensim. Getting Started with CMC - OpenSim Documentation. URL https://simtk-confluence.stanford.edu:8443/display/OpenSim/Getting+Started+with+CMChttps://simtk-confluence.stanford.edu/display/OpenSim/Getting+Started+with+CMC.

[51] OpenSim. API: OpenSim::FiberForceLengthCurve Class Reference, . URL https://simtk.org/api{_}docs/opensim/api{_}docs33/classOpenSim{_}1{_}1FiberForceLengthCurve.html.

[52] OpenSim. API: OpenSim::TendonForceLengthCurve Class Reference, . URL https://simtk.org/api{_}docs/opensim/api{_}docs33/classOpenSim{_}1{_}1TendonForceLengthCurve.html.

[53] OpenSim. Getting Started with RRA - OpenSim Documentation, . URL https://simtk-confluence.stanford.edu:8443/display/OpenSim/Getting+Started+with+RRA.

[54] OpenSim. Scaling - OpenSim Documentation, . URL https://simtk-confluence.stanford.edu:8443/display/OpenSim/Scaling.

[55] M. Petrovic, C. N. Maganaris, K. Deschamps, S. M. Verschueren, F. L. Bowling, A. J.M. Boulton, and N. D. Reeves. Altered Achilles tendon function during walking in people with diabetic neuropathy: Implications for metabolic energy saving. *Journal of Applied Physiology*, 124(5): 1333–1340, may 2018. ISSN 15221601. doi: 10.1152/japplphysiol.00290.2017. URL https://pubmed-ncbi-nlm-nih-gov.tudelft.idm.oclc.org/29420151/.

[56] Margaret Phillips, Kathryn Radford, and Adrian Wills. Ankle foot orthoses for people with Charcot Marie Tooth disease - Views of users and orthotists on important aspects of use. *Disability and Rehabilitation: Assistive Technology*, 6(6):491–499, 11 2011. ISSN 17483107. doi: 10.3109/17483107.2010.549899. URL http://www.ncbi.nlm.nih.gov/pubmed/21271787.

[57] Hilde E. Ploeger, Sicco A. Bus, Merel Anne Brehm, and Frans Nollet. Ankle-foot orthoses that restrict dorsiflexion improve walking in polio survivors with calf muscle weakness. *Gait and Posture*, 40(3):391–398, 2014. ISSN 18792219. doi: 10.1016/j.gaitpost.2014.05.016. URL http://dx.doi.org/10.1016/j.gaitpost.2014.05.016.

[58] Hilde E. Ploeger, Sicco A. Bus, Frans Nollet, and Merel Anne Brehm. Gait patterns in association with underlying impairments in polio survivors with calf muscle weakness. *Gait and Posture*, 58: 146–153, oct 2017. ISSN 18792219. doi: 10.1016/j.gaitpost.2017.07.107.

[59] Hilde E. Ploeger, Niels F.J. J Waterval, Frans Nollet, Sicco A. Bus, and Merel-Anne Anne Brehm. Stiffness modification of two ankle-foot orthosis types to optimize gait in individuals with non-spastic calf muscle weakness-A proof-of-concept study. *Journal of Foot and Ankle Research*, 12(1):41, 8 2019. ISSN 17571146. doi: 10.1186/s13047-019-0348-8. URL http://www.ncbi.nlm.nih.gov/pubmed/31406508http://www.pubmedcentral.nih.gov/articlerender.fcgi?artid=PMC6686412.

[60] Jim R. Potvin and Andrew J. Fuglevand. A motor unit-based model of muscle fatigue. *PLoS Computational Biology*, 13(6), jun 2017. ISSN 15537358. doi: 10.1371/journal.pcbi.1005581.

[61] T. Pozzo, A. Berthoz, and L. Lefort. Head stabilization during various locomotor tasks in humans. *Experimental Brain Research*, 82(1):97–106, 1990. ISSN 00144819. doi: 10.1007/BF00230842.

[62] Andrew J Ries and Michael H Schwartz. Ground reaction and solid ankle–foot orthoses are equivalent for the correction of crouch gait in children with cerebral palsy. *Developmental Medicine and Child Neurology*, 61(2):219–225, feb 2019. ISSN 14698749. doi: 10.1111/dmcn.13999. URL http://doi.wiley.com/10.1111/dmcn.13999.

[63] Andrew J. Ries, Tom F. Novacheck, and Michael H. Schwartz. A data driven model for optimal orthosis selection in children with cerebral palsy. *Gait and Posture*, 40(4):539–544, 2014. ISSN 18792219. doi: 10.1016/j.gaitpost.2014.06.011.

[64] Elizabeth Russell Esposito, Kelly A. Schmidtbauer, and Jason M. Wilken. Experimental comparisons of passive and powered ankle-foot orthoses in individuals with limb reconstruction. *Journal of NeuroEngineering and Rehabilitation*, 15(1), 11 2018. ISSN 17430003. doi: 10.1186/s12984-018-0455-y.

[65] Gregory S. Sawicki and Nabil S. Khan. A Simple Model to Estimate Plantarflexor Muscle–Tendon Mechanics and Energetics During Walking With Elastic Ankle Exoskeletons. *IEEE Transactions on Biomedical Engineering*, 63(5):914–923, 5 2016. ISSN 0018-9294. doi: 10.1109/TBME.2015.2491224. URL http://ieeexplore.ieee.org/document/7299271/.

[66] SCONE. ConditionalMuscleReflex [SCONE], . URL https://scone.software/doku.php?id=ref:conditional{_}muscle{_}reflex.

[67] SCONE. DofReflex [SCONE], . URL https://scone.software/doku.php?id=ref:dof{_}reflex.

[68] SCONE. GaitMeasure [SCONE], . URL https://scone.software/doku.php?id=ref:gait{_}measure.

[69] SCONE. MuscleReflex [SCONE], . URL https://scone.software/doku.php?id=ref:muscle{_}reflex.

[70] SCONE. SCONE Models [SCONE], . URL https://scone.software/doku.php?id=doc:model.

[71] Jessica C Selinger, Shawn M. O'Connor, Jeremy D Wong, and J. Maxwell Donelan. Humans Can Continuously Optimize Energetic Cost during Walking. *Current Biology*, 25(18):2452–2456, 2015. ISSN 09609822. doi: 10.1016/j.cub.2015.08.016. URL http://dx.doi.org/10.1016/j.cub.2015.08.016.

[72] Ajay Seth, Jennifer L Hicks, Thomas K Uchida, Ayman Habib, Christopher L Dembia, James J Dunne, Carmichael F Ong, Matthew S. DeMers, Apoorva Rajagopal, Matthew Millard, Samuel R Hamner, Edith M Arnold, Jennifer R Yong, Shrinidhi K Lakshmikanth, Michael A Sherman, Joy P Ku, and Scott L Delp. OpenSim: Simulating musculoskeletal dynamics and neuromuscular control to study human and animal movement. *PLoS Computational Biology*, 14(7), 2018. ISSN 15537358. doi: 10.1371/journal.pcbi.1006223. URL https://doi.org/10.1371/journal.pcbi.1006223.g001.

[73] Barbara Silver-Thorn, Angela Herrmann, Thomas Current, and John McGuire. Effect of ankle orientation on heel loading and knee stability for post-stroke individuals wearing ankle-foot orthoses. *Prosthetics and Orthotics International*, 35(2):150–162, 2011. ISSN 03093646. doi: 10.1177/0309364611399146.

[74] SimTK. OpenSim Documentation: Millard 2012 Muscle Models, . URL https://simtk-confluence.stanford.edu/display/OpenSim/Millard+2012+Muscle+Models.

[75] SimTK. Musculoskeletal Models OpenSim, . URL https://simtk-confluence.stanford.edu/display/OpenSim/Musculoskeletal+Modelshttp://simtk-confluence.stanford.edu:8080/display/OpenSim/Musculoskeletal+Models.

[76] Madeline L. Singer, Toshiki Kobayashi, Lucas S. Lincoln, Michael S. Orendurff, and K. Bo Foreman. The effect of ankle–foot orthosis plantarflexion stiffness on ankle and knee joint kinematics and kinetics during first and second rockers of gait in individuals with stroke. *Clinical Biomechanics*, 29(9):1077–1080, 11 2014. ISSN 02680033. doi: 10.1016/j.clinbiomech.2014.09.001. URL https://linkinghub.elsevier.com/retrieve/pii/S0268003314002125.

[77] Seungmoon Song and Hartmut Geyer. A neural circuitry that emphasizes spinal feedback generates diverse behaviours of human locomotion. *Journal of Physiology*, 593(16):3493–3511, aug 2015. ISSN 14697793. doi: 10.1113/JP270228. URL http://doi.wiley.com/10.1113/JP270228.

[78] Manish Sreenivasa, Matthew Millard, Martin Felis, Katja Mombaur, and Sebastian I. Wolf. Optimal control based stiffness identification of an ankle-foot orthosis using a predictive walking model. *Frontiers in Computational Neuroscience*, 11, 4 2017. ISSN 16625188. doi: 10.3389/fncom.2017.00023.

[79] T Sumiya, Y Suzuki, and T Kasahara. Stiffness control in posterior-type plastic ankle-foot orthoses: Effect of ankle trimline. Part 2: Orthosis characteristics and orthosis/patient matching. *Prosthetics and Orthotics International*, 20(2):132–137, 8 1996. ISSN 03093646. doi: 10.3109/03093649609164431. URL http://www.ncbi.nlm.nih.gov/pubmed/8876008.

[80] Thomas K. Uchida, Jennifer L. Hicks, Christopher L. Dembia, and Scott L. Delp. Stretching your energetic budget: How tendon compliance affects the metabolic cost of running. *PLoS ONE*, 11 (3):e0150378, mar 2016. ISSN 19326203. doi: 10.1371/journal.pone.0150378. URL https://dx.plos.org/10.1371/journal.pone.0150378.

[81] Brian R Umberger, Karin G.M. Gerritsen, and Philip E Martin. A model of human muscle energy expenditure. *Computer methods in biomechanics and biomedical engineering*, 6(2):99–111, 2003. ISSN 10255842. doi: 10.1080/1025584031000091678.

[82] K. Veerkamp, N.F.J. Waterval, T. Geijtenbeek, C.P. Carty, D.G. Lloyd, J. Harlaar, and M.M. van der Krogt. Evaluating cost function criteria in predicting healthy gait. *Submitted*, 2020.

[83] Nianfeng Wang, Yihong Zhong, and Xianmin Zhang. An Improved Model to Estimate Muscle-Tendon Mechanics and Energetics During Walking with a Passive Ankle Exoskeleton. In *Lecture Notes in Computer Science (including subseries Lecture Notes in Artificial Intelligence and Lecture Notes in Bioinformatics)*, volume 11740 LNAI, pages 83–96. Springer Verlag, 2019. ISBN 9783030275259. doi: 10.1007/978-3-030-27526-6_8. URL http://link.springer.com/10.1007/978-3-030-27526-6{_}8.

[84] Robert L. Waters and Sara Mulroy. The energy expenditure of normal and pathologic gait. *Gait & Posture*, 9(3):207–231, jul 1999. ISSN 09666362. doi: 10.1016/S0966-6362(99)00009-0. URL https://linkinghub.elsevier.com/retrieve/pii/S0966636299000090.

[85] Niels F.J. Waterval, Merel Anne Brehm, Hilde E. Ploeger, Frans Nollet, and Jaap Harlaar. Compensations in lower limb joint work during walking in response to unilateral calf muscle weakness. *Gait and Posture*, 66:38–44, oct 2018. ISSN 18792219. doi: 10.1016/j.gaitpost.2018.08.016.

[86] Niels F.J. Waterval, K. Veerkamp, Thomas Geijtenbeek, Jaap Harlaar, Frans Nollet, Merel-Anne Brehm, and M. van der Krogt. Predictive simulations can validly reproduce the gait pattern of people with non-spastic bilateral calf muscle weakness. *Gait & Posture*, 73:201–202, sep 2019. ISSN 09666362. doi: 10.1016/j.gaitpost.2019.07.104. URL https://linkinghub.elsevier.com/retrieve/pii/S0966636219308446.

[87] Niels F.J. Waterval, Merel Anne Brehm, Jaap Harlaar, and Frans Nollet. Description of orthotic properties and effect evaluation of ankle-foot orthoses in non-spastic calf muscle weakness. *Journal of rehabilitation medicine*, 52(3):jrm00026, 2020. ISSN 16512081. doi: 10.2340/16501977-2642. URL www.medicaljournals.se/jrm.

[88] Niels F.J. J Waterval, Frans Nollet, Jaap Harlaar, and Merel-Anne Anne Brehm. Modifying ankle foot orthosis stiffness in patients with calf muscle weakness: Gait responses on group and individual level. *Journal of NeuroEngineering and Rehabilitation*, 16(1):120, 10 2019. ISSN 17430003. doi: 10.1186/s12984-019-0600-2. URL http://www.ncbi.nlm.nih.gov/pubmed/31623670http://www.pubmedcentral.nih.gov/articlerender.fcgi?artid=PMC6798503.

[89] Michael W. Whittle. *Gait Analysis*. Elsevier Ltd, 4th edition, 2007. ISBN 9780750688833. doi: 10.1016/B978-0-7506-8883-3.X5001-6.

[90] Wikipedia. Coefficient of determination - Wikipedia, 2020. URL https://en.wikipedia.org/wiki/Coefficient{_}of{_}determination.

[91] Kirby A Witte, Pieter Fiers, Alison L Sheets-Singer, and Steven H Collins. Improving the energy economy of human running with powered and unpowered ankle exoskeleton assistance. *Science Robotics*, 5(40):9108, 2020. ISSN 24709476. doi: 10.1126/scirobotics.aay9108. URL http://robotics.sciencemag.org/.

[92] Gary T. Yamaguchi and Felix E. Zajac. A PLANAR MODEL OF THE KNEE JOINT TO CHARACTERIZE THE KNEE EXTENSOR MECHANISM, jan 1989. ISSN 00219290.

[93] Masataka Yamamoto, Koji Shimatani, Masaki Hasegawa, Takuya Murata, and Yuichi Kurita. Estimation of compressive tibiofemoral force using over resistance of ankle-foot orthosis on gait. In *2018 40th Annual International Conference of the IEEE Engineering in Medicine and Biology Society (EMBC)*, volume 2018-July, pages 2056–2059. IEEE, 7 2018. ISBN 978-1-5386-3646-6. doi: 10.1109/EMBC.2018.8512690. URL http://www.ncbi.nlm.nih.gov/pubmed/30440806https://ieeexplore.ieee.org/document/8512690/.

[94] Amir Abbas Zadpoor and Ali Asadi Nikooyan. The relationship between lower-extremity stress fractures and the ground reaction force: A systematic review, jan 2011. ISSN 02680033.

[95] Juanjuan Zhang, Pieter Fiers, Kirby A Witte, Rachel W Jackson, Katherine L Poggensee, Christopher G Atkeson, and Steven H Collins. Human-in-the-loop optimization of exoskeleton assistance during walking. *Science*, 356(6344):1280–1284, 2017. ISSN 10959203. doi: 10.1126/science.aal5054.

Appendix A

Slow-twitch fiber ratio settings

Table A.1: Slow-twitch fiber ratio settings of the muscles in the used musculoskeletal model

Muscle name	Slow-twitch fiber ratio
TA	0.721
SOL	0.759
GAS	0.546
VAS	0.484
RF	0.500
BFSH	0.500
HAMS	0.499
ILIO	0.500
GMAX	0.550

B

Appendix B

Passive fiber- and tendon force-length curve parameters

Table B.1: Passive fiber force-length curve parameters for soleus and gastrocnemius muscles in healthy and weakened conditions

			Passive fiber force-length curve parameters				
Muscle name	**Condition**	**Maximum isometric force (F_o^m) [N]**	**Fiber strain at zero force [-]**	**Fiber strain at F_o^m [-]**	**Normalized fiber stiffness at F_o^m [-]**	**Normalized fiber stiffness at the end of the low force region [-]**	**Fiber curve bend from linear (0) to maximum bend (1)**
SOL	60% weakness	2858	0.0	0.472	6.80	0.5	0.60
GAS	60% weakness	896	0.0	0.472	6.80	0.5	0.60
SOL	healthy (default)	7147	0.0	0.700	2.86	0.2	0.75
GAS	healthy (default)	2241	0.0	0.700	2.86	0.2	0.75

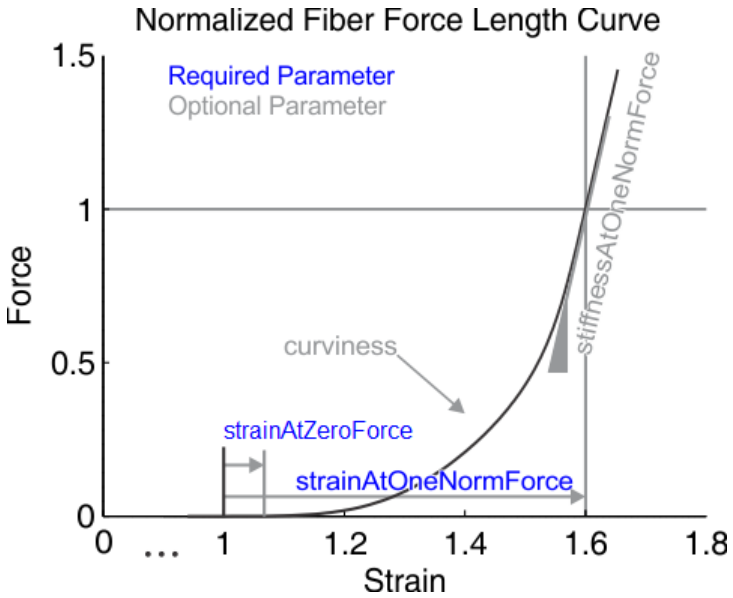

Figure B.1: Interpretation of the parameters in Tab.B.1 [51]. (Force is normalized by F_o^m)

Table B.2: Passive tendon force-length curve parameters for soleus and gastrocnemius muscles in healthy and weakened conditions

		Passive tendon force-length curve parameters					
Muscle name	**Condition**	**Maximum isometric force (F_o^m) [N]**	**Tendon strain at F_o^m [-]**	**Normalized tendon stiffness at F_o^m [-]**	**Force developed at the end of the toe region normalized by F_o^m [-]**	**Tendon curve bend from linear (0) to maximum bend (1)**	**Fiber curve bend from linear (0) to maximum bend (1)**
SOL	60% weakness	2858	0.0265	65.3	0.99	0.4	0.60
GAS	60% weakness	896	0.0265	65.3	0.99	0.4	0.60
SOL	healthy (default)	7147	0.049	28.1	0.67	0.5	0.75
GAS	healthy (default)	2241	0.049	28.1	0.67	0.5	0.75

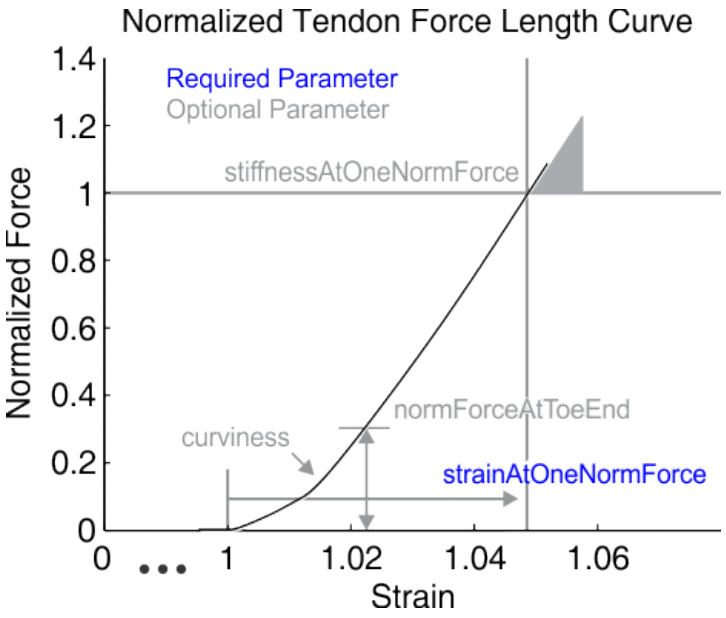

Figure B.2: Interpretation of the parameters in Tab.B.2 [52]. (Force is normalized by F_o^m)

C

Appendix C

Contact model parameter settings

Table C.1: The foot-ground contact model parameters used in the predictive simulations [82]

	Heel sphere	**Toe sphere**
Contact geometry		
x-position (m)	0.015	0.00
y-position (m)	0.019	-0.20
z-position (m)	-0.005	0.014
Radius (m)	0.040	0.020
Hunt-Crossley force parameters		
Stiffness $(\mathrm{N/m})$	2 000 000	2 000 000
Dissipation $(\mathrm{s/m})$	1	1
Frictions (static, dynamic, viscous)	1	1

Appendix D

First round optimization results with ORG init file

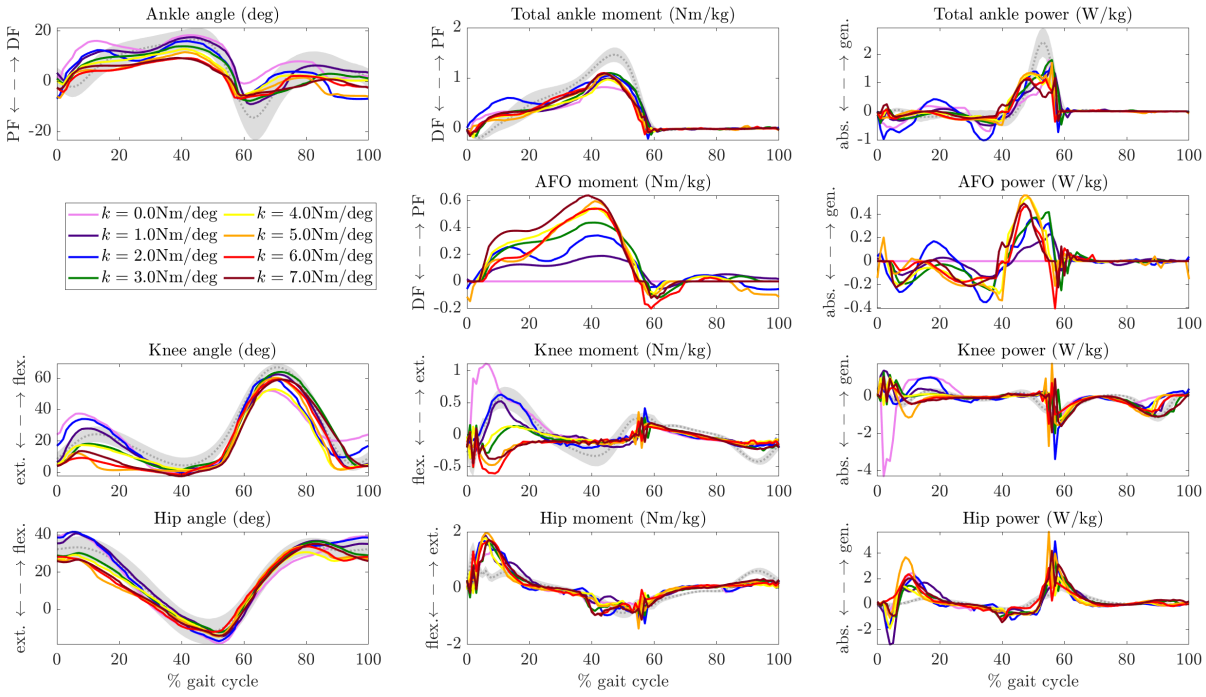

Figure D.1: First round optimization results with ORG init file. Ankle, AFO, knee and hip angles, (internal) moments and powers in the simulations with the same model with healthy calf muscle settings and with non-spastic calf muscle weakness settings wearing an AFO with stiffnesses $0 - 7\,\mathrm{Nm/deg}$. Gray curves and shading is normal data ± 1 SD [85].

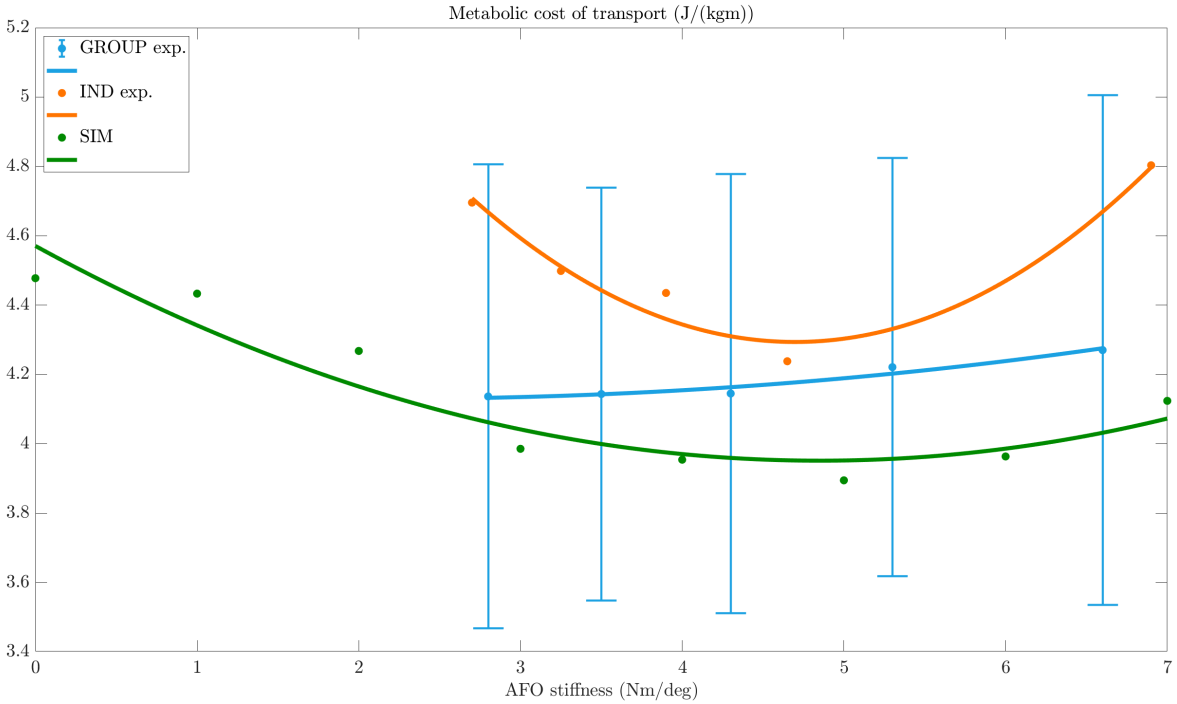

Figure D.2: First round optimization results with ORG init file. Metabolic cost of transport as AFO stiffness is varied from 0 – $7\,\mathrm{Nm/deg}$. The results of simulation (green), experimental on group level (blue) with ± 1 SD (only bilaterally affected patients results), and experimental of one of the patients (the same as the one who was used for scaling and minimum walking speed matching) (orange) is shown. The best fitting quadratic trends are plotted with the same color as the data.

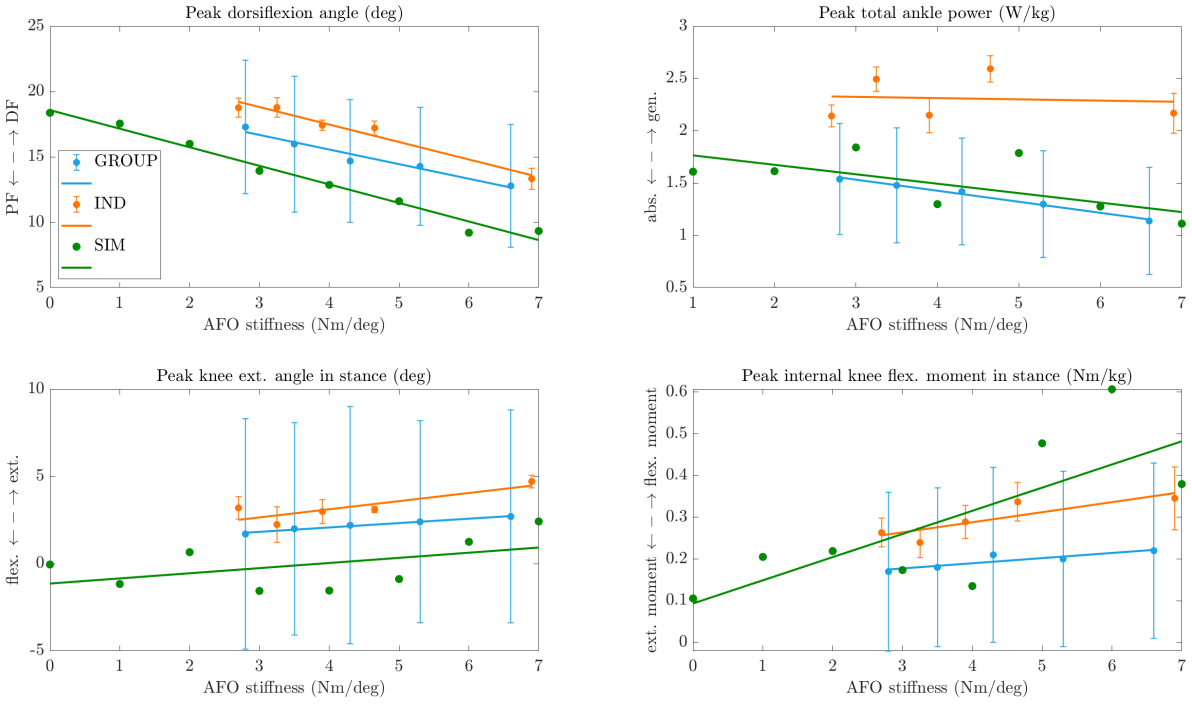

Figure D.3: First round optimization results with ORG init file. Peak dorsiflexion angle, peak total ankle power, peak knee extension angle in stance and peak internal knee flexion moment in stance as AFO stiffness is varied from 0 – 7 Nm/deg. The results of simulation (green), experimental on group level (blue) with ± 1 SD (all subjects' results), and experimental of one of the patients (the same as the one who was used for scaling and minimum walking speed matching) (orange) ± 1 SD (standard deviation of all trials) is shown. The best fitting linear trends are plotted with the same color as the data. The slope, their relative differences and the linear trends goodness of fit (R^2) value is in Tab. 3.3. The time of the peak internal knee flexion moments in stance varies in the simulation results, it depends on stiffness (see Fig. D.1.)

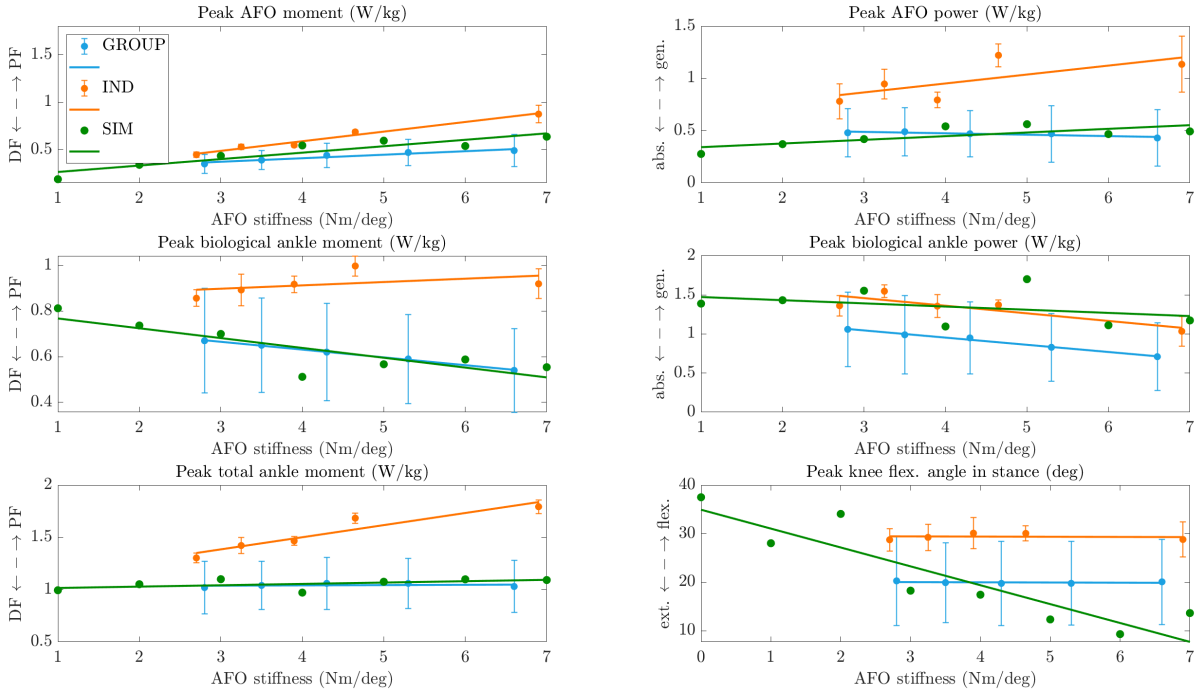

Figure D.4: First round optimization results with ORG init file. Peak AFO moment and power, peak biological ankle moment and power, peak total ankle moment and peak knee flexion angle in stance as AFO stiffness is varied from $0 - 7\,\mathrm{Nm/deg}$. The results of simulation (green), experimental on group level (blue) with ± 1 SD (all subjects' results), and experimental of one of the patients (the same as the one who was used for scaling and minimum walking speed matching) (orange) ± 1 SD (standard deviation of all trials) is shown. The best fitting linear trends are plotted with the same color as the data.

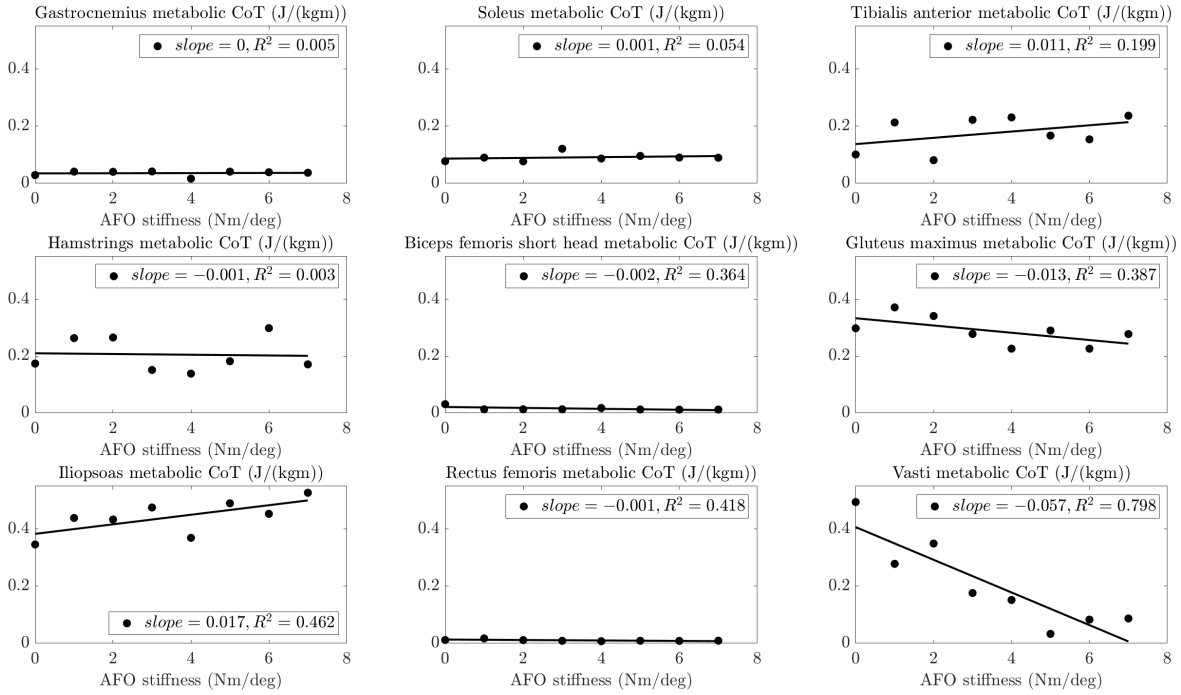

Figure D.5: First round optimization results with ORG init file. Total metabolic energy consumption of all 9 muscles during one whole gait cycle with fitted lines

Appendix E

First and second round optimization results with Patient init file

First round optimization results with Patient init file

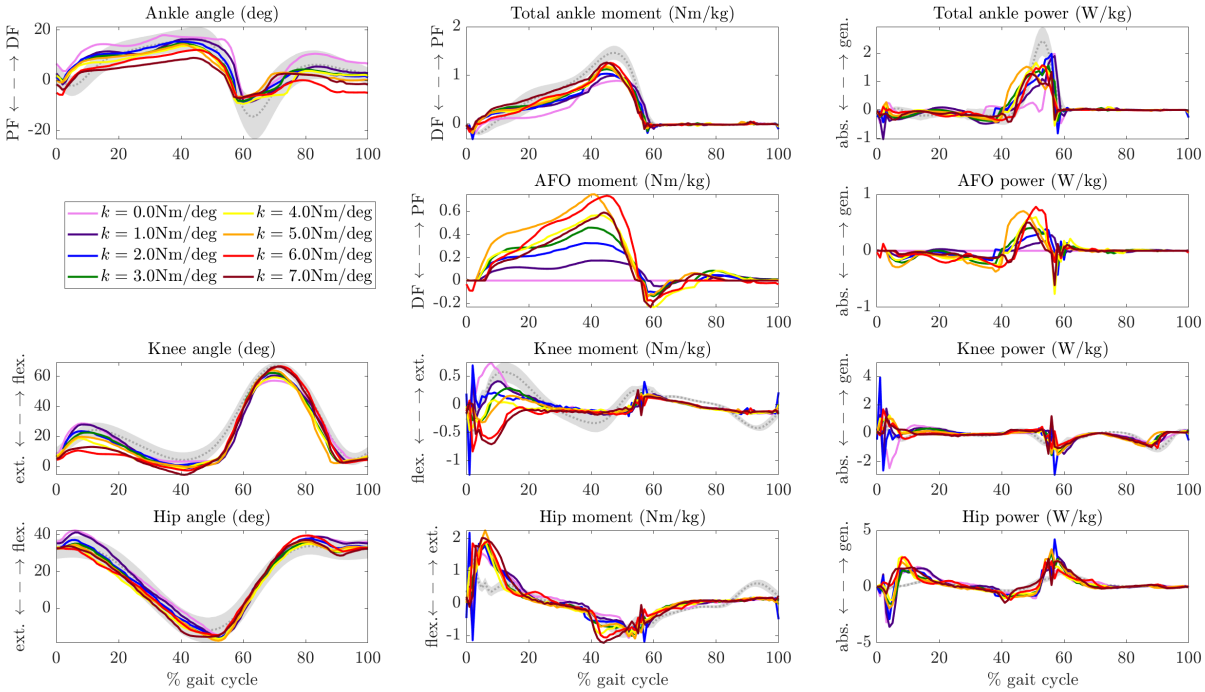

Figure E.1: First round optimization results with Patient init file. Ankle, AFO, knee and hip angles, (internal) moments and powers in the simulations with the same model with healthy calf muscle settings and with non-spastic calf muscle weakness settings wearing an AFO with stiffnesses $0 - 7\,\mathrm{Nm/deg}$. Gray curves and shading is normal data ± 1 SD [85].

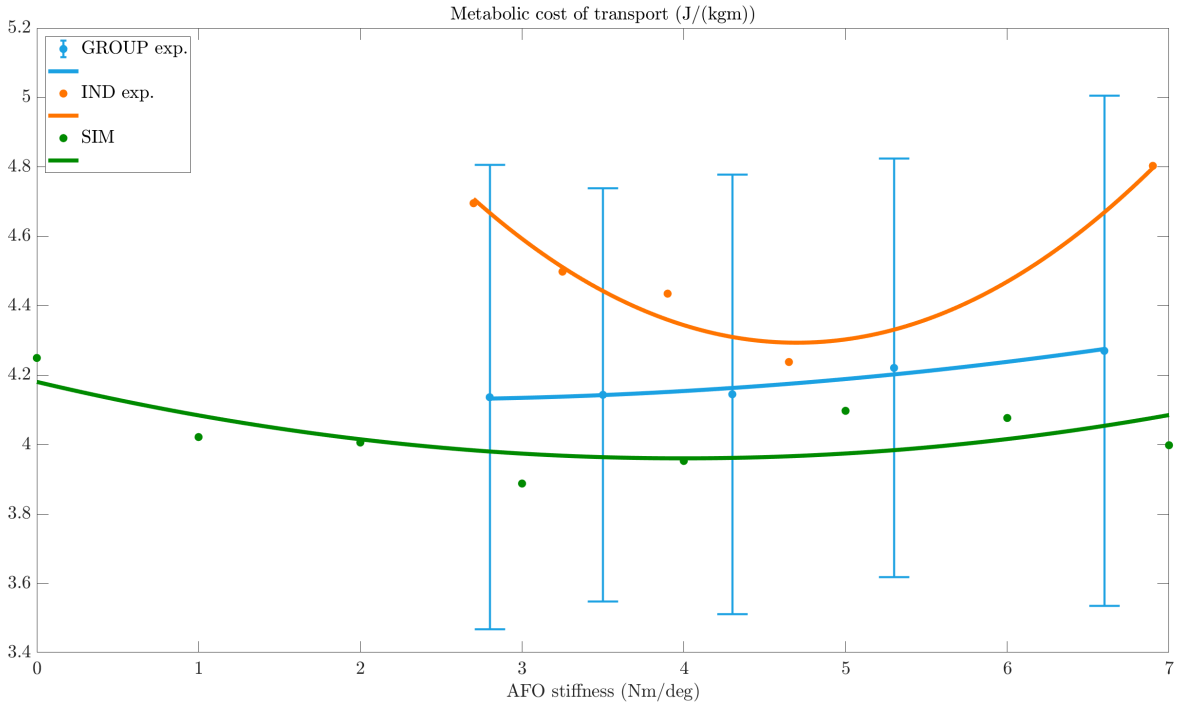

Figure E.2: First round optimization results with Patient init file. Metabolic cost of transport as AFO stiffness is varied from $0-7$ Nm/deg. The results of simulation (green), experimental on group level (blue) with ± 1 SD (only bilaterally affected patients results), and experimental of one of the patients (the same as the one who was used for scaling and minimum walking speed matching) (orange) is shown. The best fitting quadratic trends are plotted with the same color as the data.

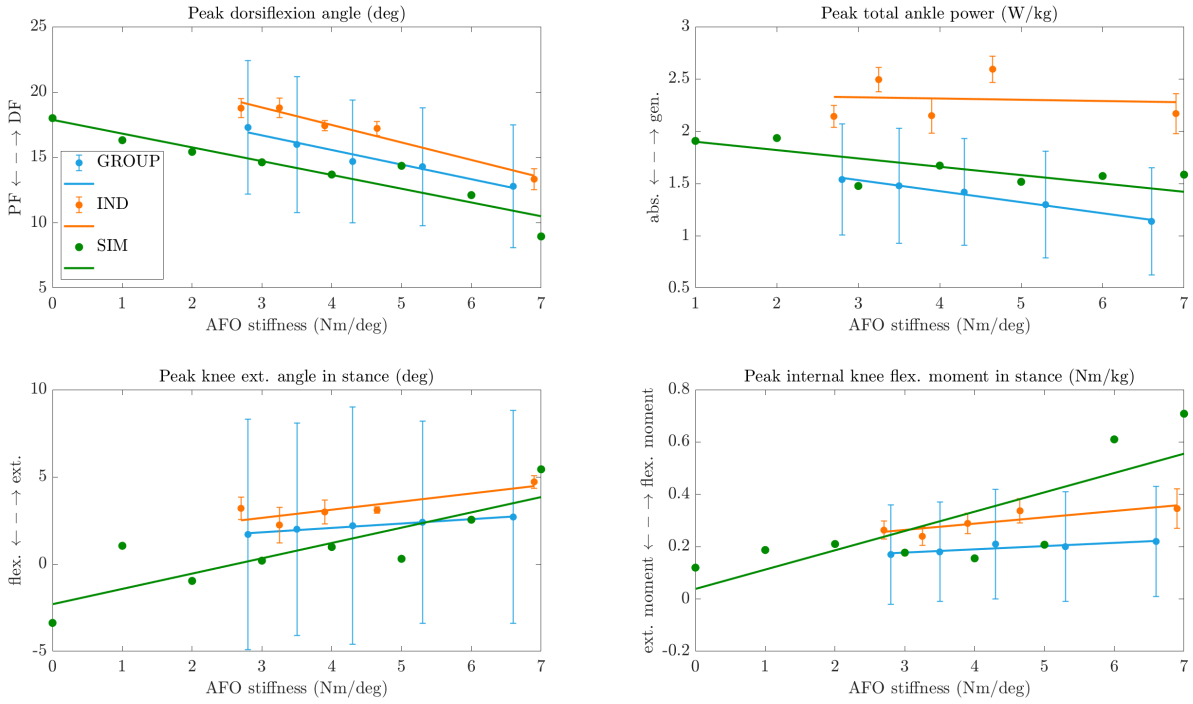

Figure E.3: First round optimization results with Patient init file. Peak dorsiflexion angle, peak total ankle power, peak knee extension angle in stance and peak internal knee flexion moment in stance as AFO stiffness is varied from $0-7$ Nm/deg. The results of simulation (green), experimental on group level (blue) with ± 1 SD (all subjects' results), and experimental of one of the patients (the same as the one who was used for scaling and minimum walking speed matching) (orange) ± 1 SD (standard deviation of all trials) is shown. The best fitting linear trends are plotted with the same color as the data. The slope, their relative differences and the linear trends goodness of fit (R^2) value is in Tab. 3.3. The time of the peak internal knee flexion moments in stance varies in the simulation results, it depends on stiffness (see Fig. E.1.)

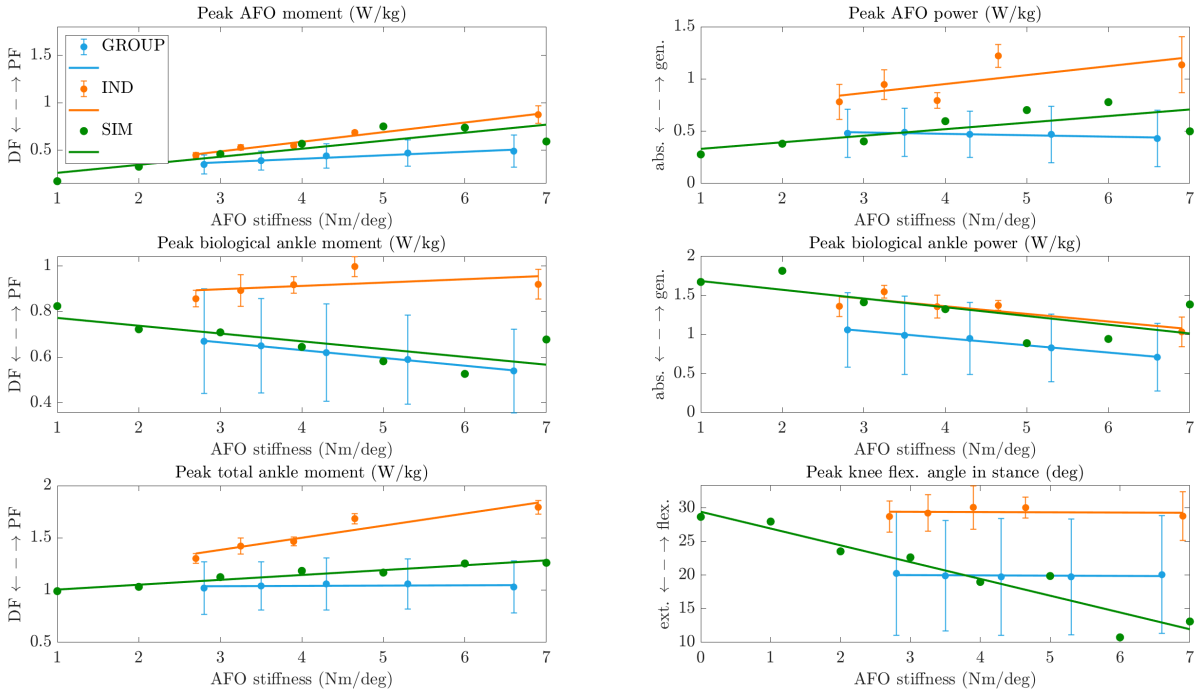

Figure E.4: First round optimization results with Patient init file. Peak AFO moment and power, peak biological ankle moment and power, peak total ankle moment and peak knee flexion angle in stance as AFO stiffness is varied from $0 - 7\,\mathrm{Nm/deg}$. The results of simulation (green), experimental on group level (blue) with ± 1 SD (all subjects' results), and experimental of one of the patients (the same as the one who was used for scaling and minimum walking speed matching) (orange) ± 1 SD (standard deviation of all trials) is shown. The best fitting linear trends are plotted with the same color as the data.

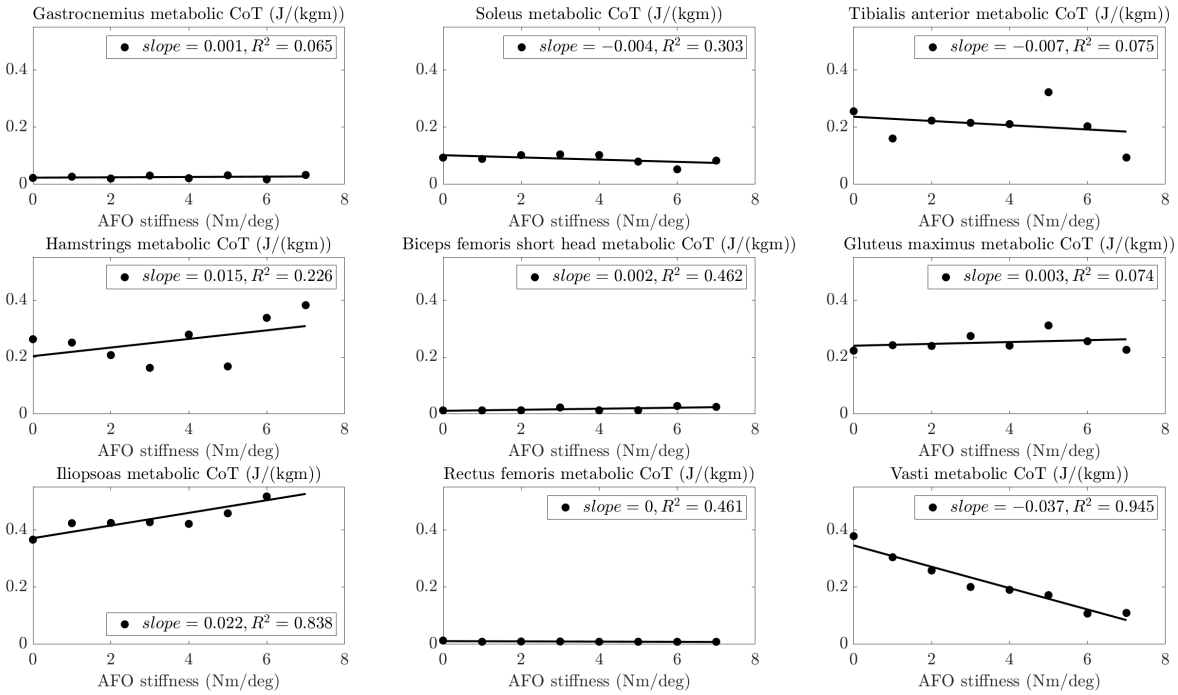

Figure E.5: First round optimization results with Patient init file. Total metabolic energy consumption of all 9 muscles during one whole gait cycle with fitted lines

Second round optimization results with Patient init file

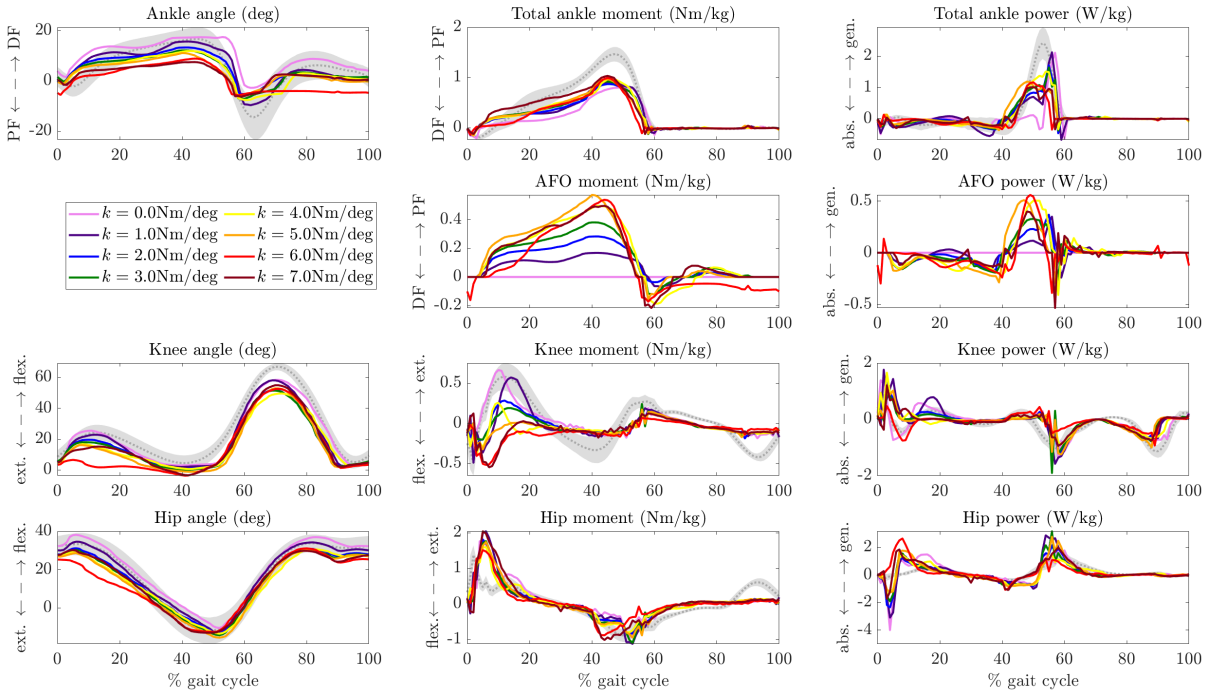

Figure E.6: Second round optimization results with Patient init file. Ankle, AFO, knee and hip angles, (internal) moments and powers in the simulations with the same model with healthy calf muscle settings and with non-spastic calf muscle weakness settings wearing an AFO with stiffnesses $0-7\,\mathrm{Nm/deg}$. Gray curves and shading is normal data ± 1 SD [85].

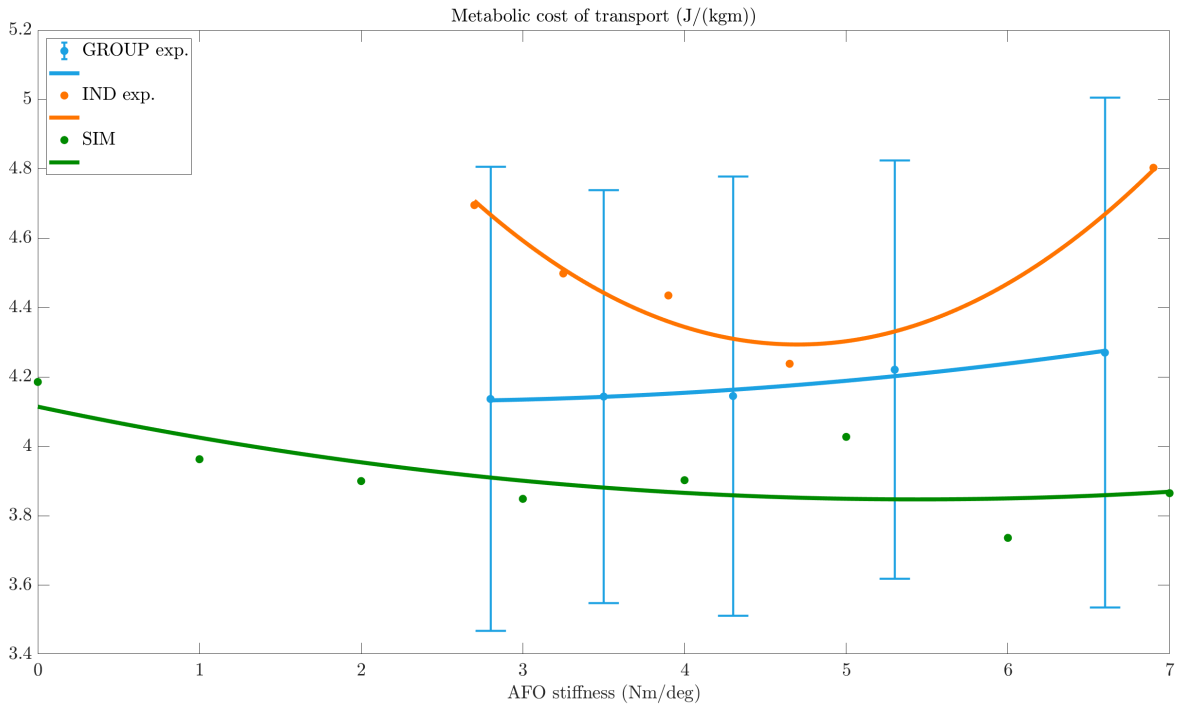

Figure E.7: Second round optimization results with Patient init file. Metabolic cost of transport as AFO stiffness is varied from $0-7\,\mathrm{Nm/deg}$. The results of simulation (green), experimental on group level (blue) with ± 1 SD (only bilaterally affected patients results), and experimental of one of the patients (the same as the one who was used for scaling and minimum walking speed matching) (orange) is shown. The best fitting quadratic trends are plotted with the same color as the data.

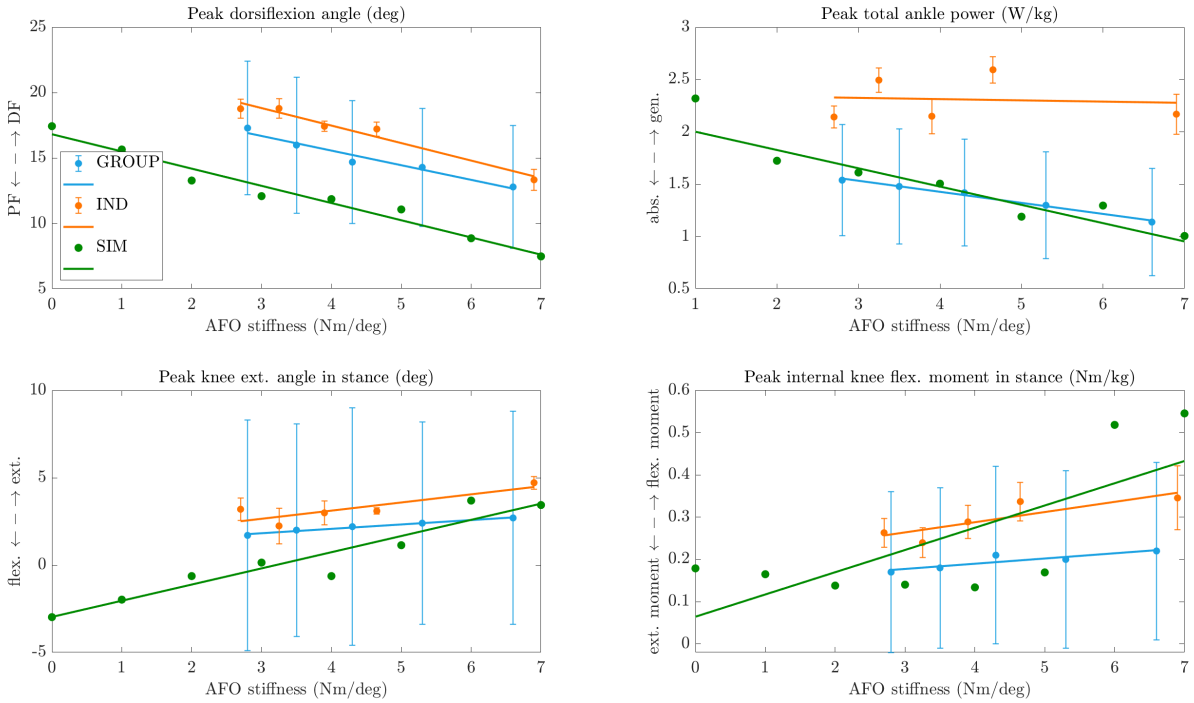

Figure E.8: Second round optimization results with Patient init file. Peak dorsiflexion angle, peak total ankle power, peak knee extension angle in stance and peak internal knee flexion moment in stance as AFO stiffness is varied from $0-7$ Nm/deg. The results of simulation (green), experimental on group level (blue) with ± 1 SD (all subjects' results), and experimental of one of the patients (the same as the one who was used for scaling and minimum walking speed matching) (orange) ± 1 SD (standard deviation of all trials) is shown. The best fitting linear trends are plotted with the same color as the data. The slope, their relative differences and the linear trends goodness of fit (R^2) value is in Tab. 3.3. The time of the peak internal knee flexion moments in stance varies in the simulation results, it depends on stiffness (see Fig. E.6.)

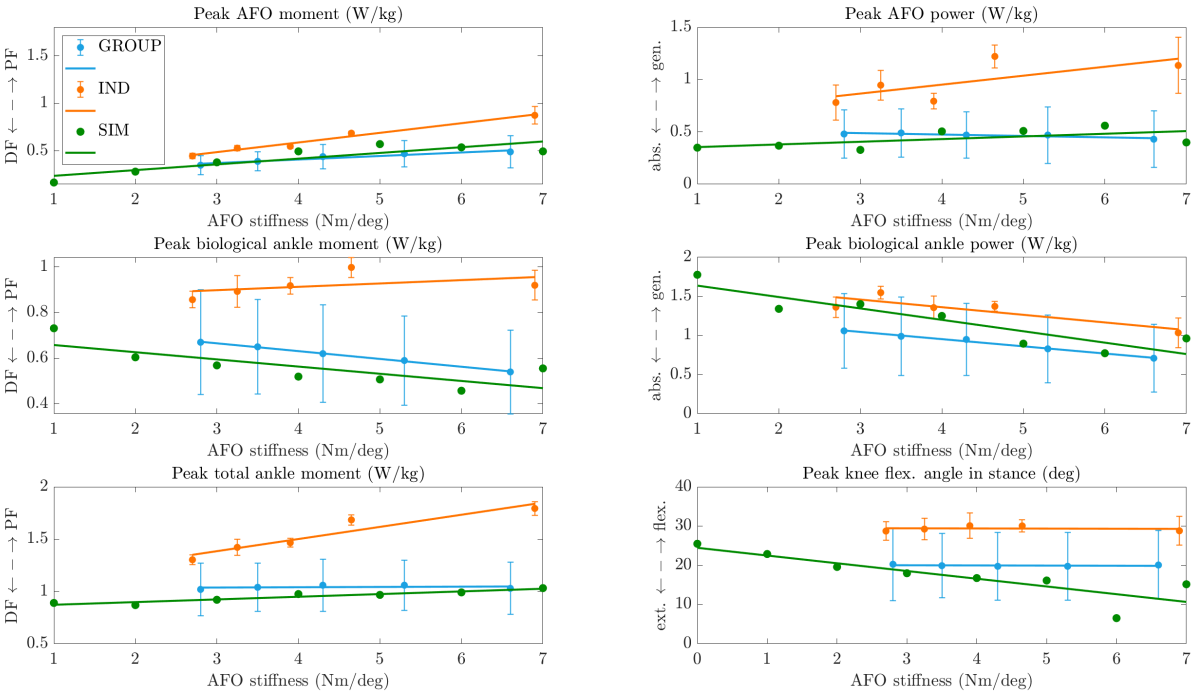

Figure E.9: Second round optimization results with Patient init file. Peak AFO moment and power, peak biological ankle moment and power, peak total ankle moment and peak knee flexion angle in stance as AFO stiffness is varied from $0-7\,\mathrm{Nm/deg}$. The results of simulation (green), experimental on group level (blue) with ± 1 SD (all subjects' results), and experimental of one of the patients (the same as the one who was used for scaling and minimum walking speed matching) (orange) ± 1 SD (standard deviation of all trials) is shown. The best fitting linear trends are plotted with the same color as the data.

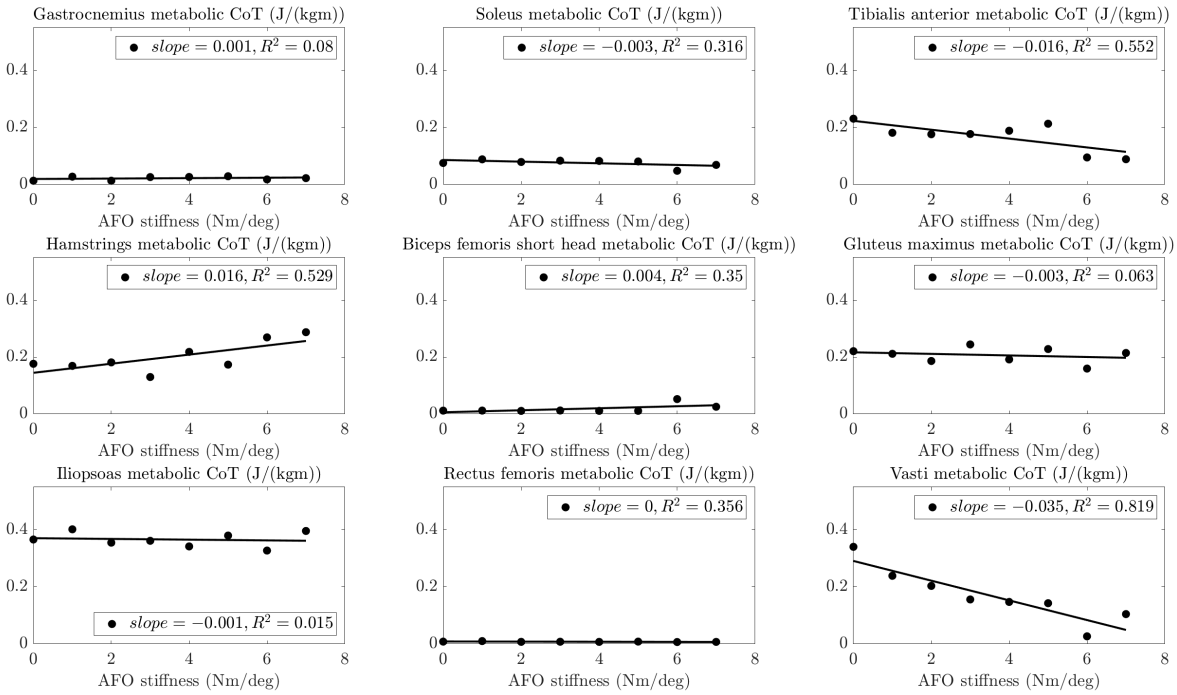

Figure E.10: Second round optimization results with Patient init file. Total metabolic energy consumption of all 9 muscles during one whole gait cycle with fitted lines